UNIVERSIDAD AUTÓNOMA DE BAJA CALIFORNIA

FACULTAD DE CIENCIAS MARINAS

INSTITUTO DE INVESTIGACIONES OCEANOLÓGICAS

LAS PROPIEDADES ÓPTICAS INHERENTES SATELITALES COMO INDICADORES DE EVENTOS DE FLORECIMIENTOS FITOPLANCTÓNICOS

T E S I S

QUE PARA CUBRIR PARCIALMENTE LOS REQUISITOS NECESARIOS
PARA OBTENER EL GRADO DE

DOCTOR EN CIENCIAS EN OCEANOGRAFÍA COSTERA

PRESENTA

JESÚS ANTONIO AGUILAR MALDONADO

ENSENADA, BAJA CALIFORNIA, MEXICO. SEPTIEMBRE 2018

Resumen

Los florecimientos fitoplanctónicos son eventos esporádicos en el tiempo y aislados en el espacio. La detección temprana de este fenómeno, así como la clasificación de un cuerpo de agua en condiciones de florecimiento o no florecimiento sigue siendo un problema no resuelto. Por esa razón, en la primera parte de la investigación se midieron las Propiedades Ópticas Inherentes (IOP) en aguas ópticamente complejas para detectar el estado de florecimiento o no florecimiento de la comunidad fitoplanctónica. Se calculó un índice de IOP a partir de los coeficientes de absorción de la Materia Orgánica Disuelta Coloreada (CDOM), el fitoplancton (phy) y el detrito (d), utilizando la longitud de onda (λ) 443 nm. La efectividad de este índice se probó con datos *in situ* de cinco eventos de florecimiento en diferentes lugares y con diferentes características en los mares mexicanos: 1. Dzilam (Mar Caribe, Océano Atlántico); 2. Holbox (Mar Caribe, Océano Atlántico); 3. Bahía de Campeche en el Golfo de México (Océano Atlántico); 4. Alto Golfo de California (UGC) (Océano Pacífico) y 5. Bahía de Todos Santos, Ensenada (Océano Pacífico). El índice se basó en las anomalías espaciales estandarizadas, que van de valores normales (-1 a 1), pasando por valores fuera de la normal (1 a 2), a valores anómalos o en florecimiento activo (2 en adelante). La diversidad de sitios mostró que el índice de IOP es un método adecuado para determinar las condiciones de un florecimiento fitoplanctónico, teniendo en cada caso de estudio por lo menos una estación en florecimiento activo.

Un vez que el índice fue probado con datos de campo se desarrolló la adaptación del índice con datos satelitales, se tomó como área de estudio la Península de Yucatán, donde la construcción de hoteles y el desarrollo de productos turísticos están asociadas con las descargas de aguas residuales de fosas sépticas. Dadas las características del acuífero kárstico de Yucatán, las descargas submarinas de aguas subterráneas son muy importantes y altamente vulnerables a la contaminación antropogénica. En esta segunda parte de la investigación se utilizaron productos satelitales a 4 km de resolución espacial y a nivel 3 de procesamiento, los productos coeficientes de absorción de fitoplancton ($\boldsymbol{a_{phy,GIOP}}$) y de detrito+CDOM ($\boldsymbol{a_{dCDOM,GIOP}}$) del modelo satelital de Propiedades Ópticas Inherentes Generalizado (GIOP), se utilizaron para calcular y mapear el índice IOP. Se elaboraron diferentes escenarios considerando las temporadas vacacionales y el régimen hidrológico, pudiendo observar la influencia de las aguas más ricas en nutrientes del Golfo de México sobre las aguas oligotróficas del norte de la península de Yucatán y los constantes bajos niveles del índice IOP en las aguas del Caribe. Además los resultados mostraron que el índice IOP satelital permite comparar diferentes puntos de observación en grandes extensiones de área.

Finalmente el índice IOP satelital fue redefinido en una concepción temporal para definir la línea base de cada pixel, determinando su comportamiento más usual a partir de series de datos que representan la variabilidad temporal. La variabilidad temporal de catorce años de datos de productos del modelo GIOP, a 1 km de resolución espacial y a nivel 2 de procesamiento, proporcionaron la definición del comportamiento promedio de dos pixeles elegidos de los meses de mayo y junio en la Bahía de Todos Santos (BTS) en Ensenada, Baja California (Océano Pacifico). La alta presencia de nubosidad en la BTS permitió probar el índice IOP satelital en condiciones donde la cantidad de datos era limitada, así es como el índice fue puesto a prueba, pudiendo diferenciar entre valores normales y valores anómalos, permitiendo la construcción de un semáforo de alerta diaria de florecimientos fitoplanctónicos.

FACULTAD DE CIENCIAS MARINAS
INSTITUTO DE INVESTIGACIONES OCEANOLÓGICAS
POSGRADO EN OCEANOGRAFÍA COSTERA

LAS PROPIEDADES ÓPTICAS INHERENTES SATELITALES COMO INDICADORES DE EVENTOS DE FLORECIMIENTOS FITOPLANCTÓNICOS

TESIS

QUE PARA CUBRIR PARCIALMENTE LOS REQUISITOS NECESARIOS PARA OBTENER EL GRADO DE

DOCTOR EN CIENCIAS EN OCEANOGRAFÍA COSTERA

PRESENTA

JESÚS ANTONIO AGUILAR MALDONADO

Aprobada por:

Dr. Eduardo Santamaría del Ángel Director de tesis	Dra. María Teresa Sebastiá Frasquet Co-Directora de tesis
Dra. Adriana González Silvera Sinodal	Dr. Omar Darío Cervantes Rosas Sinodal

Dra. Lus Mercedes López Acuña
Sinodal

Agradecimientos

Agradezco al Consejo Nacional de Ciencia y Tecnología (CONACYT) por la beca nacional, con convocatoria 291025 del año 2015, otorgada para la realización de esta investigación doctoral en el campus de Ensenada de la Universidad Autónoma de Baja California (UABC).

Debo agradecer en primer lugar a los doctores y doctoras que fueron parte de mi grupo sinodal, y que estuvieron apoyándome desde el principio y hasta el fin de la investigación doctoral.

Al Dr. Eduardo Santamaría del Ángel le agradezco de manera especial por haberme apoyado desde el primer momento en que nos conocimos, por haberme recibido en la estancia de Maestría, y después haber asistido hasta la lejana Toluca para estar presente en mi examen de titulación de Maestría. Por haberme recibido con las puertas abiertas y tenderme la mano para iniciar el doctorado, y claro, todos los consejos, apoyo, y esfuerzo que puso para que se concluyera con éxito. La amistad que hemos construido nos llevará a seguir trabajando juntos toda la vida, no importando donde nos encontremos.

A la Dra. Adriana González Silvera le agradezco su apoyo académico y personal durante toda mi estancia en Ensenada, a las Dras. Lus López Acuña y Angélica Gutiérrez Magness les agradezco su tiempo y esfuerzo que me obsequiaron para la finalización de esta investigación. De igual forma al Dr.

Omar Cervantes Rosas por su tiempo otorgado de principio a fin en este proyecto.

Por supuesto que también debo agradecer al Dr. Eduardo Santamaría por haberme dado la oportunidad de conocer a la Dra. María Terea Sebastiá Frasquet, qué además de haber sido un pilar fundamental en la construcción de la investigación, de los artículos que componen la tesis y de la tesis misma, es también la persona que me ha dado el impulso para continuar con fuerzas a pesar de las dificultades que puedan haber en el camino, pero sobre todo, mi mayor cariño y gratitud por el futuro que hemos de construir.

También mi más sincero agradecimiento y cariño a todos los POPEYES, veteranos y nuevos, que me apoyaron en campo y en la oficina, a Alejandra, Cristina, Lizbeth, Alfredo, Omar, Mariana y Diego, al clan colombiano: Daniela, Catalina, Estela y Mary.

Por último, y no por eso menos importante, sino todo lo contrario, los más importantes en mi vida, mi familia, que con su apoyo emocional y económico hicieron posible que me aventara a esta aventura. Mi madre y padre que siempre han estado conmigo y me han apoyado en cada paso que he dado. A mis hermanas Bárbara, Laura y Lola que nunca me han dejado sólo y que han sido mi sostén emocional, espiritual y económico. A Eric que ha sido un hermano. Mis queridísimos sobrinos Liliana, Wendy, Emilio y Camila que son en quienes siempre pienso. A todos gracias.

Índice

Lista de tablas

Lista de figuras

1. Introducción

La investigación desarrollada en la presente tesis doctoral se fundamenta en la importancia que tiene la detección temprana de un florecimiento fitoplanctónico. Los sistemas de previsión basados en investigaciones para los florecimientos nocivos o tóxicos son la preocupación de las redes de monitoreo de Florecimientos Algales Nocivos (FANs) [RedFAN, 2018]. Definir bajo qué condiciones un aumento en la biomasa fitoplanctónica puede considerarse un florecimiento es esencial para evitar el uso arbitrario del término [Ji et al., 2015, Brody el al., 2013, Platt et al., 2009]. Como lo expresan Carstensen et al. [2015]: "si bien no existe una definición universalmente aceptada de lo que constituye un florecimiento, la noción de una desviación sustancial por encima de la biomasa fitoplanctónica registrada en ese lugar es común a todas las definiciones". Entonces, podemos definir un florecimiento de fitoplancton como una desviación a valores más altos que los patrones estacionales estándar en un sitio específico. Los valores inusuales de biomasa alta de fitoplancton pueden ser muy diferentes entre distintos sitios. Así pues, es de vital importancia definir la línea base característica de un lugar para poder distinguir las anomalías.

La lista de variables predictoras y de seguimiento de florecimientos fitoplanctónicos utilizadas habitualmente incluye cambios en la composición de especies de fitoplancton [Schneider et al., 2006], en la cantidad de clorofila *a* [Carstensen et al., 2007], y en la concentración de macronutrientes [Huppert et al., 2002]. Asimismo, se ha propuesto la inclusión de los coeficientes de absorción de las propiedades ópticas inherentes (IOP, del inglés Inherent Optical Properties) [Cui et al., 2013]. Los coeficientes de absorción y dispersión de diversos constituyentes del agua determinan las propiedades ópticas en el océano [Preisendorfer, 1961]. Estas propiedades físicas son muy importantes en el estudio del ciclo biogeoquímico, el cambio climático, la calidad del agua y la contaminación oceánica [Cui et al., 2013]. Algunos autores han analizado la variabilidad de estas propiedades en relación con el fitoplancton y su abundancia [Loisel et al., 2011, Mercado et al., 2006]. Sin embargo, hay pocos estudios debido a la complejidad del medio, así como a la baja capacidad de observación [Cui et al., 2013].

Las propiedades de absorción de luz del medio acuático se caracterizan en términos del coeficiente de absorción $a(\lambda)$, esencialmente toda la absorción de la luz que tiene lugar en las aguas naturales es atribuible a cuatro componentes del ecosistema acuático: el agua misma, la materia orgánica disuelta coloreada (CDOM, del inglés Coloured Dissolved Organic Matter), la biota fotosintética (fitoplancton) y las partículas inorgánicas [Kirk, 2011]. Así pues, $a(\lambda)$, puede definirse como:

$$a(\lambda) = a_w(\lambda) + a_{cdom}(\lambda) + a_p(\lambda) \qquad (1)$$

donde los subíndices *w, cdom y p* representan el agua, la CDOM y la materia particulada, respectivamente. Este material particulado consiste en fitoplancton (phy) y detrito (partículas no- algales) (*d*) [Morel, 2006], así:

$$a_p(\lambda) = a_{phy}(\lambda) + a_d(\lambda) \qquad (2)$$

Cada uno de los componentes presentes en el agua de mar exhibe un espectro típico de absorción de luz, lo que significa que absorben luz con una preferencia por ciertas longitudes de onda en el espectro visible (400 a 700 nm) o ultravioleta (250 a 400 nm) [Kirk, 2011]. Así, el agua ópticamente pura $a_w(\lambda)$ absorbe la luz con una preferencia por el rojo en el espectro electromagnético de 750 a 800 nm. El fitoplancton presenta un espectro de absorción $a_{phy}(\lambda)$ caracterizado por dos picos situados en el espectro de 440 y 675 nm, que están relacionados con la absorción por clorofila *a*. El detrito, $a_d(\lambda)$, absorbe con un aumento exponencial hacia longitudes de onda más cortas, y la CDOM, $a_{cdom}(\lambda)$, absorbe con la misma tendencia, con la absorción más significativa hacia el espectro ultravioleta entre 250 y 400 nm [Santamaría-del-Ángel et al. 2015]. En base a estos tres coeficientes de absorción, Santamaría-del-Ángel et al. [2015] propuso el uso del índice llamado de propiedades ópticas inherentes (IOP). En aguas ópticamente complejas, como las aguas costeras y las aguas interiores, las propiedades ópticas están determinadas por la combinación de estos componentes del agua en proporciones variables [Santamaría-del-Ángel et al., 2011]. Este índice es calculado a partir de $a_{cdom}(\lambda)$, $a_{phy}(\lambda)$ y $a_d(\lambda)$, utilizando la longitud de onda (λ) 443 nm. El objetivo del índice IOP es identificar los florecimientos fitoplanctónicos activos y distinguirlos de los florecimientos en decaimiento. Esta distinción es muy importante frente a la metodología de observación y recuendo por microscopía, ya que las técnicas de fijación, necesarias en el pre-tratamiento de las muestras de fitoplancton, no permiten esta distinción por recuentos microscópicos y, por lo tanto, pueden conducir a conlusiones erróneas [Santamaría-del-Ángel et al., 2015].

La adaptación del índice IOP a las metodologías de sensores remotos podría reducir el costo de análisis regulares, ya que podría ayudar a determinar qué muestras deben analizarse con métodos analíticos mejor orientados antes del cierre de playas, vedas en la recolección de productos acuícolas tales como moluscos u otras decisiones de gestión. El modelo de Propiedades Ópticas Inherentes Generalizado (GIOP), desarrollado a partir de datos satelitales de los sensores de la Administración Nacional de la Aeronáutica y del Espacio de Estdos Unidos (NASA), como son los sensores Espectrorradiómetros de Imágenes de Resolución Moderada (MODIS) y el Suite de Radiómetros de Imágenes Infrarrojas y Visible (VIIRS), proporcionan el algoritmo que devuelve el coeficientes de absorción y retrodispersión marina para los constituyentes de la columna de agua (CDOM, partículas algales y no algales) en m^{-1} [NASA, 2014]. Así el desarrollo de metodologías y enfoques comunes en redes internacionales afectadas por problemas transfronterizos es importante, por lo que métodos como el índice IOP satelital pueden contribuir de forma importante a la estandarización de procedimientos [Kudela et al., 2015].

Así, como primera fase, la investigación desarrollada en esta tesis doctoral propone el uso de las IOP en aguas ópticamente complejas para detectar el estado de florecimiento o no florecimiento de la comunidad fitoplanctónica, así como detectar si se trata de un florecimiento activo o en degradación. El objetivo es probar la efectividad del índice IOP *in situ* en eventos de florecimiento en diferentes áreas costeras con características distintivas. El área 1 está compuesta por tres áreas costeras en la Península de Yucatán: Dzilam de Bravo (Dzilam) en el estado de Yucatán, Holbox en el estado de Quintana Roo y la Bahía de Campeche en el estado de Campeche; el área 2 es el Alto Golfo de California (UGC) y el área 3, Bahía de Todos Santos (TSB), es una bahía semicerrada, adyacente al Océano Pacífico, dentro de la zona de surgencia de la península de Baja California (México).

En una segunda fase, se selecciona el área 1, península de Yucatán (México), como caso de estudio para adaptar la metodología propuesta *in situ* al uso de los productos de sensores remotos. En esta región, el turismo se basa en los recursos naturales de sol, arena y playa [Padilla, 2015]. La falta de infraestructura básica; las redes de drenaje y alcantarillado, y las plantas de tratamiento de aguas residuales no existen o son ineficientes; son la principal causa de los problemas de calidad del agua en los cuerpos costeros de agua receptores [Castillo-Pavón y Méndez-Ramírez, 2015]. En esta área se seleccionan cinco puntos de monitoreo basándose en importantes destinos turísticos, distribuidos a lo largo de la costa de la Península de Yucatán, de este a oeste: Cozumel, Cancún, Holbox, Progreso y Campeche. En esta fase el denominado índice IOP satelital se basa en una serie de datos distribuidos espcialmente, provenientes de imágenes del modelo GIOP a 4 km de resolución, que permiten tomar una media y una desviación estándar que representa el comportamiento normal de esa área en ese instante.

En la tercera fase de la tesis doctoral, se pretende adaptar la metodología de cálculo del índice IOP satelital para definir la línea base temporal de un punto o un pixel. El área de estudio seleccionada es el área 3, la Bahía de Todos Santos en Ensenada, Baja California, México. Se utilizan los datos diarios de catorce años del modelo GIOP del sensor Aqua MODIS a 1 km de resolución. Al saber el comportamiento promedio de un pixel es posible deducir si su comportamiento diario, está por arriba o por debajo de lo normal. Así se puede trazar de manera sistemática el comportamiento diario de un pixel, y poder saber si está en un comportamiento normal, en un comportamiento de pre alerta o si se encuentra en alerta. Así, el desarrollo del índice IOP puede permitir identificar el grado de anomalía en el que se encuentra cada pixel y poder señalarlo en base a un semáforo de alerta, dando la oportunidad de focalizar los esfuerzos en el monitoreo de florecimiento fitoplanctónicos activos.

El desarrollo de la investigación se basó en estas tres etapas que se corresponde con los tres capítulos en los que se estructura la tesis. (Tabla 1). En primer término se definió la metodología propuesta en base a datos de campo (capítulo primero), donde las Propiedades Ópticas Inherentes (IOP), específicamente los coeficientes de absorción de fitoplancton $\boldsymbol{a_{phy}}(\boldsymbol{\lambda})$, de CDOM $\boldsymbol{a_{cdom}}(\boldsymbol{\lambda})$ y de detrito $\boldsymbol{a_{d}}(\boldsymbol{\lambda})$**,** se utilizaron como base para la identificación de anomalías espaciales, que según nuestra propuesta representan etapas o niveles de los florecimientos fitoplanctónicos. En la segunda parte del trabajo (capítulo segundo) se trasladó la metodología hacia los datos satelitales,

donde los productos de coeficiente de absorción de fitoplancton ($\boldsymbol{a_{phy,GIOP}}$) y de detrito+CDOM ($\boldsymbol{a_{dCDOM,GIOP}}$) , del modelo de Propiedades Ópticas Inherentes Generalizado (GIOP), sustituyeron los coeficientes de absorción muestreados en campo, para realizar el índice GIOP se tomaron dos áreas (Golfo de México y Mar Caribe) que permitieron definir espacialmente la línea base para las aguas de la península de Yucatán. Finalmente, la tercera parte de la investigación (capítulo tercero) fue el cambio conceptual del índice GIOP, donde se pasó de una idea espacial a una temporal, es decir, se calculó el índice para cada pixel, permitiendo obtener las anomalías puntuales de los pixeles a partir de los valores históricos de ese mismo pixel.

Tabla 1 Relación de publicaciones científicas y capítulos de la presente memoria.

N° Apartado	Titulo	Autores	Revista	Indexación	Estado
3 Capítulo Primero	Identification of Phytoplankton Blooms under the Index of Inherent Optical Properties (IOP Index) in Optically Complex Waters https://doi.org/10.3390/w10020129	Aguilar-Maldonado, Santamaría-del-Ángel, González-Silvera, Cervantes-Rosas, López-Acuña, Gutiérrez-Magness,Cerdeira-Estrada, Sebastiá-Frasquet	Water (ISSN 2073-4441)	JCR Science Edition, Factor de Impacto en 2017 de 2.067	Publicado
4 Capítulo Segundo	Mapping Satellite Inherent Optical Properties Index in CoastalWaters of the Yucatán Peninsula (Mexico) https://doi.org/10.3390/su10061894	Aguilar-Maldonado, Santamaría-del-Ángel, González-Silvera, Cervantes-Rosas, Sebastiá-Frasquet	Sustainability (ISSN 2071-10509)	JCR Science Edition, Factor de Impacto en 2017 de 2.075	Publicado
5 Capítulo Tercero	Detection of phytoplankton temporal anomalies based on satellite Inherent Optical Properties: a tool for monitoring phytoplankton blooms	Aguilar-Maldonado, Santamaría-del-Ángel, González-Silvera, Sebastiá-Frasquet	Water Research (ISSN: 0043-1354)	JCR Science Edition, Factor de Impacto en 2017 de 7.051	Enviado

2. Objetivos

El objetivo principal de la investigación es crear un semáforo de alerta y de seguimiento de florecimientos fitoplanctónicos en base al índice de Propiedades Ópticas Inherentes.

1. Comprobar el uso de las Propiedades Ópticas Inherentes (IOP), específicamente el coeficiente de absorción de luz, como indicador de que una comunidad de fitoplancton ha pasado a una condición de florecimiento.

2. Mapear el Índice de Propiedades Ópticas Inherentes (IOP) utilizando productos de teledetección del modelo de Propiedades Ópticas Inherentes Generalizado (GIOP) a 4km de resolución espacial.

3. Definir la línea base de cada pixel a partir del modelo satelital de Propiedades Ópticas Inherentes Generalizado (GIOP) a 1 km de resolución espacial.

3. Capítulo Primero.

Identification of Phytoplankton Blooms under the Index of Inherent Optical Properties (IOP Index) in Optically Complex Waters

3.1 Abstract

Phytoplankton blooms are sporadic events in time and are isolated in space. This complex phenomenon is produced by a variety of both natural and anthropogenic causes. Early detection of this phenomenon, as well as the classification of a water body under conditions of bloom or non-bloom, remains an unresolved problem. This research proposes the use of Inherent Optical Properties (IOPs) in optically complex waters to detect the bloom or non-bloom state of the phytoplankton community. An IOP index is calculated from the absorption coefficients of the colored dissolved organic matter (CDOM), the phytoplankton (phy) and the detritus (d), using the wavelength (λ) 443 nm. The effectiveness of this index is tested in five bloom events in different places and with different characteristics from Mexican seas: 1. Dzilam (Caribbean Sea, Atlantic Ocean), a diatom bloom (*Rhizosolenia hebetata*); 2. Holbox (Caribbean Sea, Atlantic Ocean), a mixed bloom of dinoflagellates (*Scrippsiella* sp.) and diatoms (*Chaetoceros* sp.); 3. Campeche Bay in the Gulf of Mexico (Atlantic Ocean), a bloom of dinoflagellates (*Karenia brevis*); 4. Upper Gulf of California (UGC) (Pacific Ocean), a diatom bloom (*Coscinodiscus* and *Pseudo-nitzschia*) and 5. Todos Santos Bay, Ensenada (Pacific Ocean), a dinoflagellate bloom

(*Lingulodinium polyedrum*). The diversity of sites show that the IOP index is a suitable method to determine the phytoplankton bloom conditions.

Keywords: absorption coefficients; phytoplankton; detritus; CDOM; water quality; monitoring

3.2 Introduction

Phytoplankton blooms are sporadic events in time and are isolated in space [1]. These complex phenomena are produced by a variety of both natural and anthropogenic causes [2]. The availability oflight and nutrients is a key factor for their development [3]. This factor is illustrated during the spring summer period. At the beginning of this period, the seasonal increase in daily irradiation eliminates the light limitation, and the end of the thermal stratification provides a supply of nutrients thanks to the turbulent and convective mixing processes, which allows the phytoplankton to proliferate [4]. However, phytoplankton blooms are not only limited to this period.

Bloom is the rapid growth of one or more species leading to an increase in the species' biomass [5]. Different adjectives have been used to characterize the degree of negative impact of these blooms according to their characteristics and those of the causative species, such as toxic, noxious or harmful [6].

Identifying phytoplankton blooms has been the target of extensive research [7–10]. Some studies have focused on detecting changes in chlorophyll a fluorescence, changes in the composition of phytoplankton species

[9], or increases in nutrient levels [11]. Measurements of the intensity of blooms have also been of great interest, including research on continuous measurements of fluorescence and chlorophyll a [12], deviations in normal biomass variations [13], ratio of two in-situ optical measurements such as chlorophyll fluorescence (Chl F) and optical particulate backscattering (bbp) [14]. Remote sensing has also been used to measure the Maximum Chlorophyll Index (MCI) of the Medium Resolution Imaging Spectrometer (MERIS) sensor [15].

Defining under which conditions an increase in phytoplankton biomass can be considered a bloom is essential to avoid the arbitrary use of the term [4,7,16]. This research proposes the use of Inherent Optical Properties (IOPs), specifically the light absorption coefficient, as an indicator that a phytoplankton community has passed into a bloom condition. The absorption and dispersion coefficients of various water constituents determine the optical properties in the ocean [17]. These physical properties are very important in the study of the biogeochemical cycle, climate change, water quality and ocean pollution [18]. Some authors have analyzed the variability of these properties in relation to phytoplankton and their abundance [19,20]. However, there are few studies due to the complexity of the environment, as well as the low observation capacity [18].

The absorption coefficient $\boldsymbol{a}(\boldsymbol{\lambda})$ characterizes light absorption properties in the aquatic environment. Light absorption in natural waters is attributable essentially to four components: water, colored dissolved organic matter (CDOM), photosynthetic biota and inorganic particles [17]. Thus, *a* (*λ*) can be expressed as:

$$\boldsymbol{a}(\boldsymbol{\lambda}) = \boldsymbol{a_w}(\boldsymbol{\lambda}) + \boldsymbol{a_{cdom}}(\boldsymbol{\lambda}) + \boldsymbol{a_p}(\boldsymbol{\lambda}) \tag{1}$$

Where the subscripts *w*, *cdom* and *p* represent water, CDOM and particulate matter, respectively. This particulate material consists of phytoplankton ($\boldsymbol{phy}$) and detritus (non-algal particles) (***d***) [18]. Thus $\boldsymbol{a_p}(\boldsymbol{\lambda})$, can be expressed as:

$$\boldsymbol{a_p}(\boldsymbol{\lambda}) = \boldsymbol{a_{phy}}(\boldsymbol{\lambda}) + \boldsymbol{a_d}(\boldsymbol{\lambda}) \tag{2}$$

Seawater components present a typical spectrum of light absorption, which means that they absorb light with a preference for specific wavelengths in the visible (400 to 700 nm) or ultraviolet (250 to 400 nm) region [21]. Optically pure water $a_w(\lambda)$ absorbs light with a preference for red in the electromagnetic spectrum of 750 to 800 nm. Phytoplankton has an absorption spectrum $a_{phy}(\lambda)$ characterized by two peaks around wavelengths 440 and 675 nm, which are related to chlorophyll *a* absorption. Detritus $a_d(\lambda)$ and CDOM $a_{cdom}(\lambda)$ absorb with an exponential increase towards shorter wavelengths, and CDOM has the most significant absorption towards the UV spectrum between 250 and 400 nm [23]. In optically complex waters, such as coastal and inland waters, the optical properties are determined by the combination of these water components in varying proportions [24]. The authors of [23] developed the IOP index with the objective of identifying phytoplankton blooms. This index is calculated from $a_{cdom}(\lambda)$, $a_{phy}(\lambda)$ and $a_d(\lambda)$, using the wavelength (λ) 443 nm.

This research proposes the use of Inherent Optical Properties (IOPs) in optically complex waters to detect the bloom or non-bloom state of the phytoplankton community, as well as detect whether it is an active or a decaying bloom. The objective is to test the effectiveness of the IOP index in bloom events in different coastal areas with distinctive characteristics.

3.3 Materials and Methods

3.3.1 Study Area

The study areas are well-known coastal areas of Mexico with distinctive characteristics where bloom events have been observed recurrently (Figure 1). These areas are as follows:

Area 1 is composed of three coastal areas in the Yucatán Peninsula: Dzilam de Bravo (Dzilam for short) in the Yucatan state (Figure 1a), Holbox in the Quintana Roo state (Figure 1b), and Campeche Bay in the Campeche state (Figure 1c). This Peninsula is a karstic region, characterized by minimal soil cover and rapid infiltration of rainwater, with the consequent high vulnerability of the aquifer to pollution [25,26]. The rainy season occurs from June through December with minimal rainfall during the rest of the year. According to [27], the Yucatán coastal aquifer is a triple porosity system, where the flow of groundwater takes place mainly through interconnected cave systems and fractures, and drains inland catchments primarily through coastal springs. In recent years, intense coastal development has taken place within the Caribbean, due to tourism, which increases the risk of aquifer pollution. This development is particularly fast on the eastern coast of the Yucatan Peninsula (Quintana Roo state). The unconfined Yucatán aquifer has submarine groundwater discharges (SGDs) threatening coastal ecosystems [26,28]. SGDs have been linked to eutrophication and harmful algal blooms [28]. Both Yucatán and Quintana Roo state coastal waters are influenced by waters of the Caribbean Sea and the Gulf of Mexico [29]. Campeche state coastal water is affected by the current system of Yucatan/Lazo/Florida [30]. This region has a predominantly cyclonic circulation [31], caused by the wind effort [32], and by an upwelling on the north coast of the Yucatan Peninsula [33].

Area 2 is the Upper Gulf of California (UGC). The Gulf of California is a semi-enclosed sea in the Eastern Pacific. The UGC is located in the Northern Gulf of California, where the Sonora and Baja California state coasts intersect at a 60° angle [34]. It is considered as one of the most biologically productive marine regions [35,36], with peak chlorophyll a concentrations of 18.2 mg m^{-3} and averages of 1.8 mg m^{-3} between 1997 and 2007 in coastal waters near the delta [37]. A complex mix of factors increases productivity. Among those are coastal upwelling, wind-driven mixing, extreme tidal mixing and turbulence, thermohaline circulation, coastal-trapped waves, regular sediment resuspension, and, to a lesser extent, agricultural runoff, released nutrients from erosion of ancient Colorado River Delta sediments and groundwater discharges [35,38,39]. After the construction of the Hoover and Glen Canyon dams in the USA in 1935 and 1964, respectively, the Colorado River only discharges variable and insignificant surface water-flows occasionally into the Gulf of California [38].

Area 3, Todos Santos Bay (TSB), is a semi-enclosed bay, adjacent to the Pacific Ocean, within the upwelling zone of the Baja California peninsula (Mexico). This area is influenced by the California Current System (CCS), which produces coastal upwelling along the coast of the Baja California peninsula. A marked seasonality is caused by the prevailing winds from the Northwest, which tend to be more intense during the spring and summer months [40–42]. Two water masses integrate the CCS, the California Current (CC), a year-round equatorward surface flow, which transports SubarcticWater (SAW), characterized by low salinity, and the California Undercurrent (CU), a poleward subsurface (100–400 m) flow that transports Equatorial Subsurface Water (ESsW), characterized by relatively high salinity, high nutrient concentration, and low dissolved oxygen content, according to a previous description [43]. The SAW is particularly important during winter and spring, while ESsW appears at the end of summer and autumn [44]. In addition to the described seasonal variability, the El Niño-Southern Oscillation (ENSO) induces oceanographic changes in the region of Baja California at an interannual scale [44]. Together, these factors control primary productivity, which is characteristically high [40,45].

Dinoflagellate algal bloom (DAB) events in this area have increased considerably in extension and frequency over the past two decades [46].

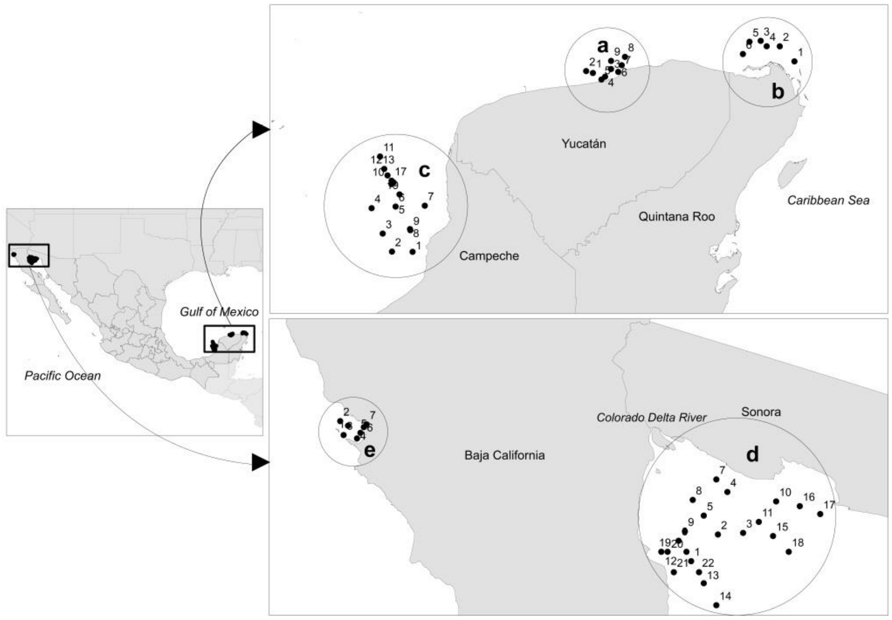

Figure 1. Sampling stations. (**a**) Dzilam de Bravo (Yucatan); (**b**) Holbox (Quintana Roo); (**c**) Campeche Bay (Campeche); (**d**) Upper Gulf of California (Baja California and Sonora) and (**e**) Todos Santos Bay (Baja California).

3.3.2 Collection of Samples

Water samples were collected in Mexico coastal waters at the stations shown in Figure 1. Four field campaigns were conducted for sampling: two in 2011 and two in 2017, during reported bloom events. Dzilam (Yucatán) and Holbox (Quintana Roo) samples were collected between 27 and 30 of August 2011 (nine and six samples, respectively). All the Dzilam and Holbox stations were sampled at the surface (1.5 m); the selection of monitoring sites was influenced by fishermen reports on fish mortality and patches of discolored water. Campeche Bay (Campeche) samples were collected between 22 and 24 of September 2011 (19 samples). Campeche Bay was also sampled at the surface (1.5 m), except for stations number 13 and 16, which were sampled at 15 m (according to the chlorophyll máximum fluorescence depth). The campaign was conducted in response to a phytoplankton bloom reported by various local, state and federal public health institutions in Campeche [47]. The Todos Santos Bay (TSB) in Ensenada (Baja California) was sampled on 2 June 2017 (seven samples) during the second week of a bloom event that lasted three weeks. This event was characterized by bioluminescence. TSB was also sampled at the surface (0.5 m). Stations 5–7 were located on the reddish patch that distinguished itself from the rest of the bay water.

These data were collected in small vessels where the samples were taken manually and stored in dark Nalgene bottles of high-density polyethylene (HDPE) until processing in the laboratory. For CDOM analysis, samples were collected in amber glass bottles and refrigerated until laboratory processing. The sampling depth was at the chlorophyll maximum fluorescence (0.5 to 15 m). The chlorophyll maximum was measured with a Phyto-PAM (HeinzWalzGmbH, Effeltrich, Germany) fluorimeter.

Sampling of the Upper Gulf of California (UGC) was carried out from 23 February to 3 March 2017,on board the research vessel “Tecolutla” of the

Mexican Navy and during the oceanographic cruise “Vaquita Marina 2017” (22 samples). Samples were taken with Niskin bottles attached to a rosette and were immediately processed in the vessel’s laboratory. Sampling depth was at the chlorophyll maximum fluorescence (10 to 40 m). The chlorophyll maximum was measured with an ECO FLNTU fluorimeter coupled to a CTD SB 19 Plus. During the oceanographic cruise, colored patches were detected in the water.

In each study area, the samples were collected inside and outside the patches with bloom evidence to capture the variability that exists in a parcel of water and to better define the baseline or mean of each campaign.

3.3.3 Absorption Coefficients Determination

Water for CDOM analysis was filtered using a 0.2 _m pore membrane filter (Nuclepore™, Merck KGaA, Darmstadt, Germany) and processed according to the methodology of [48]. The CDOM absorption coefficient, $a_{cdom}(\lambda)$, was measured in the wavelength range of 250 to 800 nm in a 10 cm long quartz cuvette using Milli-Q water as reference.

The particulate matter absorption coefficient was determined using the methodology of [48]. A volume of seawater of 0.5 to 2 L, depending on the particle load, was filtered from water stored in Nalgene bottles, with Whatman GF/F glass fiber filters 25 mm in diameter and 0.7 _m in pore size. The optical density of particulate material in the filter was measured in the wavelength range of 400 to 800 nm. Then, filters were immersed in methanol to wash out pigments and to obtain the detritus optical density for the same wavelength interval. The light absorption coefficients $a_p(\lambda)$ and $a_d(\lambda)$ were calculated following [48], and $a_{phy}(\lambda)$ was calculated by subtracting $a_d(\lambda)$ from $a_p(\lambda)$.

The optical densities of 2011 samples were read with a Perkin-Elmer Lambda 18 (PerkinElmer, Waltham, MA, USA) spectrophotometer, and the 2017 samples were read with a Cary 100 UV-Visible spectrophotometer (Agilent, Santa Clara, CA, USA).

A non-parametric one-way analysis of variance (Kruskal–Wallis) was performed to statistically assess differences in the absorption coefficients. The absorption coefficients $a_{phy}(\lambda)$, $a_d(\lambda)$ and $a_{cdom}(\lambda)$ for each sampling area were compared. Also, sampling stations under active bloom conditions were grouped according to similar phytoplankton absorption coefficients (430–550 nm), as determined by cluster analysis. Clustering dendrograms were generated using Minitab v.16. Correlation distances were calculated, and sampling areas clustered according to the average method.

3.3.4. IOP Index Determination

The IOP index was determined according to [23] following the next steps. First, the absorption coefficients $(a_{cdom}(443), a_d(443), a_{phy}(443))$ were standardized. Then, principal component analysis (PCA) was performed to reduce the number of original variables. The first principal component was selected because it accounts for the largest possible variance. This selection was based on the eigenvalues [49]. The coefficients of this principal component were named as $b_{1,1}$, $b_{1,2}$and $b_{1,3}$. Finally, the IOP index was calculated based on this first standardized empirical orthogonal function ($SEOF_1$) [24] according to Equation (3).

$$\boldsymbol{IOP_{index}} = -\mathbf{1}\left[(\boldsymbol{b_{1,1}} \times \boldsymbol{Za_{phy,443}}) + (\boldsymbol{b_{1,2}} \times \boldsymbol{Za_{CDOM,443}}) + (\boldsymbol{b_{1,3}} \times \boldsymbol{Za_{d,443}})\right] \quad (3)$$

The coefficients $b_{1,1}$, $b_{1,2}$ and $b_{1,3}$ are the first eigenvectors resulting from the $SEOF_1$, while ($Za_{phy,443}$, $Za_{CDOM,443}$ and $Za_{d,443}$) are the values derived from the Pearson correlation matrix between the absorption coefficients's standardized anomalies. Then, samples were classified as in bloom or non-bloom using factorial analysis. To describe the stages of a phytoplankton bloom, the values of the IOP index were interpreted as follows [23]: (1) values in the interval (−1, 1) show the average value of the study area and represent non-bloom conditions; (2) values in the interval (1, 2) are above the average and represent decaying bloom conditions, and (3) values higher than 2 are anomalous and indicate active bloom conditions.

3.3.5 Phytoplankton Community Characterization

The blue/red ratio ($^{\mathrm{B}}/_{\mathrm{R}}$) is an index that allows us to characterize the dominant phytoplankton size in a water sample [24, 50–55]. It is calculated as expressed in Equation (4):

$$^{\mathrm{B}}/_{\mathrm{R}} = \frac{a_{phy\,(440)}}{a_{phy\,(675)}} \quad (4)$$

If the $^{B}/_{R}$ is >3.0, dominance of picophytoplankton (<2 μm) is implied. If the ratio is <2.5, dominance of microphytoplankton (>20 μm) is implied. Ratios between 2.5 and 3.0 indicate that the structure of the community in terms of size is dominated by nanophytoplankton.

Representative samples of each sampling event were analyzed by microscopy to identify the main blooming species and/or genus. Samples were preserved in 125 mL bottles in a neutral lugol solution with a sodium acetate base in a 1:100 ratio. The samples were stored under dark and cold conditions until their identification. The Dzilam, Holbox, and Campeche samples were identified by the Florida Fish and Wildlife Conservation Commission (FWC). Phytoplankton identification was performed using an inverted Olympus IX71 microscope following a modified method of Utermöhl [56]. In the case of the UGC and TSB samples, the same method was performed using phase contrast microscopy with a Bausch and Lomb microscope. The authors [57–60] were used as taxonomic references.

For Dzilam, Holbox and Campeche, the chlorophyll *a* concentration was determined fluorometrically on methanol extracts following the method of [61], using a Turner Designs 10-AU field fluorimeter.

3.4 Results and Discussion

The IOP index was calculated from the absorption coefficients for each sampling area and sampling point. IOP index results are represented graphically in Figure 2. In Dzilam, sampling points 4 and 6 had a value in the interval (1, 2), meaning that they were above the sampling area average and in decaying bloom conditions. However, only sampling point 5 was above two and under active bloom conditions. In Figure 3, the contribution of each absorption coefficient $a_{phy}(\lambda)$, $a_d(\lambda)$ and $a_{cdom}(\lambda)$ to $a(443)$by sampling area is represented. The inner circumference shows the average contribution of each absorption coefficient to $a(443)$ for each sampling campaign. The outer circumference represents the average value of sampling points classified as active bloom according to the IOP index. In Figure 3a, Dzilam, CDOM was the major contributor to $a(443)$. $a_{cdom}(\lambda)$ contributed with 48% to total absorption, followed by $a_{phy}(\lambda)$ with 41% and $a_d(\lambda)$ with 11% (Figure 3a). At sampling point 5, we observed that the contribution of each absorption coefficient to $a(443)$ was similar to the sampling campaign average. In Holbox, only sampling point 6 was above an IOP index value of two (Figure 2), and thus under active bloom conditions. Phytoplankton was the major contributor to $a(443)$. $a_{phy}(\lambda)$, representing 59% of absorption, followed by $a_{cdom}(\lambda)$ with 27% and ad(443) with 14% (Figure 3b). At sampling point 6, we observed a higher contribution of phytoplankton to $a(443)$ than the average value of the sampling campaign ($a_{phy}(\lambda)$ of 67%). The lower average contribution of phytoplankton when considering all sampling points was related to a higher CDOM contribution under non-bloom conditions. In Campeche Bay, sampling points 12, 14, 15 and 16 were under active bloom conditions (Figure 2). Sampling point 16 showed the highest anomaly; this sample was collected at 15 m depth. In Figure 3c, the dominant absorption component was $a_{cdom}(\lambda)$ with 50%, as in Dzilam, followed by $a_{phy}(\lambda)$ with 41% of $a(443)$, and a minor contribution of $a_d(\lambda)$ (9%). At sampling point 16 (the one that is represented in the outer circumference, Figure 3c), we observed a higher contribution of phytoplankton. This was due to a higher CDOM contribution under non-bloom conditions. In the Upper Gulf of California (UGC), sampling points 8, 19 and 22 were in decaying bloom conditions (IOP index value higher than one and lower than two), while sampling station 20 was under active bloom conditions according to the IOP index (Figure 2). In Figure 3d, we observed that the highest contribution was from $a_{phy}(\lambda)$, with 43%, followed by $a_d(\lambda)$ with 35% of $a(443)$, and $a_{cdom}(\lambda)$ with 22% (Figure 3d). As in Holbox and Campeche Bay, the contribution of phytoplankton to $a(443)$ was higher than the average in the active bloom stations ($a_{phy}(\lambda)$ of 73% for sampling point 20). In Todos Santos Bay, sampling point 6 was under decaying bloom conditions, while sampling point 7 was under active bloom conditions. In Todos Santos Bay (TSB) (Figure 3e), as in Holbox, $a_{phy}(\lambda)$ represented the highest absorption percentage (77%). However, in TSB the contribution of $a_{cdom}(\lambda)$ and $a_d(\lambda)$ was characteristically low (17% and 6%, respectively). As in Holbox, Campeche Bay and UGC, we noticed a higher contribution of phytoplankton to $a(443)$ in the active bloom station ($a_{phy}(\lambda)$of 93% for sampling point 7).The $a_{cdom}(\lambda)$ and $a_d(\lambda)$ contribution was even lower than the average.

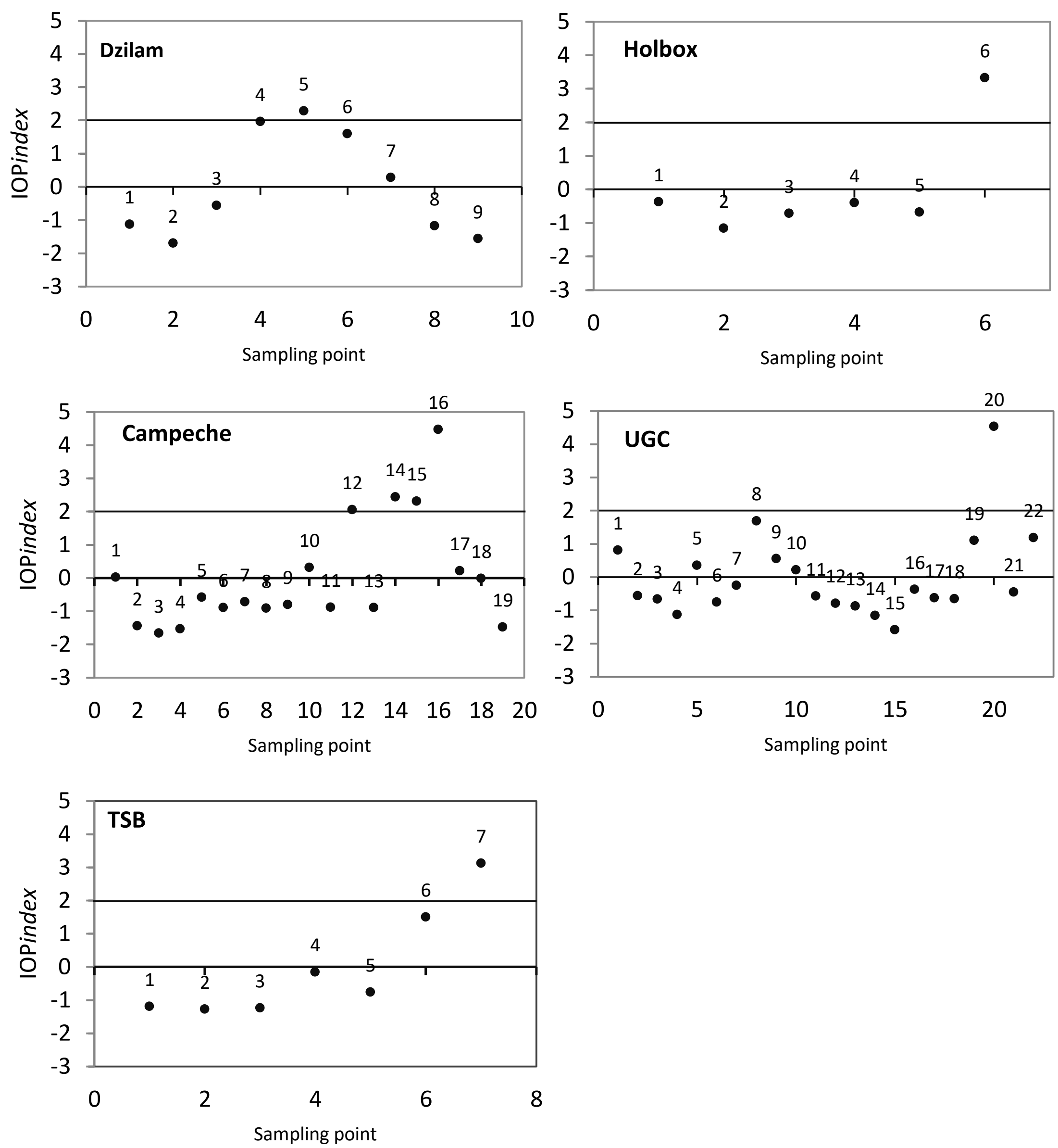

Figure 2. IOP index results for each sampling campaign and sampling point. From top to bottom and from left to right: Dzilam, Holbox, Campeche Bay, Upper Gulf of California (UGC) and Todos Santos Bay (TSB). Points located above the horizontal line, which indicates an IOP index value of two, are those under active bloom conditions.

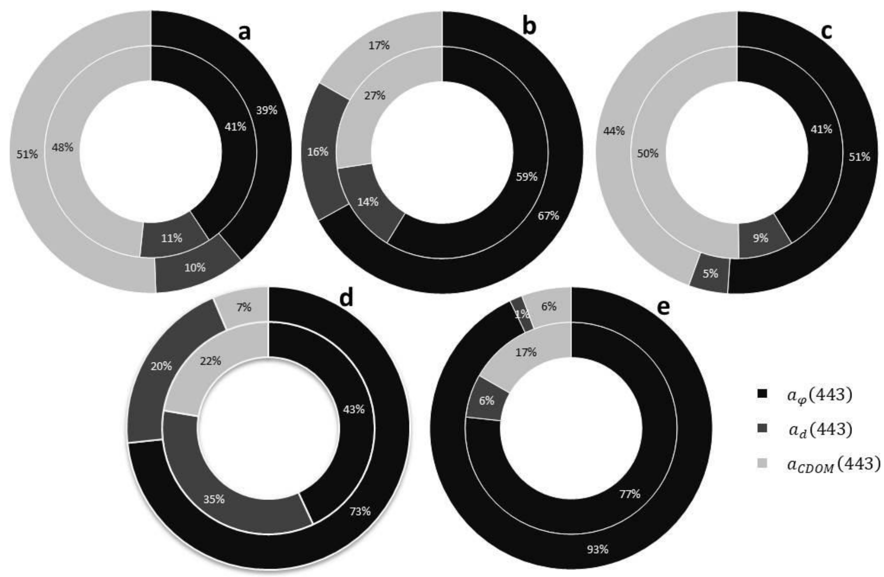

Figure 3. Contribution of each absorption coefficient ($a_{phy(\varphi)}(\lambda)$), $a_d(\lambda)$ and $a_{cdom}(\lambda)$) to $a(443)$ for each sampling area. The inner circumference shows the average contribution of each absorption coefficient to a(443) for each sampling campaign. The outer circumference represents the average value of sampling points classified as active bloom according to the IOP index. (**a**) Dzilam de Bravo; (**b**) Holbox; (**c**) Campeche Bay; (**d**) Upper Gulf of California; (**e**) Todos Santos Bay.

In Figure 4, the absorption spectrum of phytoplankton, detritus and CDOM of all the stations in bloom is compared. In the case of Campeche, the station in bloom with the greatest anomaly is represented. The phytoplankton absorption coefficient, $a_{phy}(\lambda)$, was significantly higher in TSB than in other sampling areas (p < 0.05 for a_{phy}(443)). No significant differences were observed between Dzilam and Campeche Bay (p > 0.05 for a_{phy}(443). The lowest $a_{phy}(\lambda)$ values were observed in the UGC. The detritus absorption coefficient, $a_d(\lambda)$, was significantly higher in the UGC than in all the other studied areas (p < 0.05 for $a_d(443)$). No significant differences were observed between the Yucatan Peninsula areas (Dzilam, Holbox and Campeche) or with TSB (p > 0.05 for $a_d(443)$). The CDOM absorption coefficient, $a_{cdom}(\lambda)$, was significantly higher in Dzilam and Campeche Bay than in other areas (p < 0.05 for $a_d(443)$).

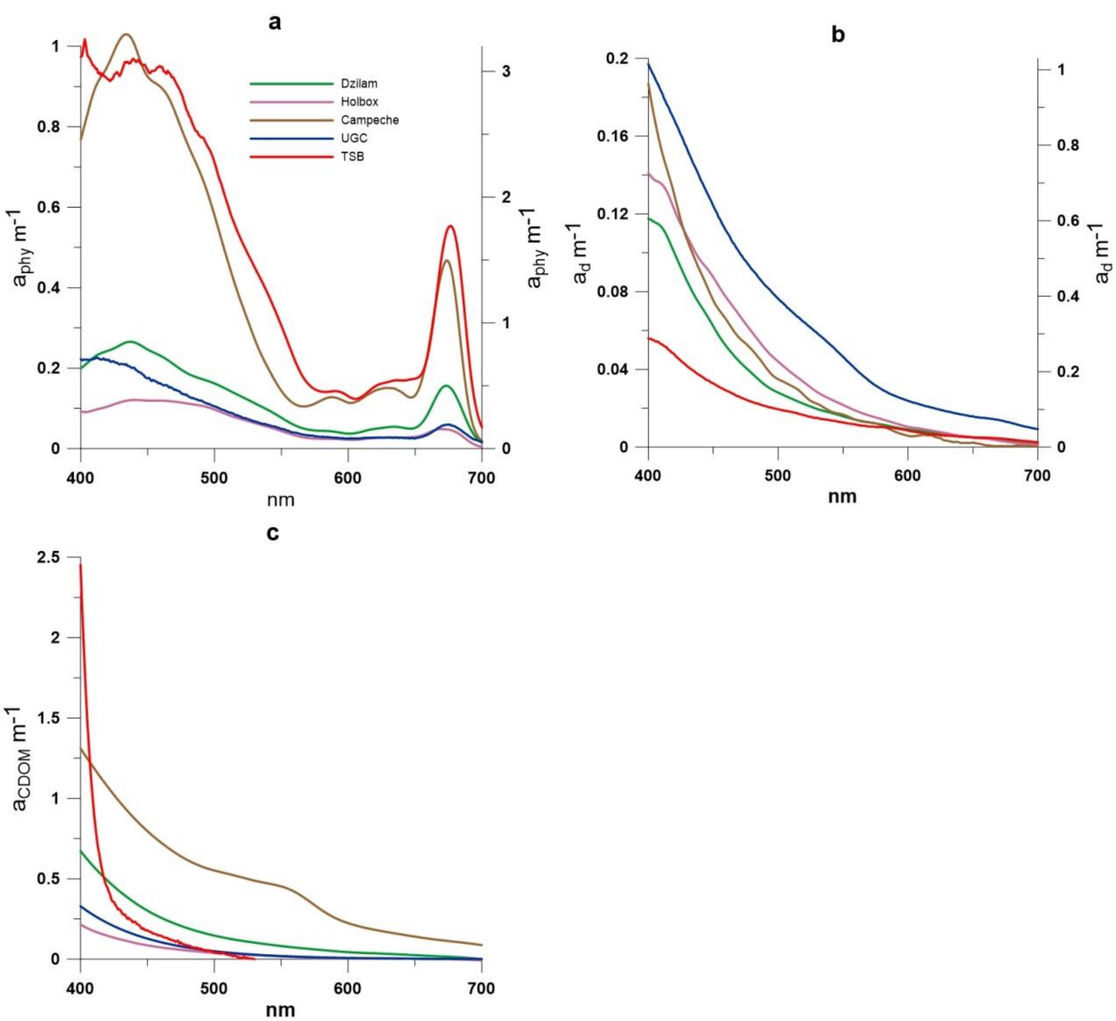

Figure 4. Absorption coefficients ($a(\lambda)$): (**a**) phytoplankton, (TSB, shown with an independent axis of greater absorption, is the one on the right), (**b**) detritus, (UGC, shown with an independent axis of greater absorption, is the one on the right) and (**c**) colored dissolved organic matter (CDOM) of sampling points under active bloom for each sampling campaign (Dzilam, Holbox, Campeche Bay, Upper Gulf of California (UGC) and Todos Santos Bay (TSB)).

In Figure 5, the ternary diagram shows the contribution to absorption of each seawater component (phytoplankton, detritus and colored dissolved organic matter) for all the sampling points. This graphical representation allowed us to compare the different study areas. In general terms, most areas have a stronger contribution from phytoplankton $(a_{phy}(443))$ and CDOM $(a_{cdom}(443))$ with the exception of UGC where some stations had a stronger contribution from detritus $(a_d(443))$. However, this high detritus contribution was much more important near the Colorado River Delta and decreased southward (Figure 5a).

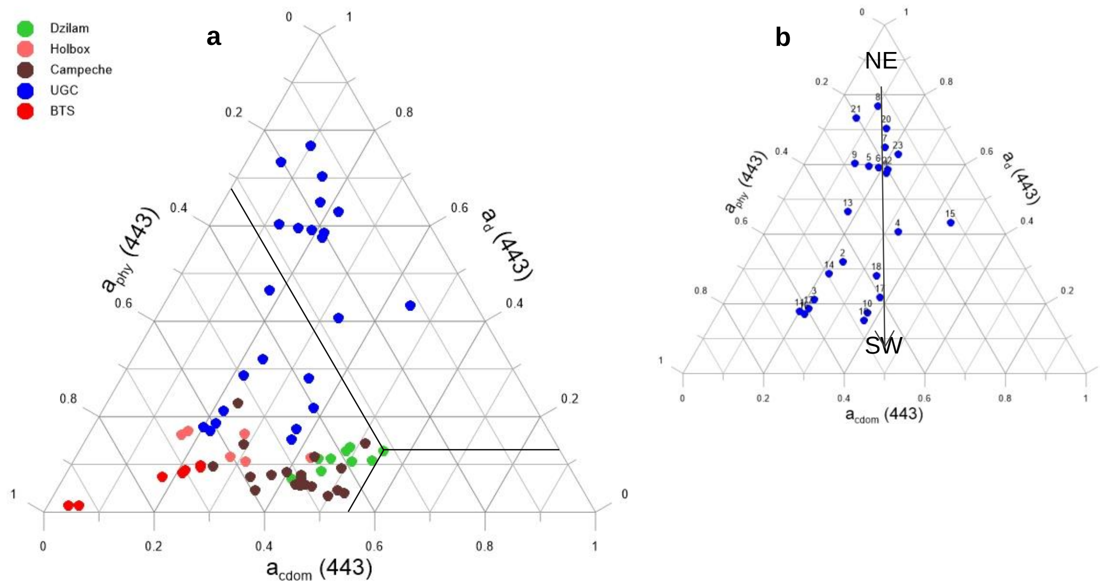

Figure 5. **(a)** Triangular diagram used to classify sampling points according to the contribution to $a(443)$ of each component: phytoplankton ($a_{phy}(443)$), colored dissolved organic matter ($a_{cdom}(443)$) and detritus ($a_d(443)$). **(b)** The UGC sampling points (1–23) are shown. The vertical arrow indicates the distribution of sampling points from northeast to southwest according to the inherent optical properties.

In order to characterize the phytoplankton community, the blue/red ratio (B/R) is shown in Table 1. As previously mentioned B/R values higher than 3 reveal a community dominated by picophytoplankton; B/R values lower than 2.5 reveal microphytoplankton dominance; and B/R values between 2.5 and 3.0 indicate that the size structure is dominated by pico/nano-phytoplankton.

In Dzilam, microphytoplankton dominated in the active bloom sampling point 5, where phytoplankton abundance exceeded 1 million cells L^{-1} (B/R =

1.71) (Table 2). According to the microscope taxonomic analysis, the dominant species was the diatom *Rhizosolenia hebetata*.

In Holbox, the B/R ratio under active bloom sample 6 was 2.57 (Table 2), which indicated a mixed picophytoplanton and nanophytoplankton community, where phytoplankton abundance almost reached 1.5 million cells L^{-1}. This was corroborated by microscope taxonomic analysis that identified the dinoflagellate *Scrippsiella* sp., and the diatoms *Chaetoceros* sp. and *Rhizosolenia hebetata*.

In Campeche Bay, B/R was lower than 2.5 in all active bloom condition points (Table 1), so microphytoplankton was dominant, and phytoplankton abundance exceeded 1 million cells L^{-1}. The dinoflagellate *Karenia brevis* was identified by microscopy as the dominant species.

In the UGC, B/R was below 2.5 in nearly all the sampling stations (Table 2). However, in sampling 15, B/R was 2.59, indicating a community dominated by the pico/nano-phytoplankton, where phytoplankton abundance just exceeded 4 thousand cells L^{-1}. The diatoms *Coscinodiscus* sp. and *Pseudo-nitzschia* sp. were identified by microscopy.

In Todos Santos Bay, B/R was below 2.5 at sampling point 7 (active bloom conditions) (Table 2), thus indicating microphytoplankton dominance, where phytoplankton abundance exceeded 40 thousand cells L^{-1}. The most abundant species in this station was the dinoflagellate *Lingulodinium polyedrum*.

In Figure 6, sampling stations under active bloom conditions are grouped according to similar phytoplankton absorption coefficients (wavelength ranging from 430 to 550 nm). The dendogram is the result of the cluster analysis. Sampling stations are named according to the study área that they represent. Dzilam, Holbox and UGC are grouped into one cluster; these sampling stations are characterized by high diatom abundance. Dzilam and Holbox share the same species (*Rhizosolenia hebetata*). Campeche and TSB are grouped into another cluster; these stations are characterized by dinoflagellates species. Thus, stations with similar species composition exhibit similar absorption spectra.

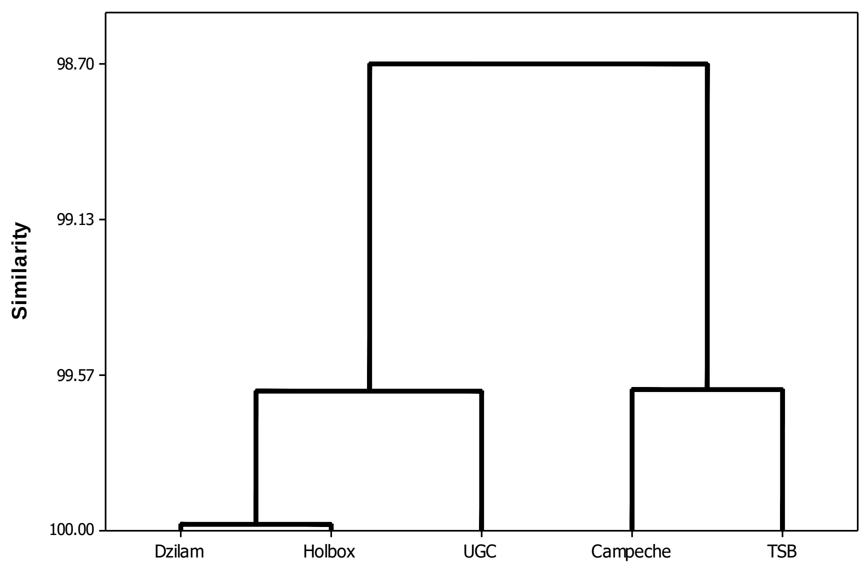

Figure 6. Dendogram. Sampling points under active bloom conditions, for each study area, clustered according to the phytoplankton absorption coefficient. Axis Y represent the similarity value according to cluster analysis.

Table 2. Specific absorption coefficients of phytoplankton (a_{phy}) at 440 nm and 675 nm (m^{-1}), and blue/red ratio (B/R) ($a_{phy}(440)/a_{phy}(675)$) based on the samples collected in the five campaigns.

Campaign	Sta.	a_{phy} (440 nm)	a_{phy} (675 nm)	Ratio B/R	Campaign	Sta.	a_{phy} (440 nm)	a_{phy} (675 nm)	Ratio B/R
Dzilam	1	0.110	0.038	2.86	UGC	1	0.039	0.078	1.99
	2	0.091	0.032	2.83		2	0.035	0.084	2.40
	3	0.167	0.061	2.75		3	0.039	0.095	2.43
	4	0.371	0.229	1.62		4	0.017	0.042	2.47
	5	0.264	0.155	1.71		5	0.041	0.085	2.07
	6	0.179	0.064	2.80		6	0.024	0.054	2.27
	7	0.170	0.072	2.36		7	0.026	0.055	2.09
	8	0.131	0.035	3.79		8	0.036	0.084	2.35
	9	0.131	0.028	4.76		9	0.048	0.105	2.16
Holbox	1	0.101	0.030	3.36		10	0.038	0.093	2.43
	2	0.076	0.023	3.37		11	0.045	0.105	2.31
	3	0.118	0.038	3.08		12	0.043	0.093	2.18
	4	0.072	0.024	3.06		13	0.031	0.073	2.33
	5	0.094	0.028	3.34		14	0.032	0.073	2.28
	6	0.387	0.151	2.57		15	0.003	0.007	2.59
Campeche	1	0.067	0.016	4.28		16	0.029	0.066	2.24
	2	0.034	0.006	5.33		17	0.032	0.071	2.21
	3	0.036	0.006	6.47		18	0.028	0.066	2.35
	4	0.032	0.006	5.24		19	0.032	0.073	2.27
	5	0.136	0.054	2.53		20	0.020	0.072	3.54
	6	0.111	0.044	2.51		21	0.059	0.201	3.39
	7	0.129	0.027	4.80		22	0.021	0.053	2.57
	8	0.132	0.028	4.77		23	0.026	0.067	2.55
	9	0.114	0.030	3.83	TSB	1	0.144	0.053	2.70
	10	0.295	0.154	1.91		2	0.139	0.047	2.96
	11	0.135	0.067	2.02		3	0.172	0.061	2.82
	12	0.685	0.338	2.03		4	0.365	0.150	2.43
	13	0.127	0.052	2.43		5	0.219	0.085	2.58
	14	0.590	0.287	2.06		6	3.077	1.773	1.74
	15	0.543	0.251	2.17		7	3.617	1.815	1.99
	16	1.006	0.464	2.17					
	17	0.370	0.172	2.16					
	18	0.243	0.114	2.13					
	19	0.065	0.021	3.09					

Dzilam (Yucatan), Holbox (Quintana Roo), and Campeche Bay (Campeche) (Figure 1a–c) are located in the karstic Yucatan Peninsula [55]. Rapid rainwater infiltration into the groundwater system and nearly no surface runoff characterize this region [25,29]. Due to its hydrological characteristics, the lowest absorption coefficient is that of detritus ($a_d(443)$ is 11%, 14% and 9%, respectively, in each area) (Figure 4). There is no relevant detritus source and no river runoff in this area (the nearest one is located in southern Campeche, far from the sampling area located in north Campeche). The climate of the region is characterized by three seasons associated with rainfall patterns: the dry season (March to May), the rainy season (June to October) and the northern wind season [62. In this region, submarine groundwater discharges (SGDs) play a significant role in driving the nutrient stoichiometry (N:Si:P ratio) in receiving waters, which is a key factor for phytoplankton assemblages. SGDs are an important source of nitrogen, particularly $\mathrm{NO_3^-}$; during the wet season (June to October), the high N:P ratio in SGDs can drive phosphorus limitation in the nearshore environment [27]. SGDs are also rich in silica, which can lead to diatom growth. Several studies have concurred that low salinity groundwater is an important source of nutrients in the Yucatan, specifically $\mathrm{NO_3^-}$ and silica, and have linked SGDs to harmful algal blooms [27]. According to [63], the HAB events in the state of Yucatan have been reported almost every year since 2001, covering an approximate area of 6000 km^2.

Our sampling was developed during the large-scale pelagic bloom event of August–December 2011. This event started in Dzilam and tended to move westward along the northern Yucatan coast [64]. In Dzilam, the dominance of the diatom *Rhizosolenia hebetata* can be explained by the input of silica from nearby springs (cenotes). The authors of [64] observed maximum chlorophyll *a* concentrations on 8 and 30 August. Our sampling was performed on 27 August. Therefore, the degradation of phytoplankton cells from the previous peak may explain the high contribution of the CDOM absorption coefficient (48% on average). The sampling point identified as being under active bloom conditions according to the IOP index had significantly higher chlorophyll *a* levels, 12.5 mg m^{-3}, which indicates non-bloom conditions, i.e., 3.1 mg m^{-3} on average.

In Holbox, the diatoms *Chaetoceros* sp. and *Rhizosolenia hebetata* were also dominant, but dinoflagellates of *Scrippsiella* sp. were also abundant. Both *Chaetoceros* sp. and *Scrippsiella* sp. were also observed in Dzilam during this HAB event according to [64]. The silica needed for this sustained diatom bloom may have been supplied by the characteristic springs (cenotes) of the Quintana Roo state [65]. The sample identified as under active bloom conditions according to the IOP index had significantly higher chlorophyll *a* levels (12.5 mg m^{-3}) than samples in non-bloom conditions (around 2.2 mg m^{-3} on average).

In Campeche Bay, the blooming species was identified as the dinoflagellate *Karenia brevis*. *Karenia brevis* blooms have been observed in all Mexican states (except Quintana Roo) [65]. Again, in this sampling campaign, the sampling point under active bloom conditions according to the IOP index had significantly higher chlorophyll *a* levels (33.2 mg m^{-3}) than sampling points in non-bloom conditions (7.0 mg m^{-3} on average). The CDOM absorption coefficient $a_{cdom}(443)$, was as high as in Dzilam (higher than in all the other study areas) (Figure 3). Our sampling was performed on 22 September 2011. Therefore, the high CDOM values could be explained by the degradation of accumulated phytoplankton cells during August and September. This region is influenced by the current system of Yucatan/Lazo/Florida [30]. It is important to note that even under very high CDOM values, the IOP index was able to distinguish an active phytoplankton bloom.

The Upper Gulf of California (UGC) and Colorado River Delta (CRD) area is a region of sediment re-suspension characterized by high detritus levels, low light extinction coefficient values (−0.05 m^{-1}) and high sedimentary loads (maximum values of 8 g/L) [34,39]. Therefore, we expected the highest detritus absorption coefficient ($a_d(\lambda)$) to be observed. It is remarkable that, also under very high detritus levels, the IOP index was able to distinguish an active phytoplankton bloom. Both genera found in the UGC, *Coscinodiscus* sp. and *Pseudo-nitzschia* sp., are indicators of marine conditions rich in nutrients or upwelling [66–68]. *Pseudo-nitzschia* abundances from 1 to 34 × 10^3 cells L^{-1} have been considered as in bloom conditions [69].

In Todos Santos Bay (TSB), the most abundant species during our study was the dinoflagellate *Lingulodinium polyedrum*. The authors of [46] have reported an increase in dinoflagellate algal blooms (DABs), with *Lingulodinium polyedrum* as the dominant species, over the past few years in coastal areas off Baja California. Our sampling took place on 2 June 2017, which is late spring, when *L. polyedrum* blooms usually occur in this area [46]. These blooms have been related to increases in irradiance, daylight hours, temperatures between 17 and 23 °C, stratification of the water column and formation of a seasonal surface thermocline [70]. They are favoured by the convergence of surface currents and winds, which induce the transport of cells that tend to concentrate near the surface and toward the coast [45, 71]. The highest phytoplankton absorption coefficient ($a_{phy}(\lambda)$) throughout the study was assigned to this bloom (Figure 4).

HAB's are often divided into toxic versus high-biomass blooms [72]. The genus observed in the UGC was *Pseudo-nitzschia*, a diatom which produces Amnesic Shellfish Poisoning and Domoic Acid Poisoning; despite that the cell concentration was too low to produce a toxic effect (approximately 1000 cell L^{-1}), it was classified as a high-biomass bloom by the IOP index. Blooms of dinoflagellates such as *Lingulodinium* are yessotoxin producers [72]. In our study area, this genus was observed in TSB with higher frequency, but they have been reported in California and along the West Coast of the US as an emerging potential threat [72].

Research-based forecast systems for toxic blooms are the preoccupation of HAB monitoring networks. The list of predictor variables includes chlorophyll *a*, macronutrients, and upwelling. Based on our results, we think that absorption coefficients must also be included in this list. Using the IOP index could reduce the cost of regulatory analysis, as it could help in determining which samples should be analyzed with more costly analytical methods, before beach closure or other management decisions. In this sense, the capability of the IOP index is crucial to distinguish between active or decaying bloom. Fixing techniques do not allow this distinction by microscopic counts and thus can lead to worse decisions. The development of common methodologies and approaches in international networks affected by transboundary problems is important. For instance, the California Harmful Algal Bloom Monitoring and Alert Program, or CalHABMAP, integrates groups across the US region but contemplates expansion to include both Mexican observations and observations from the other western states [72].

3.5 Conclusions

The selected study areas have allowed us to apply the IOP index within the wide variability of optically complex coastal waters. Within this variability, we found areas with dominance of detritus or CDOM, despite the samplings being developed in areas with observed phytoplankton blooms. The IOP index was able to discern sampling points under active bloom conditions from points in decaying bloom conditions. In the Yucatan region, the IOP index distinguished points under active bloom from points with high CDOM due to phytoplankton cell degradation from previous blooms. Also, the IOP index has been proved useful to distinguish phytoplankton blooms from the natural variability of an area. In the case of the UGC, typical high detritus levels produce a high absorption coefficient, which is not related to phytoplankton blooms. The IOP index was able to identify points under active bloom conditions from points with a high detritus load.

Continuous monitoring is essential to be able to distinguish a phytoplankton bloom from natural variability. The inherent optical properties play a key role in correctly identifying phytoplankton blooms, but are highly variable in complex coastal waters. Baseline values are unique to a coastal area and should be defined to enable the detection of anomalous events. Thus, the measurement of absorption coefficients should be considered in programs monitoring coastal waters.

In this research, the IOP index has been applied in optically complex coastal waters. However, it could also be applied to inland waters because they share the same bio-optical principle of absorption and refraction of light by particles contained in water. In inland waters, the optically active substances can vary in type and quantity in short time intervals and are often more noticeable than those occurring in the ocean [73]. Therefore, the IOP index could also be used in inland water monitoring programs, such as in the EU Water Framework Directive (Directive 2000/60/EC).

The importance of defining the baseline for the interpretation of the IOP index should be underlined. The definition of the average values of a specific area allows identifying the sampling points that have anomalous values. For this reason, it is important to have a wide range of data during the sampling, but also an adequate distribution that allows us to evaluate the variability of the studied area and to better define the baseline. The use of remote sensing can help to define IOPs from satellite reflectances, $R_{rs}(\lambda)$, and to build a baseline at a lower cost. In-situ IOP measurements could be compared to this baseline to identify active phytoplankton blooms using the IOP index. Further research is needed to test the benefits and limits of this methodology.

Acknowledgments: CONACYT supported this research with a doctorate scholarship to Jesús A. Aguilar-Maldonado, with the announcement number 251025 in 2015. María-Teresa Sebastiá-Frasquet was a beneficiary of the BEST/2017/217 grant, supported by the Valencian Conselleria d' Educació, Investigació, Cultura i Esport (Spain) during her stay at the Universidad Autónoma de Baja California (Mexico). Thanks are extended to the Strategic Action Program of the Gulf of Mexico Large Marine Ecosystem (GoM-LME), of the United Nations Industrial Development Organization (UNIDO).

Author Contributions: Jesús A. Aguilar-Maldonado carried out the tests and analyses presented in the article, drafted the text of the article and supported the sampling campaigns. Eduardo Santamaria-de-Ángel, Adriana G. Gonzalez-Silveira and Sergio Cerdeira-Estrada are authors of the methodology IOP*index* on which this article was based; the data used were obtained by resources of their research group and were part of the sampling campaigns. Maria-Teresa Sebastia-Frasquet organized the text, compiled and presented data, and formulated new ideas for this article; she was also fundamental in the writing and correction of English. Omar D. Cervantes-Rosas, Lus M. López, Angélica Gutiérrez-Magness collaborated during the entire process with ideas, corrections and advisory times.

Conflicts of Interest: The authors declare no conflict of interest. The founding sponsors had no role in the design of the study; in the collection, analyses, or interpretation of data; in the writing of the manuscript, and in the decision to publish the results.

3.6 References

1. Gower, J.; King, S.; Borstad, G.; Brown, L. Detection of intense plankton blooms using the 709 nm band of the MERIS imaging spectrometer. *Int. J. Remote Sens.* **2005**, *26*, 2005–2012. doi:10.1080/01431160500075857.
2. Carstensen, J.; Conley, D. Frequency, composition, and causes of summer phytoplankton blooms in a shallow coastal ecosystem, the Kattegat. *Limnol. Oceanogr.* **2004**, *49*, 191–201. doi:10.4319/lo.2004.49.1.0191.
3. Legendre, L. The significance of microalgal blooms for fisheries and for the export of particulate organic carbón in oceans. *J. Plankton Res.* **1990**, *12*, 681–699. doi:10.1093/plankt/12.4.681.
4. Ji, R.; Edwards, M.; Mackas, D.; Runge, J.; Thomas, A. Marine plankton phenology and life history in a changing climate: Current research and future directions, *J. Plankton Res.* **2010**, *32*, 1355–1368. doi:10.1093/plankt/fbq062
5. Richardson, K. Harmful or exceptional phytoplankton blooms in the marine ecosystem. *Adv. Mar. Biol*. **1997**, *31*, 301–385. doi:10.1016/S0065-2881(08)60225-4.
6. Smayda, T.J. What is a bloom? A commentary. *Limnol. Oceanogr*. **1997**, *42*, 1132–1136. doi:10.4319/lo.1997.42.5_part_2.1132
7. Brody, S.R.; Lozier, M.S.; Dunne, J.P. A comparison of methods to determine phytoplankton Bloom initiation. *J. Geophys. Res. Oceans* **2013**, *118*, 2345–2357. doi:10.1002/jgrc.20167.
8. Platt, T.; Fuentes-Yaco, C.; Frank, K.T. Spring algal Bloom and larval fish survival. *Nature* **2007**, *423*, 398–399. doi:10.1038/423398b.
9. Schneider, B.; Kaitala, S.; Maunula, P. Identification and quantification of plankton bloom events in the Baltic Sea by continuous pCO2 and chlorophyll a

measurements on a cargo ship. *J. Mar. Syst.* **2006**, *59*, 238–248. doi:10.1016/j.jmarsys.2005.11.003.

10. Gittings, J.A.; Raitsos, D.E.; Racault, M.F.; Brewin, R.J.; Pradhan, Y.; Sathyendranath, S.; Platt, T. Seasonal phytoplankton blooms in the Gulf of Aden revealed by remote sensing. *Remote Sens. Environ.* **2017**, *189*, 56–66. doi:10.1016/j.rse.2016.10.043.
11. Huppert, A.; Blasius, B.; Stone, L. A Model of Phytoplankton Blooms. *Am. Nat*. **2002**, *159*, 156–171. doi:10.1086/324789.
12. Fleming, V.; Seppo Kaitala, S. Phytoplankton spring bloom intensity index for the Baltic Sea estimated for the years 1992 to 2004, *Hydrobiologia* **2006**, *554*, 57–65. doi:10.1007/s10750-005-1006-7.
13. Carstensen, J.; Henriksen, P.; Heiskanen, A.-S. Summer algal blooms in shallow estuaries: Definition, mechanisms, and link to eutrophication. *Limnol. Oceanogr*. **2007**, *52*, 370–384. doi:10.4319/lo.2007.52.1.0370.
14. Cetinic, I.; Perry, M.J.; D'Asaro, E.; Briggs, N.; Poulton, N.; Sieracki, M.E.; Lee, C.M. A simple optical index shows spatial and temporal heterogeneity in phytoplankton community composition during the 2008 North Atlantic Bloom Experiment. *Biogeosciences* **2015**, *12*, 2179–2194. doi:10.5194/bg-12-2179-2015.
15. Alikas, K.; Kangro, K.; Reinart, A. Detecting cyanobacterial blooms in large North European lakes using the Maximum Chlorophyll Index. *Oceanologia* **2010**, *52*, 237–257.
16. Platt, T.; Sathyendranath, S.; White, G.; Fuentes-Yaco, C.; Zhai, L.; Devred, E.; Tang, C. Diagnostic properties of phytoplankton time series from remote sensing. *Estuaries Coasts* **2009**, *33*, 428–439. doi:10.1007/s12237-009-9161-0.
17. Preisendorfer, R.W. *Application of Radiative Transfer Theory to Light Measurements in the Sea*. IUGG: Potsdam, Germany, **1961**; Volume 10, pp. 11–30.
18. Cui, T.; Cao, W.; Zhang, J.; Hao, Y.; Yu, Y.; Zu, T.; Wang, D. Diurnal variability of ocean optical properties during a coastal algal bloom: Implications for ocean colour remote sensing. *Int. J. Remote Sens.* **2013**, *34*, 8301–8318. doi:10.1080/01431161.2013.833356.
19. Loisel, H.; Vantrepotte, V.; Norkvist, K.; Mériaux, X.; Kheireddine, M.; Ras, J.; Pujo-Pay, M.; Combet, Y.; Leblanc, K.; Dall'Olmo, G.; et al. Characterization of the Bio-

Optical Anomaly and Diurnal Variability of Particulate Matter, as Seen from Scattering and Backscattering Coefficients, in Ultra-Oligotrophic Eddies of the Mediterranean Sea. *Biogeosciences* **2011**, *8*, 3295–3317.

20. Mercado, J.M.; Ramírez, T.; Cortés, D.; Sebastián, M.; Reul, A.; Bautista, B. Diurnal Changes in the Bio-Optical Properties of the Phytoplankton in the Alborán Sea (Mediterranean Sea). *Estuar. Coast. Shelf Sci.* **2006**, *69*, 459–470
21. Kirk, J.T.O. *Light and Photosynthesis in Aquatic Ecosystems*, 3rd ed.; Cambridge Univ. Press: Cambridge, UK, 2011; ISBN 9780521151757.
22. Morel, A. Meeting the Challenge of Monitoring Chlorophyll in the Ocean from Outer Space. In *Chlorophylls and Bacteriochlorophylls: Biochemistry, Biophysics, Functions and Applications*; Grimm, B., Porra, R., Rüdiger, W., Scheer, H., Eds.; Springer: Dordrecht, The Netherlands, 2006; Volume 25, pp. 521–534, ISBN 978-1-4020-4516-5.
23. Santamaría-del-Angel, E.; Soto, I.; Millán-Nuñez, R.; González-Silvera, A.; Wolny, J.; Cerdeira-Estrada, S.; Cajal-Medrano, R.; Muller-Karger, F.; Cannizzaro, J.; Padilla-Rosas, Y.; et al. Experiences and Recommendations for Environmental Monitoring Programs. In *Environmental Science, Engineering and Technology*; Sebastia-Frasquet, M.-T., Ed.; Nova Science Publishers: Hauppauge, NY, USA, 2015; p. 32, ISBN 978-1-63482-189-6.
24. Santamaría-del-Angel, E.; González-Silvera, A.; Millán-Nuñez, R.; Callejas-Jiménez, M.E.; Cajal-Medrano, R. Determining Dynamic Biogeographic Regions using Remote Sensing Data. In *Handbook of Satellite Remote Sensing Image Interpretation: Applications for Marine Living Resources Conservation and Management*; Morales, J., Stuart, V., Platt, T., Sathyendranath, S., Eds.; EU PRESPO and IOCCG: Dartmouth, Canada, 2011; Chapter 19, pp. 273–293.
25. Hernández-Terrones, L.; Rebolledo-Vieyra, M.; Merrino-Ibarra, M.; Soto, M.; LeCossee, A.; Monroy-Rios, E. Groundwater pollution in karstic region (NE Yucatán): Baseline nutrient content and flux to coastal ecosystems. *Water Air Soil Pollut.* **2011**, *218*, 517–528. doi:10.1007/s11270-010-0664-x.
26. Moore, Y.H.; Stoessell, R.K.; Easley, D.H. Fresh-Water/Sea-Water Relationship within a Ground-Water Flow System, Northeastern Coast of the Yucatan Peninsula. *Groundwater* **1992**, *30*, 343–350. doi:10.1111/j.1745-6584.1992.tb02002.x.

27. Beddows, P.A.; Smart, P.L.; Whitaker, F.F.; Smith, S.L. Decoupled fresh-saline groundwater circulation of a coastal carbonate aquifer: Spatial patterns of temperature and specific electrical conductivity. *J. Hydrol.* **2007**, *346*, 18–32. doi:10.1016/j.jhydrol.2007.08.013.
28. Hernández-Terrones, L.M.; Null, K.A.; Ortega-Camacho, D.; Paytan, A. Water quality assessment in the Mexican Caribbean: Impacts on the coastal ecosystem. *Cont. Shelf Res*. **2015**, *102*, 62–72. doi:10.1016/j.csr.2015.04.015
29. Herrera-Silveira, J.A.; Morales-Ojeda, S.M. Subtropical Karstic Coastal Lagoon Assessment, Southeast Mexico. The Yucatan Peninsula Case. In *Coastal Lagoons: Critical Habitats of Environmental Change*; Kennish, M.J., Paerl, H.W., Eds.; CRC Press: Boca Raton, FL, USA, 2010; p. 26, ISBN 9781420088304 1420088300.
30. Sánchez, F.J.; Gámez, D.; Guevara, G.; Shirasago, G.; Obeso, M. Análisis de la circulación superficial de mesoescala en la bahía de Campeche mediante sensores activos y pasivos. *Geos* **2010**, *30*, 204.
31. Monreal-Gómez, M.A.; Salas de León, D.A. Simulación de la circulación en la Bahía de Campeche. *Geofís. Int.* **1990**, *29*, 101–111.
32. Merrell, W., Jr.; Morrison, J. On the circulation of the western Gulf of Mexico with observations from April 1978. *J. Geophys. Res.* **1981**, *86*, 4181–4185. doi:10.1029/JC086iC05p04181.
33. Cochrane, J.D. Investigations of the Yucatan current; the region of cold surface water. In *Oceanography and Meteorology of the Gulf of Mexico*; McLellan, H.J., Ed.; Annual Report Rep 61-15F; Department of Oceanography, Texas A&M University: College Station, Texas, 1961; pp. 5–6.
34. Carriquiry, J.D.; Sanchez, A. Sedimentation in the Colorado River delta and Upper Gulf of California after nearly a century of discharge loss. *Mar. Geol.* **1999**, *158*, 125–145. doi:10.1016/S0025-3227(98)00189-3.
35. Brusca, R.C.; Álvarez-Borrego, S.; Hastings, P.A.; Findley, L.T. Colorado River flow and biological productivity in the Northern Gulf of California, Mexico. *Earth Sci. Rev.* **2017**, *164*, 1–30. doi:10.1016/j.earscirev.2016.10.012.
36. Santamaría-del Ángel, E.; Millán-Núñez, R.; De la Peña, G. Efecto de la turbidez en la productividad primaria en dos estaciones en el Área del Delta del Río Colorado. *Cienc. Mar.* **1996**, *22*, 483–493.

37. Daessle, L.W.; Orozco, A.; Struck, U.; Camacho-Ibar, V.F.; van Geldern, R.; Santamaría-del-Ángel, E.; Barth, J.A.C. Sources and sinks of nutrients and organic carbon during the 2014 pulse flow of the Colorado River into Mexico. *Ecol. Eng.* **2017**, *106*, 799–808. doi:10.1016/j.ecoleng.2016.02.018.

38. Orozco-Durán, A.; Daesslé, L.W.; Camacho-Ibar, V.F.; Ortiz-Campos, E.; Barth, J.A.C. Turnover and release of P-, N-, Si-nutrients in the Mexicali Valley (Mexico): Interactions between the lower Colorado River and adjacent ground-and surface water systems. *Sci. Total Environ.* **2015**, *512–513*, 185–193. doi:10.1016/j.scitotenv.2015.01.016.

39. Aguilar-Maldonado, J.A.; Santamaría-del-Ángel, E.; Sebastiá-Frasquet, M.T. Reflectances of SPOT multispectral images associated with the turbidity of the Upper Gulf of California. *Rev. Teledetec.* **2017**, *49*, 1–16. doi:10.4995/raet.2017.7795

40. Cepeda-Morales, J.; Durazo, R.; Millán-Nuñez, E.; De la Cruz-Orozco, M.; Sosa-Ávalos, R.; Espinosa-Carreón, T.L.; Soto-Mardones, L.; Gaxiola-Castro, G. Response of primary producers to the hydrographic variability in the southern region of the California Current System. *Cienc. Mar.* **2017**, *43*, 123–135.

41. Delgadillo-Hinojosa, F.; Camacho-Ibar, V.; Huerta-Díaz, M.A.; Torres-Delgado, V.; Pérez-Brunius, P.; Lares, L.; Castro, R. Seasonal behavior of dissolved cadmium and Cd/PO 4 ratio in Todos Santos Bay: A retention site of upwelled waters in the Baja California peninsula, Mexico. *Mar. Chem.* **2015**, *168*, 37–48. doi:10.1016/j.marchem.2014.10.010.

42. Durazo, R.; Gaxiola-Castro, G.; Lavaniegos, B.; Castro-Valdez, R.; Gómez-Valdés, J.; Da S. Mascarenhas, A., Jr. Oceanographic conditions west of the Baja California coast, 2002-2003: A weak El Niño and subarctic water enhancement. *Cienc. Mar.* **2005**, *31*, 537–552.

43. Linacre, L.; Durazo, R.; Hernández-Ayón, J.M.; Delgadillo-Hinojosa, F.; Cervantes-Díaz, G.; Lara-Lara, J.R.; Camacho-Ibar, V.; Siqueiros-Valencia, A.; Bazán-Guzmán, C. Temporal variability of the physical and chemical water characteristics at a coastal monitoring observatory: Station Ensenada. *Cont. Shelf Res.* **2010**, *30*, 1730–1742. doi:10.1016/j.csr.2010.07.011.

44. Espinosa-Carreón T.L.; Gaxiola-Castro, G.; Durazo, R.; De la Cruz-Orozco, M.E.; Norzagaray-Campos, M.; Solana-Arellano, E. Influence of anomalous subarctic

water intrusion on phytoplankton production off Baja California. *Cont. Shelf Res.* **2015**, *92*, 108–121. doi:10.1016/j.csr.2014.10.003.

45. Millán-Núñez, E.; Macias-Carballo, M. Phytogeography associated at spectral absorption shapes in the southern region of the California current. *CAlCOFI* **2014**, *55*, 183–196.
46. Gutierrez-Mejia, E.; Lares, M.L.; Huerta-Diaz, M.A.; Delgadillo-Hinojosa, F. Cadmium and phosphate variability during algal blooms of the dinoflagellate Lingulodinium polyedrum in Todos Santos Bay, Baja California, Mexico. *Sci. Total Environ.* **2016**, *541*, 865–876. doi:10.1016/j.scitotenv.2015.09.081.
47. COFEPRIS. State Sanitary Emergencies by Red Tide (Mexico). Available online: Http://www.cofepris.gob.mx/AZ/Paginas/Marea%20Roja/EmergenciasSanitariasEstatales.aspx (accessed on 24 January 2018).
48. Mitchell, B.G.; Kahru, M.; Wieland, J.; Stramska, M. Determination of spectral absorption coefficients of particles, dissolved material and phytoplankton for discrete water samples. In *Ocean Optics Protocols for Satellite Ocean Color Sensor Validation*; NASA, Mueller, J.L., Fargion, G.S., Eds.; Flight Space Center: Greenbelt, MD, USA, 2002; Volume 3, pp. 231–257.
49. Santamaría-del-Angel, E.; Millán-Núñez, R.; González-Silvera, A.; Callejas-Jiménez, M.; Cajal-Medrano, R.; Galindo-Bect, M. The response of shrimp fisheries to climate variability off Baja California, México. *ICES J. Mar. Sci.* **2011**, *68*, 766–772. doi:10.1093/icesjms/fsq186.
50. Hirata, T.; Aiken, J.; Smyth, T.J.; Barlow, R.G. An absorption model to derive phytoplankton size classes from satellite ocean colour. *Remote Sens. Environ.* **2008**, *112*, 3153–3159. doi:10.1016/j.rse.2008.03.011
51. Aiken, J.; Hardman-Mountford, N.; Barlow, R.; Fishwick, J.; Hirata, T.; Smyth, T. Functional links between bioenergetics and bio-optical traits of phytoplankton taxonomic groups: An overarching hypothesis with applications for ocean colour remote sensing. *J. Plankton Res*. **2008**, *30*, 165–181. doi:10.1093/plankt/fbm098
52. Stuart, V.; Sathyendranath, S.; Platt, T.; Maass, H.; Irwin, B.D. Pigments and species composition of natural phytoplankton populations: Effect on the absorption spectra. *J. Plankton Res*. **1998**, *20*, 187–217. doi:10.1093/plankt/20.2.187.

53. Lohrenz, S.E.; Weidemann, A.D.; Tuel, M. Phytoplankton spectral absorption as influenced by community size structure and pigment composition. *J. Plankton Res.* **2003**, *25*, 35–61. doi:10.1093/plankt/25.1.35.
54. Wu, J.; Hong, H.; Shang, S.; Dai, M.; Lee Z. Variation of phytoplankton absorption coefficients in the northern South China Sea during spring and autumn. *Biogeosci. Discuss.* **2007**, *4,* 1555–1584. doi:10.5194/bgd-4-1555-2007.
55. Millán-Nuñez, E.; Millán-Nuñez, R. Specific Absorption Coefficient and Phytoplankton Community Structure in the Southern Region of the California Current during January 2002. *J. Oceanogr.* **2010**, *66*, 719–730.
56. Utermöhl, H. Zur velvollkommung der quantitative phytoplankton-Methodik*. Mitt. Int. Ver. Theor. Angew. Limnol*. **1958**, *9*, 1–38.
57. Haywood, A.J.; Steidinger, K.A.; Truby, E.W.; Bergquist, P.R.; Bergquist, P.L.; Adamson, J.; MacKenzie, L. Comparative morphology and molecular phylogenetic analysis of three new species of the genus Karenia (Dinophyceae) from New Zealand. *J. Phycol.* **2004**, *40*, 165–179. doi:10.1111/j.0022-3646.2004.02-149.x.
58. Steidinger, K.A.; Wolny, J.L.; Haywood, A.J. Identification of Kareniaceae (Dinophyceae) in the Gulf of Mexico. *Nova Hedwigia* **2008**, *133*, 269–284.
59. Gárate-Lizárraga, I.; Okolodkov, Y.; Cortés-Altamirano, R. Microalgas formadoras de florecimientos algales en el Golfo de California, In *Florecimientos Algales Nocivos en México*; García-Mendoza, E., Quijano-Scheggia, S.I., Olivos-Ortiz, A., Núñez-Vázquez, E.J., Eds.; CICESE: Ensenada, México, 2016; pp. 130–145.
60. Quijano, S.I.; Barajas, M.; Chang, H.; Bates, S. The inhibitory effect of a non-yessotoxin-producing dinoflagellate, Lingulodinium polyedrum (Stein) Dodge, towards Vibrio vulnificus and Staphylococcus aureus. *Revista de Biologia Tropical* **2016**, *64*, 805–816.
61. Holm-Hansen, O.; Riemann, B. Chlorophyll a Determination: Improvements in Methodology. *Oikos* **1978**, *30*, 438–447
62. Mendoza, M.; Ortiz-Pérez, M.A. Caracterización geomorfológica del talud y la plataforma continentales de Campeche-Yucatán, México. *Investigaciones Geográficas* **2000**, *43*, 7–31.
63. Herrera-Silveira, J.A. Ecología de los productores primarios en la laguna de Celestún, México. Patrones de variación espacial y temporal. Ph.D. Thesis, Universitat de Barcelona, Barcelona, Spain, 1993

64. Aguilar-Trujillo, A.C.; Okolodkov, Y.B.; Herrera-Silveira, J.A.; Merino-Virgilio, F.D.C.; Galicia-García, C. Taxocoenosis of epibenthic dinoflagellates in the coastal waters of the northern Yucatan Peninsula before and after the harmful algal bloom event in 2011–2012. *Mar. Pollut. Bull.* **2017**, *119*, 396–406. doi:10.1016/j.marpolbul.2017.02.074.

65. Ulloa, M.J.; Álvarez-Torres, P.; Horak-Romo, K.P.; Ortega-Izaguirre, R. Harmful algal blooms and eutrophication along the mexican coast of the Gulf of Mexico large marine ecosystem. *Environ. Dev.* **2017**, *22*, 120–128. doi:10.1016/j.envdev.2016.10.007

66. Ochoa, J.L.; Hernández-Becerril, D.U.; Lluch-Cota, S.; Arredondo-Vega, B.O.; Nuñez-Vázquez, E.; Heredia-Tapia, A.; Alonso-Rodríguez, R. Marine biotoxins and harmful algal blooms in Mexico’s Pacific littoral. Harmful algal blooms in the PICES region of the North Pacific. *PICES Sci. Rep.* **2002**, *23*, 119–128.

67. Hernández-Becerril, D.U. Morfología y taxonomía de algunas especies de diatomeas del género Coscinodiscus de las costas del Pacífico mexicano. *Rev. Biol. Trop.* **2000**, *48*, 7–18.

68. Liefer, J.D.; Robertson, A.; MacIntyre, H.L.; Smith, W.L.; Dorsey, C.P. Characterization of a toxic *Pseudo-nitzschia* spp. bloom in the Northern Gulf of Mexico associated with domoic acid accumulation in fish. *Harmful Algae* **2013**, *26*, 20–32. doi:10.1016/j.hal.2013.03.002

69. Schnetzer, A.; Miller, P.E.; Schaffner, R.A.; Stauffer, B.A.; Jones, B.H.; Weisberg, S.B.; Caron, D.A. Blooms of Pseudo-nitzschia and domoic acid in the San Pedro Channel and Los Angeles harbor areas of the Southern California Bight, 2003–2004. *Harmful Algae* **2007**, *6*, 372–387. doi:10.1016/j.hal.2006.11.004

70. Peña Manjarrez, J.; Gaxiola-Castro, G.; Helenes-Escamilla, J. Environmental factors influencing the variability of *Lingulodinium polyedrum* and *Scrippsiella trochoidea* (Dinophyceae) cyst production. *Cienc. Mar.* **2009**, *35*, 1–14. doi:10.7773/cm.v35i1.1406.

71. Ruiz-de la Torre, M.C.; Maske, H.; Ochoa, J.; Almeda-Jauregui, C.O. Maintenance of Coastal Surface Blooms by Surface Temperature Stratification and Wind Drift. *PLoS ONE* **2013**, 8, e58958. doi:10.1371/journal.pone.0058958.

72. Kudela, R.M.; Bickel, A.; Carter, M.L.; Howard, M.D.; Rosenfeld, L. The monitoring of harmful algal blooms through ocean observing: The development of the

California Harmful Algal Bloom Monitoring and Alert Program. *Coast. Ocean Obs. Syst.* **2015**, 58–75. doi:10.1016/B978-0-12-802022-7.00005-5.

73. Reinart, A.; Paavel, B.; Pierson, D.; Strombeck, N. Inherent and apparent optical properties of Lake Peipsi, Estonia. *Boreal Environ. Res*. **2004**, *9*, 429–445.

4. Capítulo Segundo.

Mapping Satellite Inherent Optical Properties Index in CoastalWaters of the Yucatán Peninsula (Mexico)

4.1 Abstract

The Yucatán Peninsula hosts worldwide-known tourism destinations that concentrate most of the Mexico tourism activity. In this region, tourism has exponentially increased over the last years, including wildlife oriented tourism. Rapid tourism development, involving the consequent construction of hotels and tourist commodities, is associated with domestic sewage discharges from septic tanks. In this karstic environment, submarine groundwater discharges are very important and highly vulnerable to anthropogenic pollution. Nutrient loadings are linked to harmful algal blooms, which are an issue of concern to local and federal authorities due to their recurrence and socioeconomic and human health costs. In this study, we used satellite products from MODIS (Moderate Resolution Imaging Spectroradiometer) to calculate and map the satellite Inherent Optical Properties (IOP) Index. We worked with different scenarios considering both holiday and hydrological seasons. Our results showed that the satellite IOP Index allows one to build baseline information in a sustainable mid-term or long-term basis which is key for ecosystem-based management.

Keywords: eutrophication; satellite images; phytoplankton blooms; Gulf of Mexico; Caribbean Sea; tourism; MODIS

4.2 Introduction

Tourism is an industry highly dependent on natural resources, and is key for the economy of many regions [1,2]. Specifically, coastal and marine tourism is one segment of the tourism market that has experienced the most important development in recent years [1,3]. This fast development has increased attention on the impacts that tourism activity produces on the same natural resources that attract tourists, especially in the absence of a sustainable planning [1]. Water pollution is one of its major impacts on environment [4]. Decreased water clarity caused by eutrophication processes and harmful algal blooms (HABs) affects trip satisfaction, and consequently, the likelihood of a tourist coming back to the same destination [2]. A sustainable tourism industry must aim to encourage repeat visits [2], and thus, must preserve the original values that once encouraged the first visitors. To be able to accomplish this objective, tourism cannot develop isolated from urban and non-urban planning. According to Bentz et al. [1] the Wildlife Tourism model suggested by Duffus and Dearden [5], which is used widely to assess the sustainability of marine wildlife tourism, states that wildlife-based tourism is particularly vulnerable to the demise of the natural attraction due to increasing impacts. For instance, whale shark tourism can be seen as a non-consumptive use, but the impacts of tourism have undesired effects on the target species [3]. Stankey et al.'s [6] Limits of Acceptable Change (LAC) model has been used to identify standards of quality and to define appropriate limits for tourism activity. As Bentz et al. [1] describe, the process of establishing LAC identifies desirable ecological conditions, choice indicators of these conditions, assesses current conditions, identifies management actions, and monitors and evaluates implemented management actions. In this framework, the choice of the indicator is a key step. As eutrophication processes and increased HAB frequency are two of the major impacts on coastal waters [7–9], we propose to monitor these impacts using an indicator which can give continuous information to assess current conditions.

In this paper, we focus on the case study of the touristic Yucatán Peninsula (Mexico). In this region, tourism is based upon the natural resources of sun, sand, and sea. Coastal recreation offers activities such as sailing, boat tours, cruise tourism, scuba diving (in coral reefs and cenotes), whale, whale shark and dolphin watching, swimming with dolphins, and sport fishing. Since the 1960s economic crisis in Mexico, the Mexican government encouraged the development of the tourism industry as an opportunity for economic recovery [4]. The current development of the Yucatan Peninsula started in the 1970s and cause a dramatic change in a short span of 40 years [10]. This fast development has been involved in direct and massive alterations of the coastal environment [4]. The lack of basic infrastructure, drainage and sewerage networks, and non-existent or inefficient wastewater treatment plants are the main causes of water quality problems in the receiving wáter bodies [11]. Padilla [4] studied the environmental effects of tourism in Cancún (Quintana Roo State). She estimated that hotel industry generates about 95% of total sewage water which is not inside the limits of wastewater treatment plants. In addition, she also identified other problems that cause wáter pollution such as septic tanks discharging into the karstic aquifer, recreational vehicles discharging wastewater into coastal waters, extensive deforestation, and destruction of mangroves and wetland areas. Eutrophication problems cause non-aesthetically attractive coastal recreational waters, but also HABs that can produce severe health effects [8,12–14]. Mexican authorities registered a HAB in Mérida (Yucatán State) in August 2003 with an 81 km extension and thousands of dead marine animals [15].

In general, the Yucatan Basin has been described as an oligotrophic region devoid of nutrients in the surface layer [16]. According to [17], in stations sampled in front of Holbox, Cabo Catoche, and Campeche, between July and August of 1994, the values of superficial Chlorophyll a did not exceed 1.65 mg m^{-3}, the foregoing descriptions of the trophic states of other authors [18–20] show that values above 2 mg m^{-3} are values that show eutrophic conditions. The episodes of HABs have increased in frequency in recent years, and at least 40 species of toxic or potentially toxic algae are known to occur [21]. The Mexican authorities recently presented a “Permanent Monitoring Program of Harmful Algal Blooms” [15], which involves several federal and state authorities ((Health Secretary, SAGARPA (Ministry of Agriculture, Livestock, Rural Development, Fisheries and Food), Secretary of Fisheries and Aquaculture of the State Government, SEMAR (Marine Secretary) and PROFEPA (Federal Attorney for Environmental Protection)), universities, and research centers (CICIMAR

(Interdisciplinary Center for Marine Sciences), CIBNOR (Northwest Center for Biological Research), and UABCS (Autonomous University of Baja California Sur)). However, this monitoring program is based on reporting HAB episodes to the State Health Authority by individuals, state institutions of the affected federal entity, participants of the State Committee of the Mexican Bivalve Mollusks Health Program, and by independent institutions. This monitoring relies on direct observation and does not offer a continuous information system, neither in time nor in coverage. In order to be able to undertake corrective and management measures, more complete information is needed. In this sense, both remote sensing and modeling are complimentary tools that can help. Among modeling tools, we can cite as an example of a eutrophication/water quality model that of Reference [22] based on CE-QUAL-ICM.

The objective of our study is to map the Inherent Optical Properties Index using remote sensing products from the Generalized Inherent Optical Property (GIOP) model. The use of remote sensing technology allows one to have a synoptic view of the entire area, at moderate- or high-spatial resolution resolution and high-temporal resolution, and permits long-time monitoring which is essential to draw the baseline of a specific region and detect deviations from this [23,24]. Satellite and airborne measurements of spectral reflectance (i.e., ocean color) have proved to be effective for monitoring phytoplankton blooms [25–27]. There is plenty of research that analyzes the advantages of remote sensing in highly variable coastal waters [28–31]. Remote sensing of inherent optical properties (IOP) can provide essential information on the concentration of the optically important components present in water masses as in situ measurements [32]. Satellite ocean color instruments, such as the NASA Moderate Resolution Imaging Spectroradiometer (MODIS), provide daily global estimates of marine IOPs [33]. The analysis of IOPs is especially important in optically complex waters, because in this type of water, water color depends on three main constituents: colored detritus matter (CDM), colored dissolved organic matter (CDOM), and phytoplankton [34,35]. In this study, we apply the Inherent Optical Properties (IOP) Index developed by Santamaría et al. [36] to satellite products. The IOP Index has proven to be able to discern sampling points under active bloom conditions from points in decaying bloom conditions. In the Yucatan region, Aguilar-Maldonado et al. [23] found that the IOP Index distinguished points under active bloom from points with high CDOM due to phytoplankton cell degradation from previous blooms. Also, the IOP Index was able to identify points under active bloom conditions from points with a high CDM load.

4.3 Materials and Methods

4.3.1 Case Study Regions

Our study area (Figure 7) comprises the coastal regions of three states of the Yucatán Peninsula: Campeche, Yucatán, and Quintana Roo.

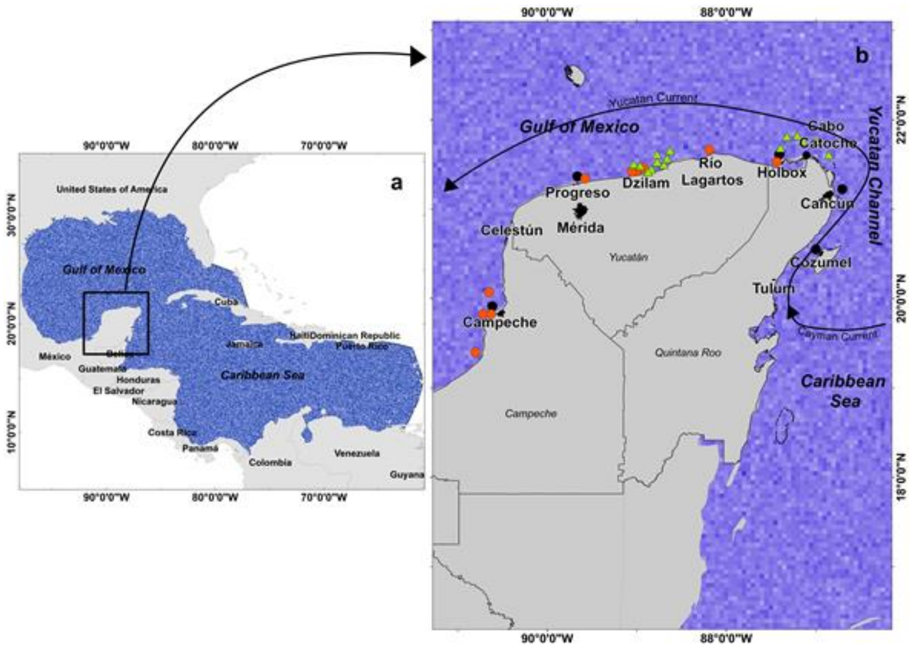

Figure 7. Study area. (**a**) Gulf of Mexico and Caribbean Sea basins. (**b**) Study area detail, where black dots are selected monitoring points, red dots are areas with historic harmful algal bloom (HAB) reports, and green triangles are points sampled in situ for validation.

The Yucatán Peninsula separates the Gulf of Mexico Large Marine Ecosystem (GoM-LME) and the Caribbean Sea Large Marine Ecosystem (CS-LME). The Yucatán Current flows into the Gulf of Mexico adjacent to the Yucatán Shelf carrying different water masses from the Caribbean and Atlantic [37] (Figure 7). According to the climatic classification of Koppen modified for Mexico [38], the Yucatán Peninsula has a climatic regime which is predominantly hot and sub-humid, with a dry season from March to May, a rainy season from June to October, and a “Nortes” or post-rainy season from November to February. During the dry season, rainfall is almost absent (1.4 mm)

[39,40]. The hydrological unit area of the Yucatán Peninsula Aquifer includes the states of Yucatán, Campeche, and Quintana Roo [41]. It is the most extensive karstic aquifer in the world [42]. It is an unconfined aquifer, except in the coastal zone, characterized by a very low hydraulic gradient on the order of 7–10 mm/km [42]. Nowadays, the aquifer is threatened due to population and tourism infrastructure growth. Among water quality problems, high levels of nutrients and fecal organisms are generalized in both rural and urban areas. The origin of nitrogen and phosphorus concentrations is anthropogenic [43]. López-Maldonado et al. [41] found that 75% of the wastewater from the household sector goes to septic tanks and the remainder is discharged directly into the aquifer, which is in agreement with INEGI (National Institute of Statistic and Geography) [44] statistics. Agriculture and livestock are the other important anthropogenic sources. Particularly, small farms in the livestock sector generate more important direct outputs into the aquifer without treatment than larger farms [41,45]. The connectivity of submarine groundwater discharge to the nearshore coastal environment is an important impact for coastal water quality [46–48].

In Figure 8, land uses in the Yucatán Peninsula are represented, and adapted from INEGI 2014 land use cartography (scale 1:250,000). In general terms, the three states show different land uses. In Quintana Roo State, the major land uses in the coastal areas are tall semi-deciduous forests, in Yucatan State, the main use is farmland, and in Campeche State, the extent of the mangrove swamp is remarkable.

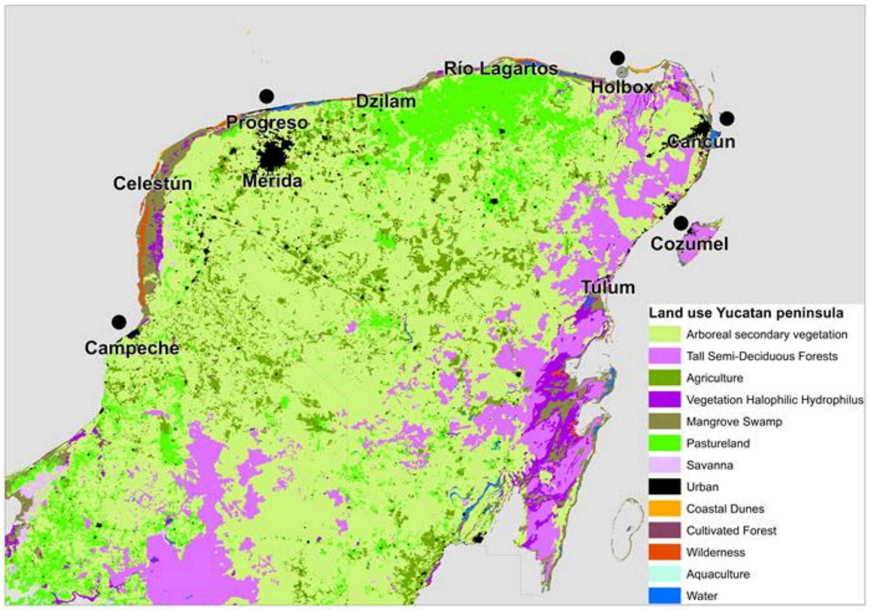

Figure 8. Land use in the Yucatán Peninsula adapted from INEGI (National Institute of Statistic and Geography) 2014 land use cartography. Black dots are selected monitoring points.

We selected five monitoring points distributed along the coast of the Yucatán Peninsula (black dots in Figures 7 and 8). The selection was based on important tourist destinations, from east to west: Cozumel, Cancún, Holbox, Progreso, and Campeche. Progreso can be considered as Mérida’s beach. We also took into account historic HABs reported between 2003 and 2017 by COFEPRIS (Comisión Federal para la Protección contra Riesgos Sanitarios/Federal Commission for Protection against Health Risks) [15] in this region (red dots in Figure 7). The population in these municipalities has notably increased over the last years (Table 3).

Table 3. Inhabitants' evolution in monitored municipalities (source: INEGI) and monitoring point coordinates.

ID	Coordinate X	Coordinate Y	Location	1990	2000	2010
1	-87.000	20.551	Cozumel	33,884	58,673	77,236
2	-86.705	21.224	Cancun	159,723	392,643	628,306
3	-87.408	21.614	Holbox	927	1,193	1,486
4	-89.663	21.367	Progreso	35,280	43,850	37,369
	-89.630	20.980	Mérida	522,849	658,698	777,615
5	-90.613	19.914	Campeche	148,211	189,817	220,389

The Mexican Caribbean Sea is 40 km wide by 865 km long, which gives an approximate área of 34,000 km2 that essentially comprises the coast of the state of Quintana Roo, and indirectly and partially the coast of the state of Yucatán. The Riviera Maya, located along the Caribbean Sea in the state of Quintana Roo, is an internationally known tourist destination, with important tourist centers like Cancún, Holbox, Cozumel, and Tulum (Figure 7). During the decade of the nineties, the hotel sector in the region expanded into a residential hotel corridor of more than 130 km that reaches from Cancún to Tulum. It developed as a massive sun and beach tourism model [49]. More recently, some destinations have sought to differentiate what they offer, such as Holbox Island—a small island on the northeastern tip of the Yucatán Peninsula (Figure

7). Holbox is one of the largest whale shark watching industries in the world, thanks to the congregation of this species from May to September in its plankton rich waters [3]. The high tourism season is summer (from June to September), but there is also an important visitors' affluence in spring due to Easter holidays and to spring-breakers. Spring-breakers from the USA exceeded 40,000 visitors in 2013–2014 [49].

4.3.2 Image Processing and Satellite IOP Index Calculations

The satellite IOP Index was calculated based on the methodology proposed for the in situ IOP index by Santamaría-del-Ángel et al. [36], and later applied by Aguilar-Maldonado et al. [23] following the next steps. First, the absorption coefficients of phytoplankton and CDM plus CDOM were obtained from the GIOP satellite model. The GIOP model of MODIS Terra and MODIS Aqua sensors were obtained from NASA's Ocean Color Web. The GIOP model is the result of two international IOP algorithm workshops that were hosted by NASA in conjunction with the Ocean Optics XIX (October 2008) and XX (September 2010) conferences. (Please, see https://oceancolor.gsfc.nasa.gov/atbd/giop/ for more information). We used daily images, processed at level 3, and with 4 km spatial resolution, to form three-day aggregates. Cloud cover prevented us from using daily images. We used the NASA SeaDAS software (https://seadas.gsfc.nasa.gov/) to make composites of the minimum number of days which had good coverage, which in this case was 3 days. The band 443 was selected because satellite products for absorption coefficients were obtained from this one. The GIOP model was obtained from the satellite reflectances [50], which are first converted to their subsurface values [51]. Each component can be expressed as the product of its concentration-specific absorption coefficient (eigenvector; a^*) and its concentration or amplitude (eigenvalue; A) [33]:

$$a(\lambda) = a_w + \sum_{i=1}^{N_\phi} A_{\phi_i}\, a^*_{\phi_i}(\lambda) + \sum_{i=1}^{N_d} A_{d_i}\, a^*_{d_i}(\lambda) + \sum_{i=1}^{N_g} A_{CDOM_i}\, a^*_{CDOM_i}(\lambda) \quad (1)$$

where the subscripts indicate contributions by water (w), phytoplankton (Φ), CDM (d) and CDOM. Both $a^*_{d_i}(\lambda)$ and $a^*_{CDOM_i}(\lambda)$ are commonly expressed as

$$a^*_{d,CDOM}(\lambda) = \exp\left(-S_{d,CDOM}\lambda\right) \quad (2)$$

where S determines the spectral dependence a_{CDOM} and is found to be approximately 0.014 nm^{-1} [51]. S_d and S_{CDOM} typically vary between 0.01 and 0.02 nm^{-1} in natural waters [52]. As the spectral shapes of NAP and CDOM absorption differ only in their exponential slopes, the two components are typically combined for satellite applications [33].

Then, absorption coefficients of phytoplankton, and NAP plus CDOM were standardized for the wavelength of 443 nm using the equation:

$$z = \frac{x - \bar{x}}{SD} \quad (3)$$

where: (x): the value to be standardized; ($\bar{x}$): the average; and (*SD*) the standard deviation.

The standardization was calculated for the entire GoM and CS area (Figure 1a) in order to better define baseline conditions and normal patterns.

Then, the satellite IOP index was calculated based on a Principal Component Analysis (PCA) of the standardized pixel values of each three-day composite. The first principal component was selected because it accounts for the largest possible variance. This selection was based on the eigenvalues. The coefficients of this principal component were named as $\boldsymbol{b}_{\mathbf{1},\mathbf{1}}$ and $\boldsymbol{b}_{\mathbf{1},\mathbf{2}}$. Finally, the IOP index was calculated based on this first standardized empirical orthogonal function ($SEOF_1$) according to Equation (3).

$$IOP_{index\ satellite} = \left[(b_{\mathbf{1},\mathbf{1}} * Za_{\phi,GIOP}) + (b_{\mathbf{1},\mathbf{2}} * Za_{dCDOM,GIOP})\right] \quad (4)$$

Where $Za_{\phi,GIOP}$ and $Za_{dCDOM,GIOP}$ they are the standardized values of phytoplankton and CDM plus CDOM, respectively, obtained from the GIOP satellite model.

Chlorophyll *a* concentration and temperature daily images were downloaded and processed equally to absorption coefficients.

Images of the dry period (i.e., April) and the wet period (i.e., June, July, and August) of the year 2011 were used. The year 2011 was chosen based on the report of a very extensive bloom in time (it lasted about 150 days from August to December 2011) and space in this region already analyzed from other points of view by other authors [7,23].

To describe the stages of a phytoplankton bloom, the values of the IOP Index were interpreted as follows [23,31]: (1) values in the interval (-1, 1) show the normal values of the specific site or non-bloom conditions; (2) values in the interval (1, 2) are above the average and represent a transition from anomalous values to normal values or decaying bloom conditions; and (3) values higher than 2 are anomalous and indicate eutrophic or bloom conditions. These thresholds are defined thanks to the standardization of the data. In a normal distribution, the Inverse Cumulative Distribution Function (ICDF) defines 1.96 standard deviations as the limit of values without noise with 95% confidence. This value was rounded to 2 standard deviations to define the limit of the anomalous conditions.

A Spearman correlation analysis was performed between GIOP model absorption coefficients and in situ measures of absorption coefficients published in Aguilar-Maldonado et al. [23]. In situ sampling points are represented in Figure 1b. These points are located in Dzilam (Yucatán) and Holbox (Quintana Roo). Nine samples were collected on 27 August and six samples on 30 August 2011. Colored detritus matter and CDOM were added to be compared with the satellite product $a_{dCDOM,GIOP}$. Each sampled point was related to the pixel value corresponding to that point.

4.4 Results

Spearman correlation analysis showed high positive and significant correlation between in situ absorption coefficients and satellite products. Colored detritus matter plus CDOM obtained from the GIOP model has a 0.533 relation with CDM plus CDOM obtained from in situ measures, while phytoplankton coefficients have a 0.937 relation.

In Figure 9, we can see the satellite IOP index results for April 2011. Inherent Optical Properties Index values above two indicate active bloom conditions and they are represented by a yellow to red color scale. Red areas show the highest anomalies. White areas are not covered by satellite due to clouds. April 2011 was the driest month according to SMN (National Meteorological Service) [53] with a 21.9 mm average precipitation. In 2011, spring break was from 15 March to 15 April and approximately 30,000 visitors were registered [48]. The first April fortnight, we observe bloom conditions in the coastal area of Campeche State (Figure 9a,b, red areas), and with less intensity around Holbox Island (Figure 9a,b yellow areas). During the second fortnight, bloom conditions expand on the North Campeche coast (Figure 9c,d, red areas), and extend from Holbox to Río Lagarto (Figure 9c,d red areas). During the last April days, from the 28 to 30, the phytoplankton blooms were considerably reduced (Figure 9e, yellow and orange areas). During this period, no phytoplankton bloom was detected in the southern coastal region of Quintana Roo State. In Figure 10, we represent the satellite IOP Index values for the five selected monitoring points: Holbox, Cancún, Cozumel, Progreso, and Campeche. These points are represented as black dots on Figures 7 and 8, and their coordinates are included in Table 3. Figure 10 is supplementary to Figure 3, and includes the whole April period for the monitoring points. As we can see, satellite coverage in the Cancún area was less than for the rest of the Yucatán Peninsula; white areas in Figure 9 are those without satellite images due to cloud cover, and in Figure 10 correspond to no data. However, the Cozumel monitoring point, which is the closest point to Cancún in Quintana Roo State, had a better coverage and satellite IOP Index, which was always between (-1, 0), which indicates non-bloom conditions. The Progreso monitoring point showed values in the interval (1, 2) which were above the average and represented decaying bloom conditions. Only during 19 to 21 April did the IOP Index exceeds 2 (2.16), indicating an active bloom. On the other hand, Campeche and Holbox showed the highest values. The IOP Index was above two during the entire month at the Campeche monitoring point, with maximum values from 16 to 21 April (IOP index from 5.94 to 6.77). The Holbox monitoring point was above two from 13 to 27 April, with a maximum value of 9.16 from 19 to 21 April.

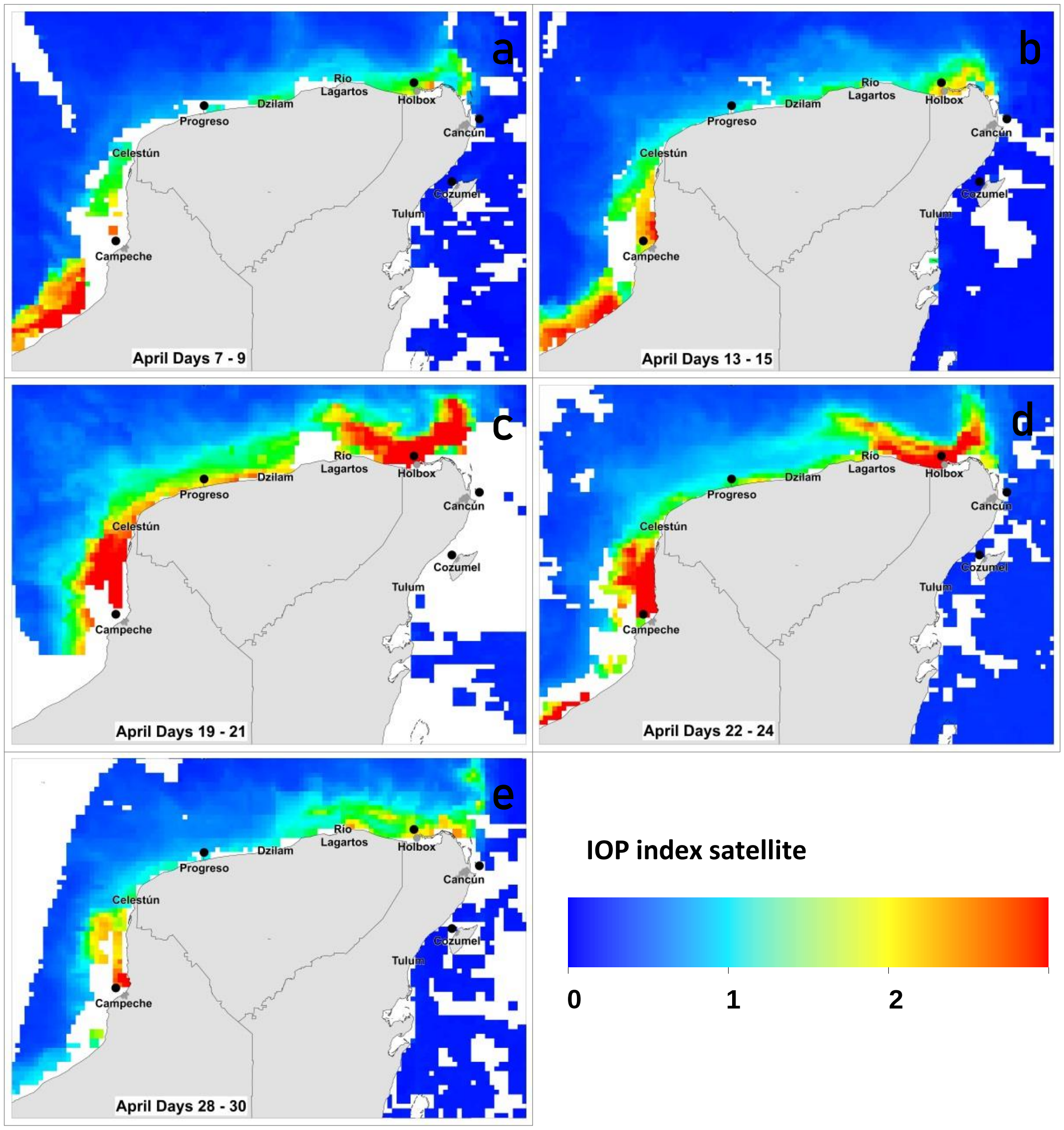

Figure 9. Satellite IOP index in the coastal waters of the Yucatán Peninsula during the dry period. White areas are not covered by satellite due to clouds. (**a**) 7 to 9 April, (**b**) 13 to 15 April, (**c**) 19 to 21 April, (**d**) 22 to 24 April and (**e**) 28 to 30 April.

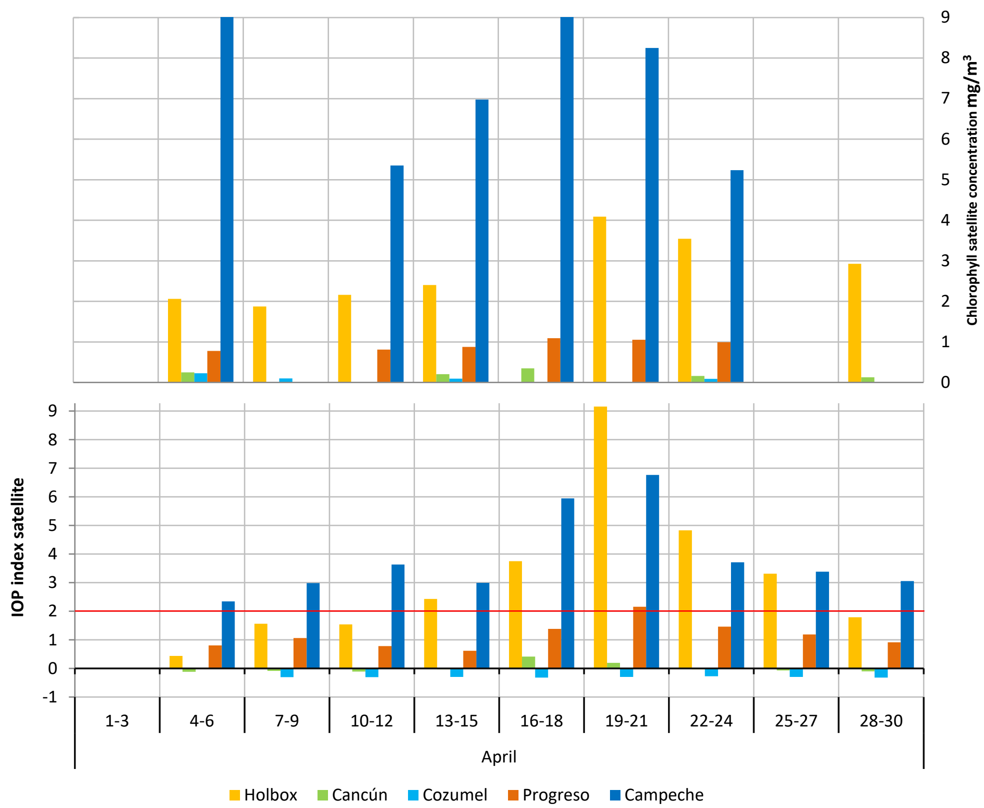

Figure 10. (**a**) chlorophyll *a* values and (**b**) satellite Inherent Optical Properties (IOP) Index in the selected monitoring points (black dots in Figure 7 and Figure 8) in April 2011. IOP index values above two indicate active bloom conditions. An absence of bars indicates that no satellite information was available due to clouds.

10 shows the relationship of the satellite IOP index with satellite chlorophyll *a*. We observe that anomalous values of the index (>2), which mean active bloom conditions are characterized by the highest chlorophyll *a* concentrations. In Campeche region, all points with an IOP index value above two had chlorophyll *a* concentrations between 5 to 9 mg/m^3. In

Holbox, points classified as in active bloom had chlorophyll *a* concentrations between 2 to 4 mg/m^3. Due to clouds not all monitoring points had chlorophyll *a* data for the whole study period, this is reflected in the absence of bars in Figure 10 for those data.

Figure 11 illustrates sea surface temperature in the coastal waters of the Yucatán Peninsula during the dry period. A cooler water mass can be observed in the northern region approximately from Progreso to Holbox, while in the east a warmer water mass predominated. It can be seen that the satellite IOP Index is related to the movement of water masses. In general, cooler waters from the Gulf of Mexico are associated with anomalous values.

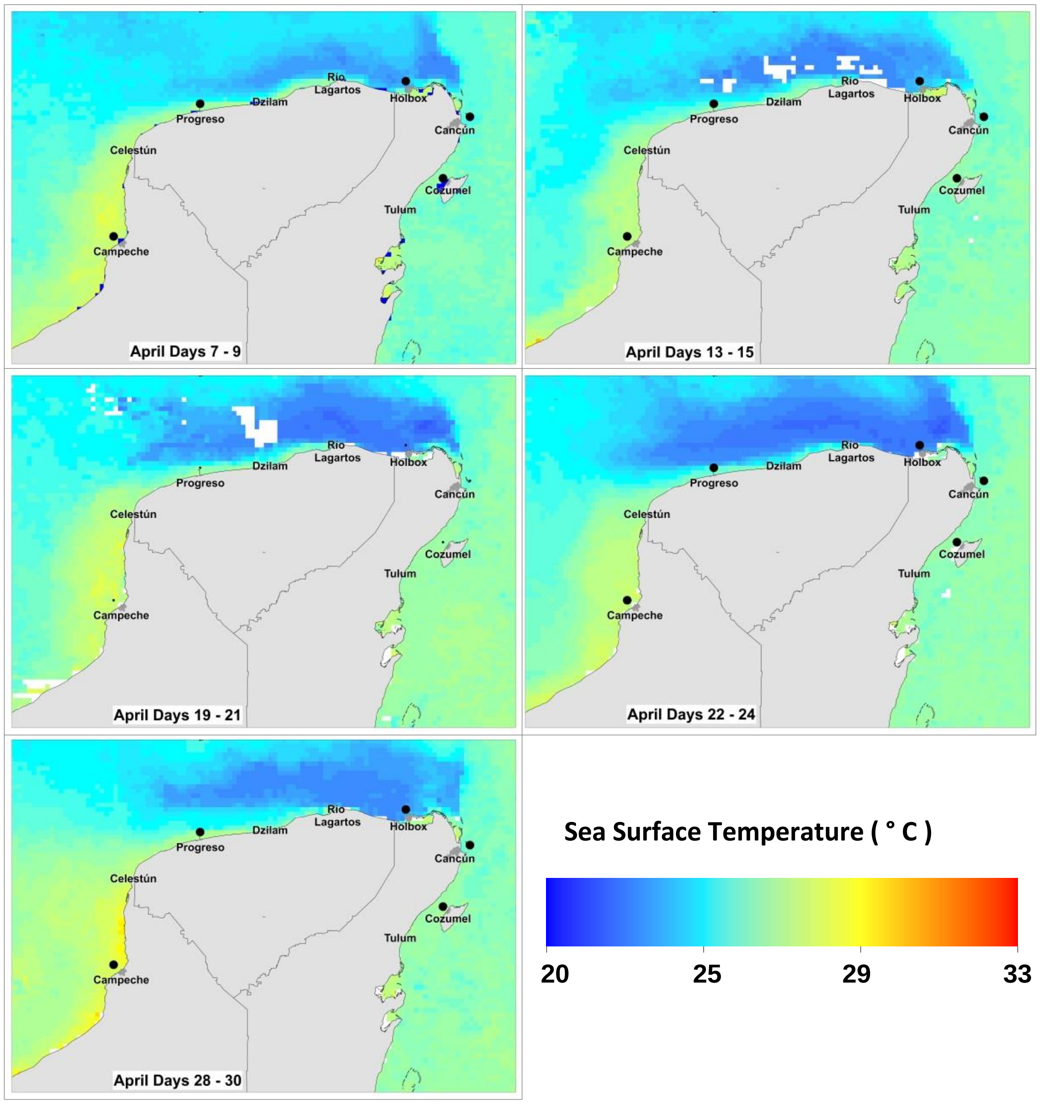

Figure 11. Sea surface temperatures in the coastal waters of the Yucatán Peninsula during the dry period. (**a**) 7 to 9 April, (**b**) 13 to 15 April, (**c**) 19 to 21 April, (**d**) 22 to 24 April and (**e**) 28 to 30 April.

In Figure 12, we represent a selection for the wet period (i.e., June–August 2011) which coincides with summer and the highest visitor number period. June was the rainiest month according to SMN (National

Meteorological Service) [53], with a 234.3 mm average precipitation. During this period, the entire coastal area of the Yucatán and Campeche states, and the Holbox area (Quintana Roo), show satellite IOP Index values higher than two, depicted by a yellow to red color scale (Figure 12). As in April, no phytoplankton bloom was detected in the southern coastal region of Quintana Roo State, which includes the Cozumel and Cancún municipalities (Figure 12).

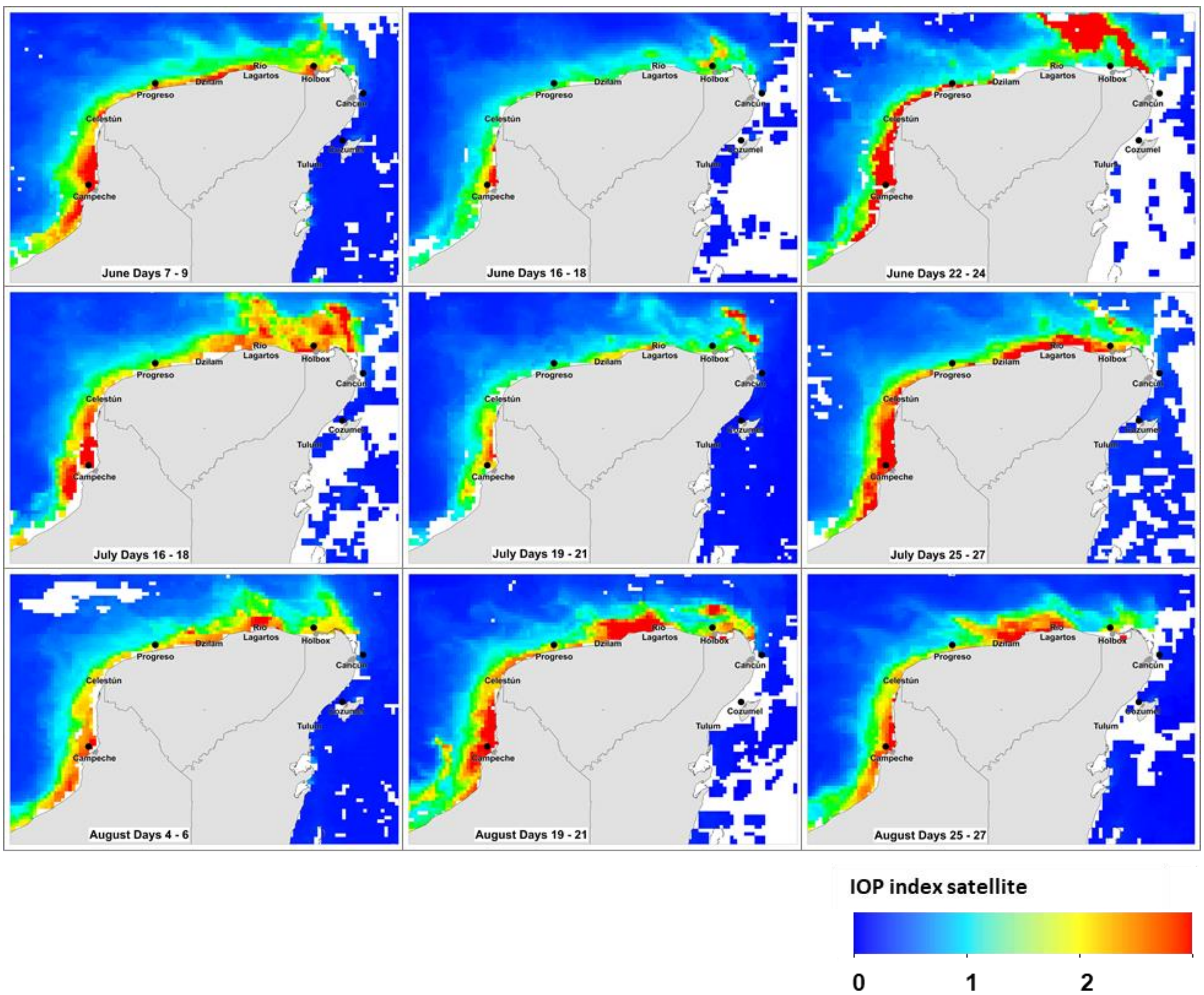

Figure 12. Satellite IOP index in the coastal waters of the Yucatán Peninsula during the wet period. White areas are not covered by satellite due to clouds. (**a**) 7 to 9 June, (**b**) 16 to 18 June, (**c**) 22 to 24 June, (**d**) 16 to 18 July, (**e**) 19 to 21 July, (**f**) 25 to 27 July, (**g**) 4 to 6 August, (**h**) 19 to 21 August and (**i**) 25 to 27 August.

Figure 13, Figure 14 and Figure 15 are supplementary to Figure 12, and include the whole June to August period for the selected monitoring points. During the wet period, Cancún and Cozumel remained in the interval (−1, 1) which represents the average value for the CS-LME, and represents non-bloom conditions. At the Progreso monitoring point, which was in the interval (1, 2) in June, showed IOP index values above two from 4 to 12 June (Figure 13), and punctually between 16 to 18 July (Figure 14), and from 13 to 15 August (Figure 15). Holbox was in bloom conditions mainly during the first June fortnight (Figure 13) and the second July fortnight (Figure 14), but also for some days in August (Figure 15, 4 to 9 August and 28 to 30 August). Campeche was in active bloom conditions (IOP Index > 2) during nearly the entire wet period (Figure 13, Figure 14 and Figure 15), and only sporadically showed values in the interval (1, 2) which represent decaying bloom conditions (e.g., Figure 13, 4 to 6 June).

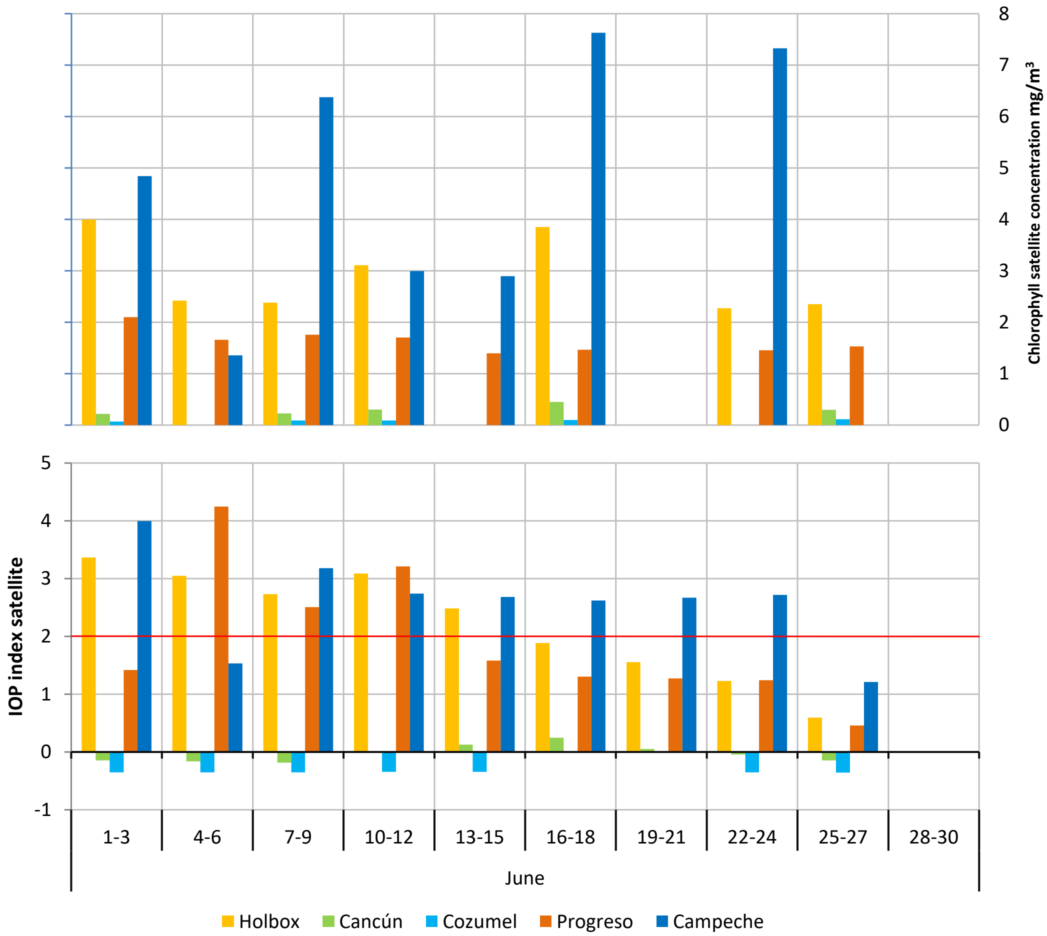

Figure 13. (**a**) Chlorophyll *a* values and (**b**) satellite IOP Index at the selected monitoring points (black dots in Figure 7 and Figure 8) June 2011. IOP Index values above two indicate active bloom conditions. An absence of bars indicates that no satellite information was available due to clouds.

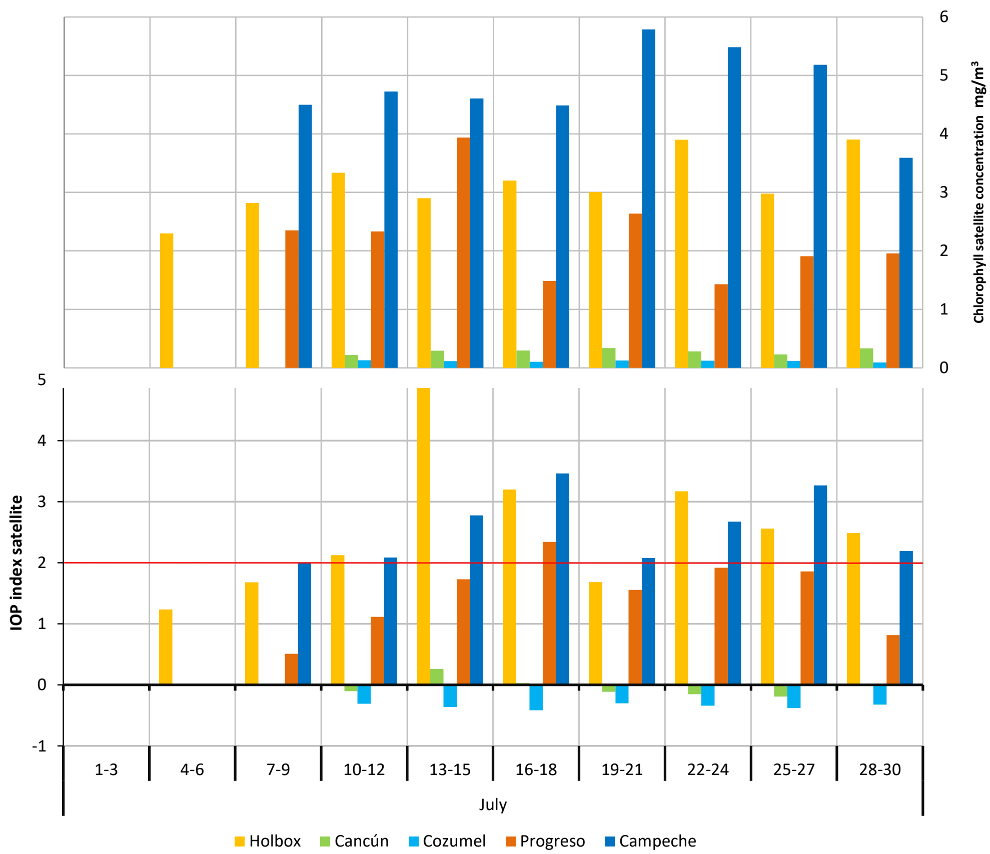

Figure 14 (**a**) Chlorophyll *a* values and (**b**) satellite IOP Index at the selected monitoring points (black dots on Figure 7 and Figure 8) July 2011. IOP Index values above two indicate active bloom conditions. An absence of bars indicates no satellite information was available due to clouds.

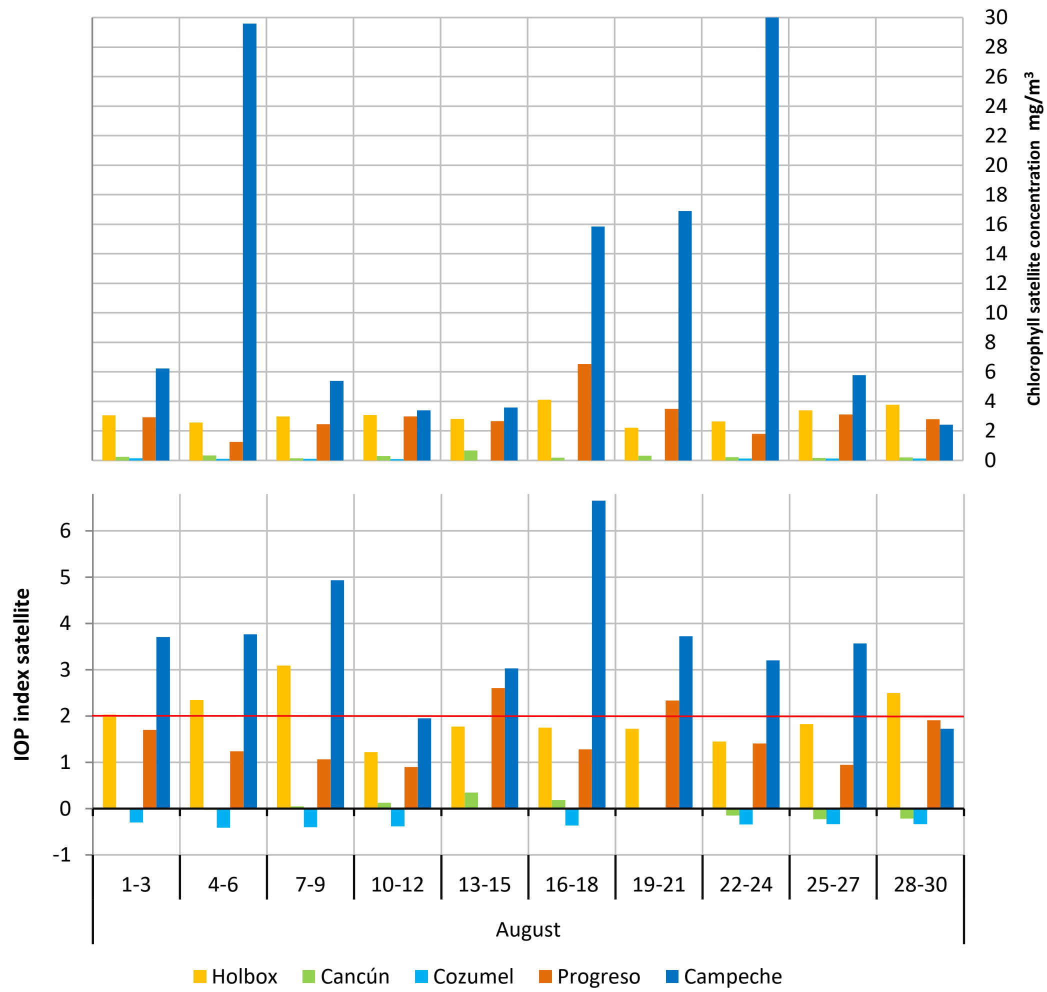

Figure 15. (**a**) Chlorophyll *a* values and (**b**) satellite IOP Index at the selected monitoring points (black dots on Figure 7 and Figure 8) August 2011. IOP Index values above two indicate active bloom conditions. An absence of bars indicates no satellite information was available due to clouds.

In these same figures, chlorophyll *a* concentrations are shown. The anomalous values of the IOP Index are associated with the highest chlorophyll *a* concentrations. In the Campeche region, all points with an IOP

Index value above two had chlorophyll *a* concentrations approximately between 3 to 30 mg/m^3. The highest chlorophyll *a* concentrations were detected in August. Higher concentrations of chlorophyll *a* than in the dry period were observed. In Holbox, points classified as in active bloom had chlorophyll *a* concentrations between 2 to 4 mg/m^3.

The satellite IOP Index is based on the three optically important components of water, not just phytoplankton. Sometimes, high values of chlorophyll *a* are linked to low IOP Index values close to the threshold between active bloom and decaying bloom conditions. This is because the concentration of CDOM is very high due to the degradation of organic matter, that is, the degradation of the dead phytoplankton that formed the bloom. Therefore, although the concentration of chlorophyll *a* remains high, it is considered that the bloom is in decay when the value of the IOP is less than two. A downward trend in the value of the IOP indicates an increase in the processes of degradation of organic matter or external contributions of CDM.

Figure 16 illustrates sea Surface Temperature in the coastal waters of the Yucatán Peninsula during the wet period (June to August), and a significant surface water warming was observed.

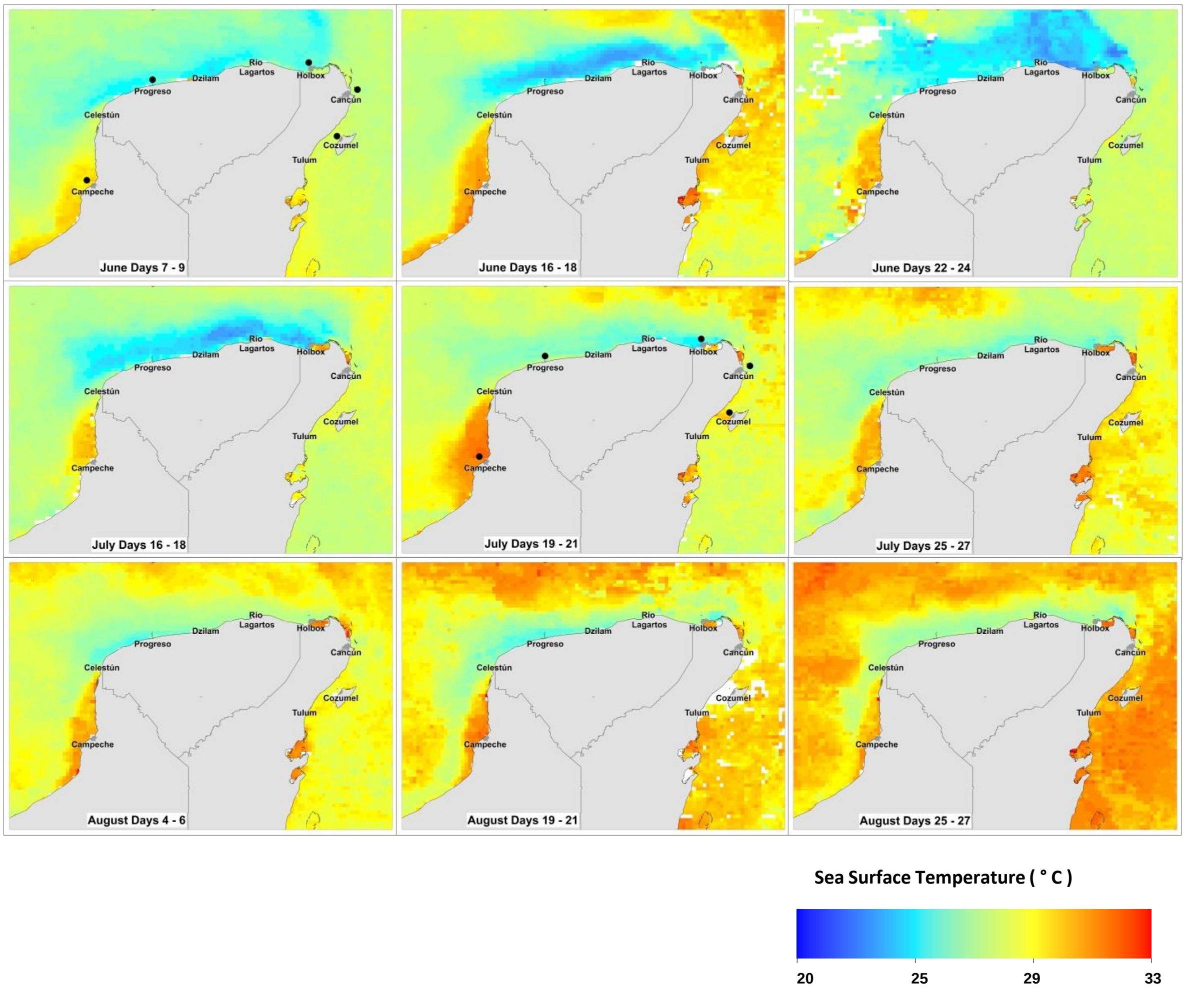

Figure 16. Sea surface temperatures in the coastal waters of the Yucatán Peninsula during the wet period. (**a**) 7 to 9 June, (**b**) 16 to 18 June, (**c**) 22 to 24 June, (**d**) 16 to 18 July, (**e**) 19 to 21 July, (**f**) 25 to 27 July, (**g**) 4 to 6 August, (**h**) 19 to 21 August and (**i**) 25 to 27 August.

4.5 Discussion

As stated by Carstensen et al. [54], “while there is no universally accepted definition of what constitutes a bloom, the notion of a substantial deviation above background phytoplankton biomass is common to all definitions". So, we can define a phytoplankton bloom as a deviation to higher values than standard seasonal patterns at a specific site. Unusual high phytoplankton biomass values can be very different between sites. For instance, Carstensen et al. [54] studied long-term monitoring data from a diverse set of marine ecosystems in North America and Northwestern Europe and observed an important difference in biomass scale between sites. The Yucatan Basin has been described as an oligotrophic region devoid of nutrients in the surface layer [16]. In the absence of phytoplankton blooms, chlorophyll *a* levels observed in this area by other studies did not exceed 1.65 mg m^{-3} [17]. Chlorophyll *a* levels above 2 mg m^{-3} have been classified as a eutrophic regime by several authors [18,19,20]. In this study, we found that chlorophyll *a* values above 2 mg m^{-3} in the Holbox area have been classified as in bloom conditions according to the IOP Index. This may seem a reduced chlorophyll *a* value, but it is not for this specific area, since it represents a substantial deviation from background values.

Biomass patterns in estuarine-coastal ecosystems can change abruptly [55]. In general, it is a recognized one seasonal pattern that starts with a spring bloom dominated by large, fast-growing diatoms, followed by a number of summer blooms comprised of diatoms, flagellates, and dinoflagellates. However, there are many deviations from this classical pattern [54]. The high variability of coastal waters promotes different strategies at different times and a unique pattern of bloom occurrence cannot be defined [56,57]. The presence of a quasi-permanent bloom in the Campeche region could be explained because of the succession of different species, and sustained due to all the processes that have been identified to trigger blooms at the land-sea interface, including coastal upwelling, wind induced entrainment of bottom water, neap-spring variability of tidal mixing and stratification, seasonal winds that enhance water retention in bays, and seasonal changes in temperature and solar radiation, among others [54]. The temporal and spatial distribution of phytoplankton blooms shown in the results section is the consequence of several factors, including both oceanographic and continental processes. Among them, upwelling events, oceanographic currents, and submarine groundwater discharges (SGDs). The northeastern coast of Yucatan is nourished by seasonal coastal upwelling events which have positive effects such as enhancing fisheries and promoting the presence of the whale shark, but also undesired effects like algal bloom events [37]. It is known to upwell during spring and summer. While upwelling could be suppressed during the northerly winds season (90–129 m/s), these winds contribute to the cooling and mixing of the water column from October to April [21,37]. In our study, we selected April, June, July, and August as the study period taking into account not only tourist activity but also these upwelling events. The surface circulation in the central portion of the Gulf is dominated by the Loop Current, where surface waters enter into the Gulf through the Yucatán channel and exit through the Florida Strait [21,58]. North of Cabo Catoche (Figure 13), a cyclonic gyre formation marks the area of most intensive upwelling in the Yucatan region. According to Pérez et al. [59], this gyre, in addition, may define a focus of convergence of upwelled and Yucatan Current waters. Another feature described by Pérez et al. [59] is a permanent countercurrent, which flows to the southwest along the slope of the Yucatan Peninsula which may be related to the upwelling-convergence processes. In Figure 11 and Figure 16, we observed that the nearest coastal stripe was characterized by more constant sea surface temperatures, and it is well marked both during the dry and wet periods. These authors [59] found high concentrations of chlorophyll, organic particles, and phytoplankton around the northeast of Cabo Catoche in the summer. These high concentrations match our results in Figure 12, where we observe high IOP Index values, due to phytoplankton blooms, in the Río Lagartos-Holbox area. In the Campeche area, inside the Gulf of Mexico, the Campeche bank has been described as one of the most important upwelling regions in the western ocean margin [60]. Both in Figure 10 and Figure 12, we can observe characteristic high IOP Index values.

Submarine groundwater discharges in the Yucatán karstic aquifer, where the aquifer is connected hydraulically with the sea, provides a direct input of nutrients such as nitrogen (N) and phosphorus (P) to coastal waters. Several authors have found evidence that water quality is strongly related to SGD, and variations in phytoplankton community structure are related to local nutrient loading and hydrographic conditions, turbulence, and human impacts [47,48]. This nutrient input is usually characterized by N:P ratios higher than 16, which is the optimal ratio for algae in coastal areas (Redfield ratio), especially in agricultural areas [61]. Groundwater quality is also influenced by the amount and distribution of precipitation [62]. Muñoz et al. [63] found higher levels of phosphate during the wet season in the Dzilam area, which is characterized by livestock uses (Figure 8). Pacheco et al. [62] found high nitrate concentrations under the biggest city in Yucatan State (Mérida) and in the agricultural zone, which cause an increase in this ratio. But, phosphorus inputs from domestic and municipal sewage can also modify the Redfield ratio. While nitrate inputs are usually linked to agriculture, phosphorus inputs can be linked to tourism, as their main source is domestic sewage [64]. However, this karst system is characterized by delayed groundwater discharge [42], and a lag may exist before peak discharge of groundwater and nutrients to the coast occurs [46]. In our results, we observed important phytoplankton blooms in the Holbox-Río Lagarto area since 19 to 24 April. This year, 2011, the spring break was from 15 March to 15 April. So, blooms in this area started approximately one month after the beginning of the maximum hotel occupation. Upwelling events also happened during spring, but it seems that the added effect of SGDs could have triggered phytoplankton blooms.

In our results we observed that phytoplankton blooms extended from Holbox (most eastern area with bloom events) to South Campeche, while no blooms were observed in the Cancún-Cozumel area. Historic COFEPRIS reports of HABs from 2003 to 2017 [10], which are represented with red dots in Figure 7, show the same spatial distribution. This can be due to the effect of the Yucatan Current, which flows into the Gulf of Mexico adjacent to the Yucatan Shelf carrying different water masses from the Caribbean and Atlantic (Figure 7 arrow indicates the Yucatán current direction). Enriquez et al. [65] already noticed that a bloom seeded in the Cabo Catoche (CC) region will move along the coast travelling westwards. During the dry period, no blooms were reported by COFEPRIS [15], although we found blooming areas in Campeche and Holbox. During the 2011 wet period, COFEPRIS [15] did report blooms. COFEPRIS [15] reported a HAB of *Scrippsiella trochoidea*, *Pleurosigma sp.*, and *Cylindrotheca closterium* between 22 July to 16 December on Río Lagartos (Yucatán state), but no sanitary closure was implemented. However, we observed satellite IOP Index values above two from 1 June in the Holbox-Río Lagartos area, which indicated an active phytoplankton bloom. The next HAB reported by COFEPRIS was on 15 October and lasted until 18 October on Holbox (Quintana Roo state). This HAB did imply the sanitary closure and the death of 4 tons of fish was quantified [15]. So, no HAB was detected in Holbox until October, but we have shown that active bloom conditions were present along the June–August period, and also after the spring break. These active bloom conditions were characterized by a high phytoplankton biomass, as corroborated by satellite chlorophyll *a* graphs included in the results section (Figure 10 and Figure 13–9). Also, the studies of References [7,23] confirm high phytoplankton biomass blooms. The Permanent Monitoring Program of Harmful Algal Blooms [10] is based not on regular monitoring but on direct observation and reporting to the authorities. The major consequence of this type of monitoring is that HAB events can go unnoticed. In addition, water color in optically complex waters depends on its three main constituents: CDM, CDOM, and chlorophyll *a* [34,35]. So, observing water color is not a confident way to detect blooms because it can confuse it with high CDM or high CDOM content. The advantage of the IOP Index is that it can discern phytoplankton biomass blooms from discoloration due to CDM or CDOM as proven by Reference [23]. The IOP Index cannot give information on phytoplankton taxonomic composition, so by its results we are not able to detect the presence of toxic species. But it has proven very useful to map blooming areas, which is essential to plan in situ sampling and optimize sampling efforts. Not all HABs produce fish mortalities as can be appreciated in COFEPRIS reports, but they have other undesired effects such as reduced water transparency. Ziegler et al. [3] identified the most important motivations for participating in the whale shark tour on Holbox as good underwater visibility and proximity to whale sharks. However, a significant proportion of tour participants were dissatisfied with underwater visibility (22.9%), the variety of marine life (20.2%), and abundance of marine life (19.5%). All these environmental features can be seriously affected by phytoplankton bloom events. Understanding tourist needs and expectations can help inform management decisions and improve the quality of services offered at a particular tourism destination.

Continuous monitoring is of paramount importance for implementing preventive and corrective measures. The use of satellite products can enhance in situ monitoring possibilities, as it offers higher spatial and temporal resolution at a lower cost [23,24,25,26]. However, these products must be used with caution. Our methodology offers a more precise technology because the satellite IOP Index has taken into account all the water constituents (i.e., phytoplankton, CDOM, and CDM) to identify an active bloom [23,36]. Other products such as the diffuse attenuation coefficient K490 (m^{-1}) is not able to distinguish active bloom conditions, because high KD490 values can be due to other water constituents rather than to chlorophyll *a* [7]. The application of the satellite IOP Index can help to build baseline information in a sustainable mid-term or long-term basis which is key for ecosystem-based management. Following the approach of Stankey et al. [6], we could use the satellite IOP Index as an indicator to determine the Limits of Acceptable Change (LAC). The first step in the process of establishing LAC is identifying desirable ecological conditions and choosing indicators of these conditions. Ecological desired conditions are IOP Index values below two, which indicate an absence of an active phytoplankton bloom. The second step is assessing current conditions, which will imply determining the location, extension, and frequency of active blooms. Long-term monitoring data is necessary to define the standard seasonal pattern of a specific site. The following steps are identifying management actions, and monitoring and evaluating those implemented management actions. The advantage of remote sensing is that due to its reduced cost, it is more feasible for implementing an economically sustainable monitoring program. Tourism satisfaction with water quality and transparency could be related to the presence of active or decaying bloom conditions which produce reduced water clarity. Natural processes, such as the Yucatán Current, avoid that the impact of tourist industry can be seen in the main tourism centers (e.g., Cancún to Tulum, in the Riviera Maya). But, this does not mean that wastewater discharges to septic tanks have no effect, it rather means that their effect is observed in areas further away (e.g., Holbox). In this framework, management actions, cannot be local actions, but must move a step forward to take into account regional processes. In this sense, remote sensing can be a useful tool in monitoring programs.

Author Contributions: J.A.A.-M., E.S.-D.-Á., and M.-T.S.-F. conceived and designed the experiments. J.A.A.-M. carried out the tests and analyses presented in the article. Both J.A.A.-M. and M.-T.S.-F. wrote the article. E.S.-D.-Á., A.G.-S., and O.D.C.-R collaborated with advisory times.

Funding: This research was funded by CONACYT with a doctorate scholarship to Jesús A. Aguilar-Maldonado, with the announcement number 251025 in 2015. María-Teresa Sebastiá-Frasquet was a beneficiary of the BEST/2017/217 post-doctoral research grant, supported by the Valencian Conselleria d'Educació, Investigació, Cultura i Esport (Spain) during her stay at the Universidad Autónoma de Baja California (Mexico). The Secretariat of Public Education of Mexico (SEP) under the Program for Professional Development Teacher, covered the costs of publication in open access.

Acknowledgments: We would like to thank the anonymous reviewers who helped to improve the original manuscript.

Conflicts of Interest: The authors declare no conflict of interest. The founding sponsors had no role in the design of the study; in the collection, analyses, or interpretation of data; in the writing of the manuscript; and in the decision to publish the results.

4.6 References

1. Bentz, J.; Lopes, F.; Calado, H.; Dearden, P. Sustaining marine wildlife tourism through linking Limits of Acceptable Change and zoning in the Wildlife Tourism Model. *Mar. Policy*, **2016**, 68, 100-107. DOI: https://doi.org/10.1016/j.marpol.2016.02.016.
2. Jarvis, D.; Stoeckl, N.; Liu, H. The impact of economic, social and environmental factors on trip satisfaction and the likelihood of visitors returning. *Tourism Manage.*, **2016**, 52, 1-18 DOI: https://doi.org/10.1016/j.tourman.2015.06.003.

3. Ziegler, J.; Dearden, P.; Rollins, R. But are tourists satisfied? Importance-performance analysis of the whale shark tourism industry on Isla Holbox, Mexico. *Tourism Manage.*, **2012**, 33 (3), 692-701. DOI: https://doi.org/10.1016/j.tourman.2011.08.004.
4. Padilla, N.S. The environmental effects of Tourism in Cancun, Mexico. *Int. J. Environ. Sci.,* **2015**, 6 (1), 282-294, DOI:10.6088/ijes.6032.
5. Duffus, D.A. & Dearden, P. Non-consumptive wildlife-oriented recreation, a conceptual framework. *Biol. Conserv*., **1990**, 53, 213 – 231. DOI: http://dx.doi.org/ 10.1016/0006-3207(90)90087-6.
6. Stankey, G.H.; McCool, S.F.; Stokes, G.L. Limits of acceptable change: a new framework for managing the Bob Marshall wilderness complex. *Western Wildlands,* **1984**,10, 33–37.
7. Aguilar-Trujillo, A.C.; Okolodkov, Y.B.; Herrera-Silveira, J.A.; Merino-Virgilio, F.D.C.; Galicia-García, C. Taxocoenosis of epibenthic dinoflagellates in the coastal waters of the northern Yucatan Peninsula before and after the harmful algal bloom event in 2011–2012. *Mar. Pollut. Bull*., **2017**, 119, 396–406. DOI: https://doi.org/10.1016/j.marpolbul.2017.02.074s
8. Ulloa, M.J.; Álvarez-Torres, P.; Horak-Romo, K.P.; Ortega-Izaguirre, R. Harmful algal blooms and eutrophication along the Mexican coast of the Gulf of Mexico large marine ecosystem. *Environ. Dev*. **2017**, 22, 120–128. DOI: 0.1016/j.envdev.2016.10.007
9. Henrichs, D. W., Hetland, R. D., & Campbell, L. Identifying bloom origins of the toxic dinoflagellate Karenia brevis in the western Gulf of Mexico using a spatially explicit individual-based model. *Ecological modelling*, **2015**, 313, 251-258. https://doi.org/10.1016/j.ecolmodel.2015.06.038
10. Murray, G. Constructing Paradise: The Impacts of Big Tourism in the Mexican Coastal Zone. *Coast Manage*, **2007**, 35, 339–355, DOI: 10.1080/08920750601169600.
11. Castillo-Pavón, O. & Méndez-Ramírez, J.J. The tourist developments and their environmental effects in the Mayan Riviera, 1980-2015. *Quivera*, **2017**, 19 (2), 101-118.
12. Heisler,J.; Glibert, P.M,; Burkholder, J.M.; Anderson, D.M.; Cochlan, W.; Dennison, W.C.; Dortch, Q.; Gobler, C.J.; Heil, C.A.; Humphries, E.; Lewitus, A.; Magnien, R.;

Marshall, H.G.; Sellner, K.; Stockwell, D.A.; Stoecker, D.K.; Suddleson, M. Eutrophication and harmful algal blooms: A scientific consensus. *Harmful Algae*, **2008**, 8 (1), 3-13, https://doi.org/10.1016/j.hal.2008.08.006.

13. Smayda, T. J. Complexity in the eutrophication–harmful algal bloom relationship, with comment on the importance of grazing. *Harmful Algae*, **2008**, 8(1), 140-151. https://doi.org/10.1016/j.hal.2008.08.018
14. Klemas, V. Remote sensing of algal blooms: An overview with case studies. *J. Coast. Res*., **2012**, 28(1), 34-43. DOI: 10.2112/JCOASTRES-D-11-00051.1
15. COFEPRIS (Comisión Federal para la Protección contra Riesgos Sanitarios/ Federal Commission for Protection against Health Risks) Available online: https://www.gob.mx/cofepris/acciones-y-programas/antecedentes-en-mexico-76707 (accessed on 09/03/2018)
16. Okolodkov, Y. B. A review of Russian plankton research in the Gulf of Mexico and the Caribbean Sea in the 1960-1980s. *Hidrobiológica*, **2003**. 13(3), 207-221.
17. Signoret, M., Bulit, C., & Pérez, R. Patrones de distribución de clorofila ay producción primaria en aguas del Golfo de México y del Mar Caribe. *Hidrobiológica*, **1998**. 8(2), 81-88.
18. Antoine, D., & Morel, A. Oceanic primary production: 1. Adaptation of a spectral light-photosynthesis model in view of application to satellite chlorophyll observations. *Global biogeochemical cycles*, **1996**. 10(1), 43-55. DOI: https://doi.org/10.1029/95GB02831
19. Barocio-León, Ó. A., Millán-Núñez, R., Santamaría-del-Ángel, E., González-Silvera, A., & Trees, C. C. Spatial variability of phytoplankton absorption coefficients and pigments off Baja California during November 2002. *Journal of oceanography*, **2006**. 62(6), 873-885. DOI: https://doi.org/10.1007/s10872-006-0105-z
20. Smith, V. H., Tilman, G. D., & Nekola, J. C. Eutrophication: impacts of excess nutrient inputs on freshwater, marine, and terrestrial ecosystems. *Environmental pollution*, **1999**. 100(1-3), 179-196. DOI: https://doi.org/10.1016/S0269-7491(99)00091-3
21. Limoges, A.; Londeix, L.; de Vernal, A. Organic-walled dinoflagellate cyst distribution in the Gulf of Mexico. *Mar. Micropaleontol.*, **2013**, 102, 51-68. DOI: https://doi.org/10.1016/j.marmicro.2013.06.002

22. Jiang, L., Xia, M., Ludsin, S.A, Rutherford, E.S., Mason, D.M., Pangle, K.L., Marin Jarrin, J.R. Biophysical modeling assessment of the drivers for plankton dynamics at western Lake Erie. *Ecological Modelling*, **2015**, 308, 18-33.
23. Aguilar-Maldonado, J.A.; Santamaría-del-Ángel, E.; González-Silvera, A.; Cervantes-Rosas, O.; López, L.M.; Gutiérrez-Magness, A.; Cerdeira-Estrada, S.; Sebastiá-Frasquet, M.T. Identification of Phytoplankton Blooms under the Index of Inherent Optical Properties (IOP Index) in Optically Complex Waters. *Water,* **2018**, *10*(2), 129; doi:10.3390/w10020129
24. Sebastiá Frasquet, MT.; Estornell Cremades, J.; Rodilla Alamá, M.; Marti Gavila, J.; Falco Giaccaglia, SL. Estimation of chlorophyll «A» on the Mediterranean coast using a QuickBird image. *Revista de Teledetección*, **2012**, 37, 23-33. http://hdl.handle.net/10251/36141
25. Caroppo, C.; Odermatt, D.; Philipson, P.; Bruno, M. Using satellite remote sensing of harmful algal blooms (HABs) in a coastal European site. *Phycologia*, **2017**, *56*(4), 28.
26. Wei, G.; Tang, D.; Wang, S. Distribution of chlorophyll and harmful algal blooms (HABs): A review on space based studies in the coastal environments of chinese marginal seas. *Advances in Space Research,* **2008**, *41*(1), 12-19. DOI: http://dx.doi.org/10.1016/j.asr.2007.01.037
27. Urquhart, E.A.; Schaeffer, B.A.; Stumpf, R.P.; Loftin, K.A.; Werdell, P.J. A method for examining temporal changes in cyanobacterial harmful algal bloom spatial extent using satellite remote sensing, *Harmful Algae,* **2017**, 67, 144-152, DOI: https://doi.org/10.1016/j.hal.2017.06.001.
28. Harvey, E. T., Kratzer, S., & Philipson, P. Satellite-based water quality monitoring for improved spatial and temporal retrieval of chlorophyll-a in coastal waters. *Remote Sensing of Environment*, **2015**,158, 417-430
29. Malthus, Tim J., and Peter J. Mumby. "Remote sensing of the coastal zone: an overview and priorities for future research." **2003**: 2805-2815.
30. Matthews, M. W. A current review of empirical procedures of remote sensing in inland and near-coastal transitional waters. *International Journal of Remote Sensing*, **2011**, 32(21), 6855-6899.

31. Miller, R. L., & McKee, B. A. Using MODIS Terra 250 m imagery to map concentrations of total suspended matter in coastal waters. *Remote sensing of Environment*, **2004**, 93(1-2), 259-266.
32. Loisel, H.; Vantrepotte, V.; Norkvist, K.; Mériaux, X.; Kheireddine, M.; Ras, J.; Pujo-Pay, M.; Combet, Y.; Leblanc, K.; Dall'Olmo, G.; et al. Characterization of the Bio-Optical Anomaly and Diurnal Variability of Particulate Matter, as Seen from Scattering and Backscattering Coefficients, in Ultra-Oligotrophic Eddies of the Mediterranean Sea. *Biogeosciences* **2011**, 8, 3295–3317.
33. Werdell, P. J.; Franz, B. A.; Bailey, S. W.; Feldman, G. C.; Boss, E., Brando, V. E.; Dowell, M.; Hirata, T.; Lavender, S. J.; Lee, Z.; Loisel, H.; Maritorena, S.; Mélin, F.; Moore, T. S.; Smyth, T. J.; Antoine, D. A.; Devred, E.; Fanton d'Andon, O. H.; Mangin, A. Generalized ocean color inversion model for retrieving marine inherent optical properties. *Applied optics*, **2013**, 52(10), 2019-2037. DOI: https://doi.org/10.1364/AO.52.002019
34. Brezonik, P. L., Olmanson, L. G., Finlay, J. C., & Bauer, M. E. Factors affecting the measurement of CDOM by remote sensing of optically complex inland waters. *Remote Sensing of Environment*, **2015**, 157, 199-215.
35. Odermatt, D., Gitelson, A., Brando, V. E., & Schaepman, M.. Review of constituent retrieval in optically deep and complex waters from satellite imagery. *Remote sensing of environment*, **2012**, 118, 116-126. https://doi.org/10.1016/j.rse.2011.11.013
36. Santamaría-del-Angel, E.; Soto, I.; Millán-Nuñez, R.; González-Silvera, A.; Wolny, J.; Cerdeira-Estrada, S.; Cajal-Medrano, R.; Muller-Karger, F.; Cannizzaro, J.; Padilla-Rosas, Y.; et al. Experiences and Recommendations for Environmental Monitoring Programs. In *Environmental Science, Engineering and Technology*; Sebastia-Frasquet, M.-T., Ed.; Nova Science Publishers: Hauppauge, NY, USA, **2015**; p. 32. ISBN 978-1-63482-189-6.
37. Enriquez, C.; Mariño-Tapia, I.; Jeronimo, G.; Capurro-Filograsso, L. Thermohaline processes in a tropical coastal zone. *Cont Shelf Res.,* **2013**, 69, 101-109. DOI: https://doi.org/10.1016/j.csr.2013.08.018
38. García, E. Modificaciones al sistema climático de Köppen para la República Mexicana. 5ta Edición. Publisher: *Instituto de Geografía*, UNAM, Ciudad de Mexico, Mexico, **2004**, ISBN 970-32-1010-4

39. CONAGUA (Comisión Nacional del Agua/ National Water Comission). **2016.** Estadísticas del Agua en México. Secretaría de Medio Ambiente y Recursos Naturales. Available online: http://201.116.60.25/publicaciones/EAM_2016.pdf (accessed on 2 February 2018).
40. Arcega-Cabrera, F.; Garza-Pérez, R.; Noreña-Barroso, E.; Oceguera-Vargas, I. Impacts of geochemical and environmental factors on seasonal variation of heavy metals in a coastal lagoon Yucatan, Mexico. *Bull Environ Contam Toxicol*., **2015,** 94(1), 58-65. doi: 10.1007/s00128-014-1416-1
41. Lopez-Maldonado, Y.; Batllori-Sampedro, E.; Binder, C.R.; Fath, B.D. Local groundwater balance model: stakeholders' efforts to address groundwater monitoring and literacy, *Hydrolog Sci J.*, **2017**, 62 (14), 2297-2312. DOI: 10.1080/02626667.2017.1372857
42. Derrien, M.; Arcega-Cabrera, F.; Velazquez Tavera, N.L.; Kantún Manzano, C.A.; Capella Vizcaino, S. Sources and distribution of organic matter along the Ring of Cenotes, Yucatan, Mexico: Sterol markers and statistical approaches. *Science of The Total Environment*, **2015**, 511, 223-229, DOI: https://doi.org/10.1016/j.scitotenv.2014.12.053
43. Marin, L.E.; Steinich, B.; Pacheo, J.; Escolero, O.A. Hydrogeology of a contaminated sole-source karst aquifer, Merida, Yucatan, Mexico. *Geofís. Int*., **2000** 39, 359–365. http://www.redalyc.org/pdf/568/56839406.pdf
44. INEGI. Available online: http://www.beta.inegi.org.mx/temas/agua/ (accessed on 09/03/2018)
45. Ramírez, R.R.; Seeliger, L.; Di Pietro, F. Price, Virtues, Principles: How to Discern What Inspires Best Practices in Water Management? A Case Study about Small Farmers in the Yucatan Peninsula of Mexico. *Sustainability*, **2016**, 8, 385; doi:10.3390/su8040385
46. Null, K.A.; Knee, K.L.; Crook, E.D.; de Sieyes, N.R.; Rebolledo-Vieyra, M.; Hernández-Terrones, L.; Paytan, A. Composition and fluxes of submarine groundwater along the Caribbean coast of the Yucatan Peninsula, *Cont Shelf Res.*, **2014**, 77, 38-50. DOI: https://doi.org/10.1016/j.csr.2014.01.011.
47. Alvarez-Gongora, C., & Herrera-Silveira, J. A. Variations of phytoplankton community structure related to water quality trends in a tropical karstic coastal zone. *Marine pollution bulletin*, **2006**, 52(1), 48-60.

48. Carruthers, T. J. B., Van Tussenbroek, B. I., & Dennison, W. C. Influence of submarine springs and wastewater on nutrient dynamics of Caribbean seagrass meadows. *Estuarine, Coastal and Shelf Science*, **2005**, 64(2-3), 191-199.
49. Monterrubio, J.; Sosa, P.; Josiam, B. Spring Break and social impact in Cancun, Mexico: A study for tourism management. *Turismo y Sociedad,* **2014**, 15, 149-166. https://papers.ssrn.com/sol3/papers.cfm?abstract_id=2646714
50. Lee, Z. P., Du, K. P., & Arnone, R. A model for the diffuse attenuation coefficient of downwelling irradiance. *Journal of Geophysical Research: Oceans*, **2005**, 110(C2).
51. Gordon, H. R.; O. B. Brown; R. H. Evans; J. W. Brown; R. C. Smith; K. S. Baker, and D. K. Clark. A semianalytic radiance model of ocean color. *J. Geophys. Res*., **1988**, 93(D9), 10909–10924, DOI:10.1029/JD093iD09p10909
52. Roesler Collin S.; Perry M. J.; Carder Kendall L. Modeling in situ phytoplankton absorption from total absorption spectra in productive inland marine waters. *Limnology and Oceanography*, **1989**, 34, 1510-1523. DOI: 10.4319/lo.1989.34.8.1510
53. SMN (Servicio Meteorológico Nacional/ National Metereological Service). 2018. Available online: http://smn.cna.gob.mx/es/climatologia/temperaturas-y-lluvias/resumenes-mensuales-de-temperaturas-y-lluvias (accessed on 09/03/2018)
54. Carstensen, J., Klais, R., & Cloern, J. E. Phytoplankton blooms in estuarine and coastal waters: Seasonal patterns and key species. Estuarine. *Coastal and Shelf Science*, 162, 98-109. DOI: https://doi.org/10.1016/j.ecss.2015.05.005
55. Winder, M. and Cloern, J.E. The annual cycles of phytoplankton biomass. *Philos. Trans. R. Soc. B: Biol Sci*. **2010**. 365, 3215-3226. DOI: 10.1098/rstb.2010.0125.
56. Cloern, J.E. and Jassby, A. Complex seasonal patterns of primary producers at the land-sea interface. *Ecol. Lett.* **2008**. 11, 1294-1303. DOI: https://doi.org/10.1111/j.1461-0248.2008.01244.x
57. Margalef, R. Life-forms of phytoplankton as survival alternatives in an unstable environment. *Oceanologica acta*, **1978**. 1(4), 493-509.
58. Athié, G.; Candela, J.; Sheinbaum, J.; Badanf, A.; Ochoa, J. Yucatán Current variability through the Cozumel and Yucatán channels. *Ciencias Marinas*, **2011**, 37(4A), 471-492. DOI: http://www.scielo.org.mx/scielo.php?script=sci_arttext&pid=S0185-38802011000400008

59. Pérez, R., Muller-Karger, F. E., Victoria, I., Melo, N., & Cerdeira, S. Cuban, Mexican, US researchers probing mysteries of Yucatan current. Eos, *Transactions American Geophysical Union*, **1999**, 80(14), 153-158.
60. Merino, M. Upwelling on the Yucatán Shelf: hydrographic evidence *J. Mar. Syst*., 1997, 101-121
61. Beusen, A. H. W.; Slomp, C. P.; bouwman, A. F. Global land–ocean linkage: direct inputs of nitrogen to coastal waters via submarine groundwater discharge. *Environ. Res. Lett.*, **2013**, vol. 8, 3, 34-35. https://doi.org/10.1088/1748-9326/8/3/034035
62. Pacheco-Castro, R.; Pacheco Avila; J.; Ye, M.; Cabrera Sansores, A. Groundwater Quality: Analysis of Its Temporal and Spatial Variability in a Karst Aquifer. *Groundwater*, **2018**, 56 (1), 62–72. https://doi.org/10.1111/gwat.12546
63. Muñoz, J., Freile-Pelegrín, Y., & Robledo, D. Mariculture of Kappaphycus alvarezii (Rhodophyta, Solieriaceae) color strains in tropical waters of Yucatán, México. *Aquaculture*, **2004**, 239(1-4), 161-177.
64. Sebastiá- Frasquet, M. T.; Rodilla, M.; Sanchis, J.A.; Altur, V.; Gadea, I.; Falco, S. Influence of nutrient inputs from a wetland dominated by agriculture on the phytoplankton community in a shallow harbour at the Spanish Mediterranean coast. *Agric. Ecosyst. Environ.*, **2012,** 152, 10-20. DOI: https://doi.org/10.1016/j.agee.2012.02.006.
65. Derrien, M.; Arcega-Cabrera, F.; Velazquez Tavera, N.L.; Kantún Manzano, C.A.; Capella Vizcaino, S. Sources and distribution of organic matter along the Ring of Cenotes, Yucatan, Mexico: Sterol markers and statistical approaches. *Science of The Total Environment*, **2015**, 511, 223-229, DOI: https://doi.org/10.1016/j.scitotenv.2014.12.053
66. Enriquez, C.; Mariño-Tapia, I. J.; Herrera-Silveira, J.A. Dispersion in the Yucatan coastal zone: implications for red tide events. *Cont Shelf Res*., **2010**, 30, 127–137. DOI: https://doi.org/10.1016/j.csr.2009.10.005

5. Capítulo Tercero.

Detection of phytoplankton temporal anomalies based on satellite Inherent Optical Properties: a tool for monitoring phytoplankton blooms

5.1 Abstract

The definition of the baseline determines the most usual behavior of any variable under study, from data series that are representative of spatial and temporal variability. The objective of this study was to define the baseline of satellite absorption coefficients in Todos Santos Bay (Baja California, Mexico) to determine the presence of phytoplankton blooms based on the satellite Inherent Optical Properties index (IOP index). Two pixels (1 km) or sampling points were selected based on historical bloom reports. To account for temporal variability, the data of phytoplankton absorption coefficients ($\boldsymbol{a_{phy,_{GIOP}}}$) and colored detritus matter (CDM) plus colored dissolved organic matter (CDOM) ($\boldsymbol{a_{dCDOM,_{GIOP}}}$) from the Generalized Inherent Optical Property (GIOP) satellite model of the NASA Moderate Resolution Imaging Spectroradiometer (MODIS) Aqua sensor was studied for the period 2003 to 2016. In situ sampling data taken during a phytoplankton bloom event on June 2017 was used to validate the use of satellite products. Correlation between in situ and satellite phytoplankton absorption coefficient was 0.809, while correlation between in situ and satellite CDM plus CDOM absorption coefficient was 0.671. The satellite IOP index methodology proposed in this study can be a supplementary tool for permanent

in situ monitoring programs. This methodology offers several advantages: a complete spatial coverage of the specific coastal area under study, appropriate temporal resolution and a tool for building an objective baseline to detect deviation from normal conditions during phytoplankton bloom events.

Keywords: satellite images; absorption coefficients; phytoplankton blooms; MODIS; Todos Santos Bay; Pacific Ocean

5.2 Intoduction

There is a need to develop more effective coastal monitoring programs with proper temporal and spatial coverage. The detection of algal blooms is one of the key issues in these monitoring programs. Phytoplankton blooms are proliferation events of micro-algal organisms in an aquatic environment. They can be quick events that start and end within a few days or can stay for several weeks (Barocio-Leon et al., 2008). In recent years, remote sensing technology has been postulated as an adequate tool for providing a synoptic view of extensive ocean or coastal areas, that is effective in complementing in situ sampling programs (Sebastiá et al. 2012a). Chlorophyll *a* (Chl*a*) has been widely used as a proxy for phytoplankton biomass. However, the term bloom is a relative concept, because it characterizes events with very different biomass concentrations. Phytoplankton blooms can occur even at extremely low Chl*a* levels (<0.1 mg m^{-3}) complicating their detection (Blondeau-Patissier et al., 2014). Harmful Algal Blooms (HABs) can produce toxins such as okadaic acid which causes the Diarrheic Shellfish Poisoning (DSP) or domoic acid which causes the Amnesic Shellfish Poisoning (ASP). However, the number of phytoplankton cells necessary for reaching toxic levels is also highly variable, such as only 200 cel/l of *Dinophysis* sp. (DSP), 1,000 cel/l of *Alexandrium* spp (PSP) or 50,000 cel/l *Pseudonitzchia* spp (ASP) (Andersen, 1996). Thus, many toxic or harmful events occur at very low biomass and can occur without noticeable changes in water color due to low cell density.

Different bloom definitions have arisen pointing out this variability. For example, Blondeau-Patissier et al. (2014) defined a phytoplankton bloom as “a biological event composed of micro-algal species that is sustained both over time and space and that results in noticeable changes in satellite radiances at wavelengths used for algal bloom proxies due to an increase in biomass (in comparison to surrounding algal bloom-free waters). Aguilar-Maldonado et al. (2018b) defined it as “a deviation to higher values than standard seasonal patterns at a specific site”. Changes in phytoplankton production, abundance and dynamics, as well as patterns, trends and cycles are difficult to detect and quantify. So to define the change, it is required to know the baseline conditions of the phytoplankton properties (Smayda et al., 2004).

Different approaches have been followed to identify the presence of algal blooms from ocean color data. A complete review can be found at Blondeau-Patissier et al. (2014). Among them bio-optical models, which are based on fundamental theories of marine optics are considered as one of the most robust ones (Garver and Siegel, 1997; Morel, 2001). Specially in optically complex waters, such as coastal waters, where optically active constituents (colored dissolved organic matter (CDOM), detritus) show their own patterns during algal bloom conditions (Blondeau-Patissier et al. 2014). Recent findings using inherent optical properties (IOPs) from bio-optical models for the detection of algal blooms point the use of phytoplankton absorption coefficient instead of Chl*a* because the latter can be affected by non-biotic optically active material (CDOM and detritus) (Goela et al. 2013). The use of IOPs from remote sensing technology may allow long-time monitoring at moderate- or high-spatial resolution and high-temporal resolution, which is essential to draw the baseline of a specific region and detect deviation.

The first objective of this study was to build the temporal baseline of phytoplankton absorption coefficient ($\boldsymbol{a_{phy,GIOP}}$) and detritus plus colored dissolved organic matter (CDOM) ($\boldsymbol{a_{dCDOM,GIOP}}$) absorption coefficients in Todos Santos Bay (Baja California, Mexico). The final aim was to develop a remote sensing monitoring methodology to determine the presence of algal blooms based on the satellite Inherent Optical Properties index (IOP index) based on deviations from the baseline. The absorption coefficients were obtained from the Generalized Inherent Optical Property (GIOP), satellite model of the NASA Moderate Resolution Imaging Spectroradiometer (MODIS).

5.3 Materials and Methods

5.3.1 Study Area

Todos Santos Bay (TSB) is a semi-enclosed bay located on the northwestern Pacific coast of Baja California state (Mexico), approximately 100 km south of the Mexico–USA border (Figure 17). The bay is limited to the north by Punta San Miguel and to the south by Punta Banda. Surface water characteristics in this area are closely related to the California Current System (CCS), which produces the upwelling of cold and nutrient-rich subsurface water along the coast of the Baja California peninsula. The predominant circulation pattern is a southeastern flux into the bay, except when there is a change of flow direction to the northeast, Punta Banda, which induces surface water to flow out of the bay (Peña-Manjarrez et al. 2009). Primary productivity in TSB is characteristically high (Cepeda-Morales et al. 2018; Millán-Núñez et al. 2014). The city of Ensenada (228 km^2, 466,815 inhabitants according to the last population census (INEGI, 2010)) is located to the east of the bay. The Ensenada Harbor is one of the most important harbors in the Mexican Pacific. Aquaculture activities of high economic importance are carried out inside or near the bay, among them, tuna fattening and the cultivation of bivalve mollusks (such as oyster, clam, mussels, mule paw and ax callus).

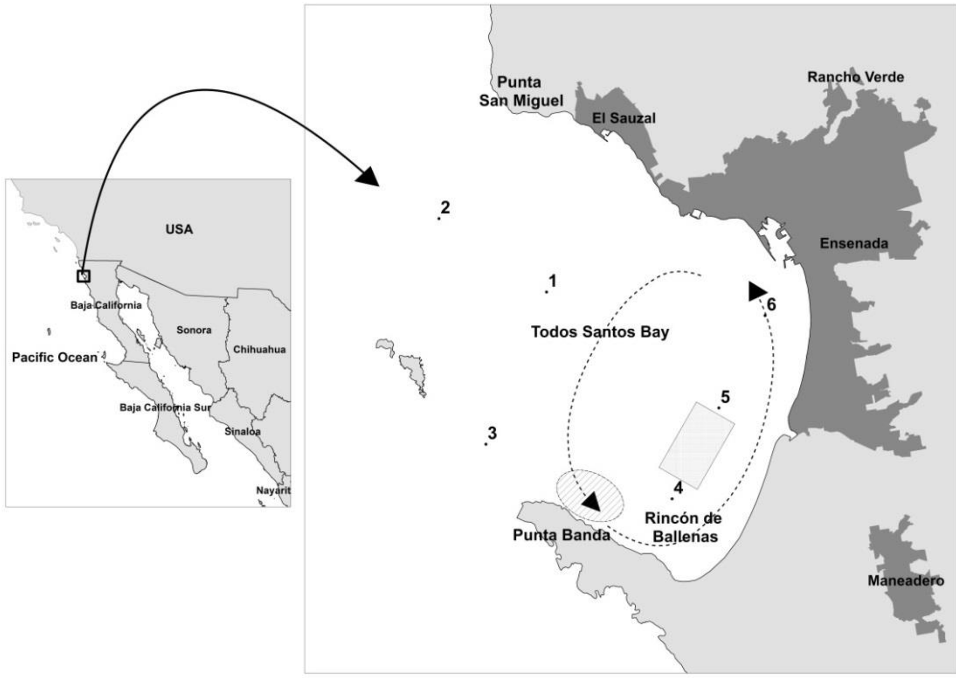

Figure 17. Location of sampling points in Todos Santos Bay (Baja California, Mexico). Sampling points are numbered 1 to 6. The rectangle shows the bivalve mollusks cultivation area and the oval the tuna fattening area. Dashed lines and arrows indicate predominant circulation pattern.

TSB is characterized by a dominance of diatoms during the upwelling season (spring - summer), which alternates with a dominance of dinoflagellates when nutrients are depleted (Almazán-Becerril et al. 2016). Recurrent dinoflagellate blooms have been observed since at least 1901 (Peña-Manjarrez et al. 2009). However, dinoflagellate algal bloom (DAB) events in this area have increased considerably in extension and frequency over the past two decades (Gutierrez-Mejia et al., 2016). Several species that produce toxins have been detected (*Pseudo-nitzschia* spp, *Dinophysis* spp, etc.) (Almazán-Becerril et al. 2016).

Pseudo-nitzschia causes the toxic syndrome of amnesic shellfish poisoning, caused by domoic acid (DA), which has caused massive mortalities of marine mammals and sea birds, especially in California state (United States) (García-Mendoza et al 2009). The dinoflagellate *Ceratium furca* caused the mass death of bluefin tuna (*Thunnus orientalis*) from tuna farms located 15 miles from Todos Santos Bay, with losses of 12-15 million dollars (Orellana-Zepeda et al., 2004).

The Mexican Federal Commission for Protection against Health Risks Historic (COFEPRIS, in Spanish Comisión Federal para la Protección contra Riesgos Sanitarios) has public reports of HABs since 2003 (COFEPRIS, 2018). In TSB recurrent blooms are detected in Rincón de Ballenas (Figure 17). Since 2003 the following blooms have been reported in this area: 21 to 31 December 2010 (okadaic acid, diarrheic toxin); 15 to 24 September 2011 (domoic acid, amnestic toxin); 2 to 16 April 2012 (okadaic acid, diarrheic toxin); 13 to 27 June 2012 (okadaic acid, diarrheic toxin); 29 June to 31 July 2012 (okadaic acid, diarrheic toxin, *Dinophysis* spp and *Prorocentrum* spp.); 17 September to 16 November 2012 (okadaic acid, diarrheic toxin); and 15 July to 23 August 2013 (okadaic acid, diarrheic toxin). During these events the extraction, commercialization and consumption of bivalve mollusks from these areas was prohibited, mainly due to the detection of okadaic acid. Measures implemented in the closed season included the monitoring of phytoplankton and mollusks. Usually, the species responsible for the toxin secretion have not been identified, only in July 2012 the presence of *Dinophysis* spp and *Prorocentrum* spp was confirmed.

5.3.2 Collection of Samples

Six stations were sampled on TSB on 2 June 2017 during the second week of a bloom event that lasted three weeks (Figure 1). This event was characterized by bioluminescence. The sampling depth was at the chlorophyll maximum fluorescence (0.5 m). The samples were collected inside and outside the patches with bloom evidence to capture the variability that exists in a parcel of water. Stations 5 and 6 were located on the reddish patch that distinguished itself from the rest of the bay water.

Samples were collected in small vessels, they were taken manually and stored in dark Nalgene bottles of high-density polyethylene (HDPE) until processing in the laboratory. For CDOM analysis, samples were collected in amber glass bottles and refrigerated until laboratory processing.

5.3.3 Absorption Coefficients Determination

The absorption coefficient $a(\lambda)$ characterizes light absorption properties in the aquatic environment. Light absorption in natural waters is attributable essentially to four components: water, colored dissolved organic matter (CDOM), photosynthetic biota and inorganic particles (Kirk, 2011). Thus, a (λ) can be expressed as:

$$\boldsymbol{a(\lambda) = a_w(\lambda) + a_{cdom}(\lambda) + a_p(\lambda)} \qquad \text{(Eq.1)}$$

Where the subscripts *w*, *cdom* and *p* represent water, CDOM and particulate matter, respectively. This particulate material consists of phytoplankton ($\boldsymbol{phy}$)

and detritus (non-algal particles) (***d***) (Morel, 2006). Thus $\boldsymbol{a_p}(\boldsymbol{\lambda})$, can be expressed as:

$$\boldsymbol{a_p}(\boldsymbol{\lambda}) = \boldsymbol{a_{phy}}(\boldsymbol{\lambda}) + \boldsymbol{a_d}(\boldsymbol{\lambda}) \qquad \text{(Eq.2)}$$

A volume of seawater of 0.5 to 2 L, depending on the particle load, was filtered from water stored in Nalgene bottles, with Whatman GF/F glass fiber filters 25 mm in diameter and 0.7 µm in pore size. The optical density of particulate material in the filter was measured in the wavelength range of 400 to 800 nm. Then, filters were immersed in methanol to wash out pigments and to obtain the detritus optical density for the same wavelength interval. The light absorption coefficients $a_p(\lambda)$ and $a_d(\lambda)$ were calculated following Mitchell et al. (2002), and $a_{phy}(\lambda)$ was calculated by subtracting $a_d(\lambda)$ from $a_p(\lambda)$.

Water for CDOM analysis was filtered using a 0.2 µm pore membrane filter (Nuclepore™, Merck KGaA, Darmstadt, Germany) and processed according to the methodology of Mitchell et al., (2002). The CDOM absorption coefficient, $a_{CDOM}(\lambda)$, was measured in the wavelength range of 250 to 800 nm in a 10 cm long quartz cuvette using Milli-Q water as reference.

The optical densities of samples were read with a Cary 100 UV-Visible spectrophotometer (Agilent, Santa Clara, CA, USA).

5.3.4 In situ IOP Index Calculations

The in situ IOP index was calculated for the absorption coefficients determined in the laboratory for the six stations which were sampled on TSB on 2 June 2017, during a bloom event that lasted from 25 May to 10 June 2017.

The first step to calculate the IOP index was to standardize the absorption coefficients ($\boldsymbol{a_{CDOM,438-448}}$, $\boldsymbol{a_{d,438-448}}$, $\boldsymbol{a_{phy,438-448}}$) obtained in laboratory measurements using Equation 1. The average absorption from 438 to 448 nm was used because it is the same band width of satellite products (see next section). This was a modification of Santamaria-del-Ángel et al. (2015) and Aguilar-Maldonado et al. (2018a) version of in situ IOP index.

$$z = \frac{x - \bar{x}}{SD} \qquad \text{(Eq.3)}$$

Where:

(x) the value to be standardized; ($\bar{x}$) the average and (*SD*) the standard deviation.

The second step was to perform a principal component analysis (PCA) to reduce the number of original variables. We selected the first principal component because according to eigenvalues it accounts for the largest possible variance. Finally, the IOP index was calculated based on the first standardized empirical orthogonal function ($SEOF_1$) according to Equation (2).

$$\boldsymbol{IOP_{index}} = \boldsymbol{-1}\left[\begin{matrix}(\boldsymbol{b_{1,1}} \times \boldsymbol{Za_{phy,438-448}}) + \\ (\boldsymbol{b_{1,2}} \times \boldsymbol{Za_{CDOM,438-448}}) + (\boldsymbol{b_{1,3}} \times \boldsymbol{Za_{d,438-448}})\end{matrix}\right] \qquad \text{(Eq. 4)}$$

The coefficients $\boldsymbol{b_{1,1}}$, $\boldsymbol{b_{1,2}}$ and $\boldsymbol{b_{1,3}}$ are the first eigenvectors resulting from the SEOF$_1$, while ($Za_{phy,438-448}$, $Za_{CDOM,438-448}$ and $Za_{d,438-448}$) are the values derived from the Pearson correlation matrix between the absorption coefficients standardized anomalies. Then, samples were classified as in bloom or non-bloom using factorial analysis.

The values of the satellite IOP index were interpreted as follows: (1) values in the interval (−1, 1) show the normal values of the specific site or non-bloom conditions; (2) values in the interval (1, 1.6) are above the average and represent a transition from anomalous values to normal values or decaying bloom conditions, and (3) values higher than 1.6 are anomalous and indicate a phytoplankton bloom. The definition of thresholds was possible thanks to the standardization of the data. The limit of the anomalous conditions was based on an Inverse Cumulative Distribution Function (ICDF), in a normal distribution, which defines 1.64 standard deviations as the limit of values without noise with 95% confidence. This value was rounded 1.6 standard deviations. The limit of anomalous conditions was modified from Santamaría-del-Ángel et al. (2015) and Aguilar-Maldonado et al. (2018a), the confidence level was increased from 90 to 95% to avoid missing active bloom conditions.

5.3.5 Image Processing and Satellite IOP Index Calculations

The IOP index was first applied by Santamaría-del-Ángel et al. (2015) and Aguilar-Maldonado et al. (2018a) for in situ data. Later, it was adapted by Aguilar-Maldonado et al. (2018b) for using satellite products and calculating the satellite IOP index. In this study, we improved the satellite IOP index by increasing spatial resolution (from 4 km to 1 km). We also modified the focus from spatial variability to temporal variability. Instead of standardizing the data for a specific area, we selected a point and standardized monthly data for a set of years to build a temporal baseline. So, the satellite IOP index was calculated for the months of May and June since 2003 to 2016 to build the temporal baseline of two selected points (sampling points 4 and 6, Figure 17).

The satellite IOP index was calculated as follows. The first step was to obtain the absorption coefficients of phytoplankton and detritus plus CDOM from the Generalized Inherent Optical Property (GIOP) satellite model. The GIOP model of MODIS Aqua sensor was obtained from NASA's Ocean Color Web (Please, see https://oceancolor.gsfc.nasa.gov/atbd/giop/ for more information). Satellite products for absorption coefficients pertain to MODIS band 9 (443nm, bandwidth 10 nm). We used daily images, processed at level 2, and with 1 km spatial resolution. Cloud cover reduced the number of available images. Then, absorption coefficients of phytoplankton, and detritus plus CDOM were standardized using Equation 1.

The satellite IOP Index was calculated based on a principal component analysis (PCA) of the standardized pixel values as for in situ IOP index. In this case, the principal component only had two coefficients named as $\boldsymbol{b_{1,1}}$ and $\boldsymbol{b_{1,2}}$. Finally, the IOP Index was calculated based on this first standardized empirical orthogonal function (SEOF1) according to Equation (3).

$$IOP_{index\ satellite} = \left[(b_{\mathbf{1,1}} * Za_{phy,_{GIOP}}) + (b_{\mathbf{1,2}} * Za_{dCDOM,_{GIOP}})\right] \qquad \text{(Eq. 5)}$$

Where $Za_{phy,_{GIOP}}$ and $Za_{dCDOM,_{GIOP}}$ are the standardized values of phytoplankton and detritus (non-algal particles) plus CDOM respectively obtained from the GIOP satellite model.

The values of the satellite IOP index were interpreted as for the in situ satellite index.

A non-parametric one-way analysis of variance (Kruskal–Wallis) was performed to statistically assess differences in the satellite absorption coefficients. The absorption coefficients $\boldsymbol{a_{phy,_{GIOP}}}$ and $\boldsymbol{a_{dCDOM,_{GIOP}}}$ for each sampling point were compared.

5.3.6 Validation

A Spearman correlation analysis was performed between GIOP satellite model absorption coefficients and in situ measures of absorption coefficients (6 sampling points in Figure 1). Laboratory absorption data of $\boldsymbol{a_{CDOM}}$, $\boldsymbol{a_d}$ and $\boldsymbol{a_{phy}}$ were averaged from 438 to 448 nm to obtain $\boldsymbol{a_{CDOM,438-448}}$, $\boldsymbol{a_{d,438-448}}$ and $\boldsymbol{a_{phy,438-448}}$, which corresponds to MODIS band 9 bandwidth. Then, laboratory colored detritus matter and CDOM were added to be compared with the satellite product $a_{dCDOM,_{GIOP}}$ (Aguilar-Maldonado et al. 2018b). Each sampled point was related to the pixel value corresponding to that point. The bloom event lasted since 25 May to 10 June 2017. So, based on bloom duration and cloud coverage we decide to form fifteen-day composites to compared with 2 June

2017 samples. Composites were done with the NASA SeaDAS software (https://seadas.gsfc.nasa.gov/).

5.4 Results and discussion

In Figure 18, the absorption spectrum of phytoplankton, detritus and CDOM of all the stations in bloom is compared. The phytoplankton absorption coefficient, a_{phy}, was significantly higher in sampling point 6 than in other sampling points ($p < 0.05$ for a_{phy}) (Figure 2a). a_{CDOM} and a_d were also significantly higher in point 6 ($p < 0.05$ for a_{CDOM} and a_d) (Figure 18b and 18c).

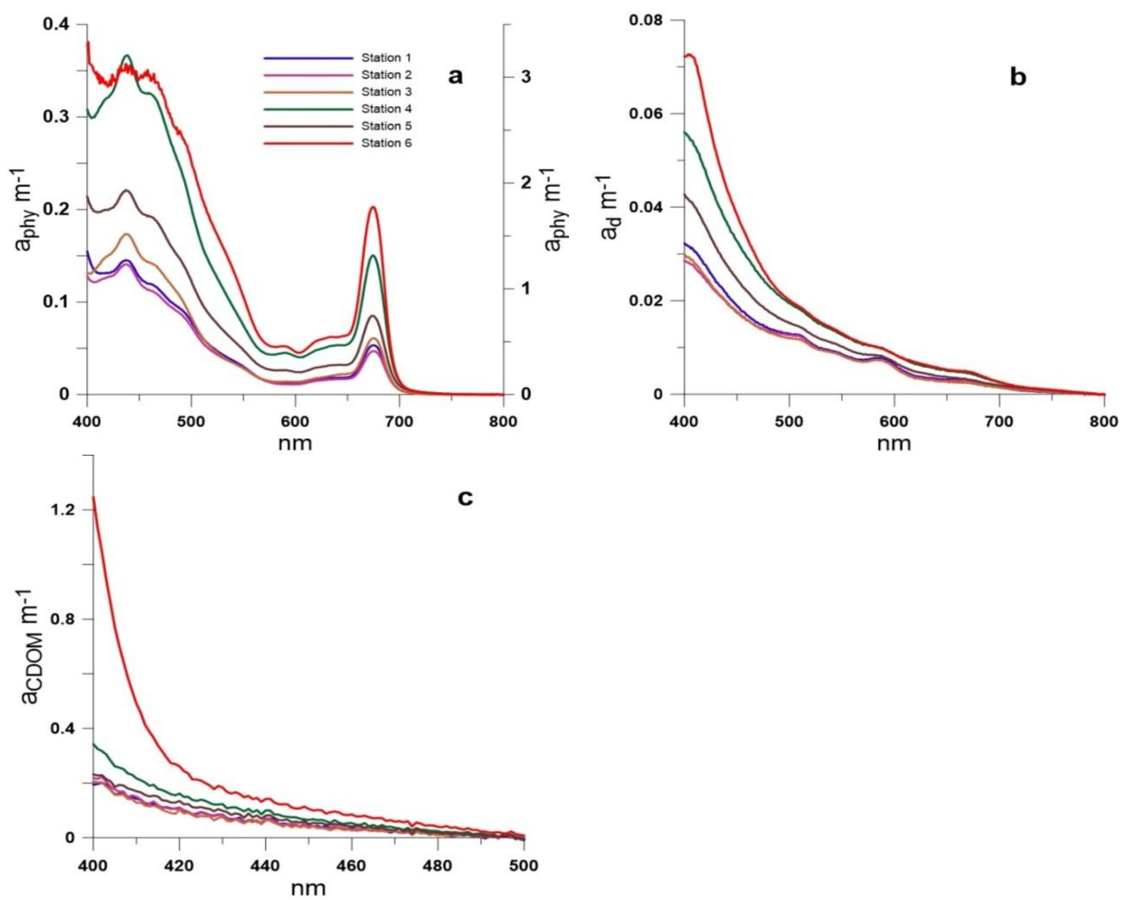

Figure 18. Absorption coefficients ((λ)): (a) phytoplankton (a_{phy}), (sampling point 6, shown with an independent axis of greater absorption, is the one on the right); (b) detritus (a_d) and (c) colored dissolved organic matter (CDOM) (a_{CDOM}) of sampling points

IOP index results are shown in Figure 19. In situ IOP index results for 2 June 2017 are represented with black dots and satellite IOP index results for 25 May to 10 June 2017 are represented with gray dots. The Spearman correlation analysis between GIOP satellite model absorption coefficients and in situ measures of absorption coefficients showed a positive statistically significant correlation. Correlation between $\boldsymbol{a_{phy\ (438-448)}}$ and $\boldsymbol{a_{phy,GIOP}}$ was 0.809, and correlation between $\boldsymbol{a_{dCDOM\,(438-448)}}$ and $\boldsymbol{a_{dCDOM,GIOP}}$ was 0.671. So, the correlation was better for phytoplankton absorption coefficient, but in both cases can be considered a good fit (Gregg and Casey 2003; Santamaría-del-Ángel et al. 2010; Sebastiá et al. 2012). In Figure 19 can be appreciated that both in situ and satellite IOP index show the same trend for all sampling points. In general, it can be observed that satellite IOP index shows higher values than in situ IOP index, but the classification of bloom condition is the same for all the sampling points, except sampling point 5. Sampling point 6 showed the highest anomaly, the IOP index value in this point was above 1.6, and it was under active bloom conditions according to the IOP index interpretation. Sampling point 5 shows the greater difference between in situ IOP index and satellite IOP index, while the first classifies this point under non-bloom conditions, the second classifies it as under active bloom conditions. Sampling points 1, 2, 3 and 4 are under non-blooms conditions, they present values that are normal for their location. A decrease in the IOP index value is observed as the distance from the coast increases, sampling points 1, 2 or 3 showed the lowest values.

The difference between in situ and satellite measures is due to several factors. Laboratory results are based on a discrete sample of a limited volume, while satellite results represent the average value of one pixel (1 km). Also, samples were taken on 2 June 2017, while satellite data were a composite of the available images since 25 May to 10 June 2017. In the specific case of sampling point 5 there were only 3 images available (less than for the other sampling points).

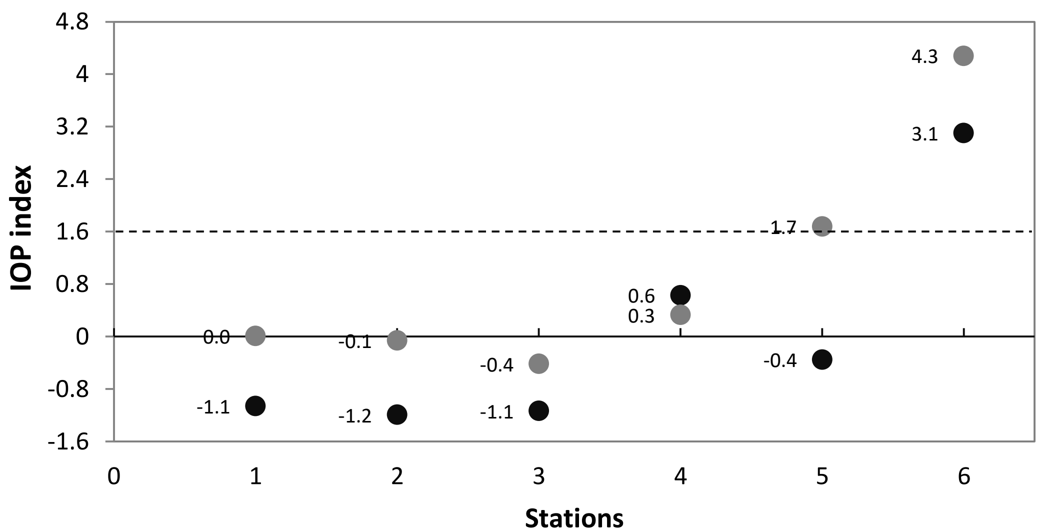

Figure 19. IOP index results in Todos Santos Bay. In situ IOP index results for 2 June 2017 are represented graphically with black dots and satellite IOP index

results for 25 May to 10 June 2017 are represented with gray dots. Dots above the dashed line indicate active bloom conditions.

Figure 20 shows a map of the satellite IOP index in Todos Santos Bay, for the composite image since 25 May to 10 June 2017. Anomalous IOP index values, that is values above 1.6 (orange to red color scale) are concentrated inside the bay, near to the coast. As the distance to the coast increases blue colors predominate, indicating normal or non-bloom conditions.

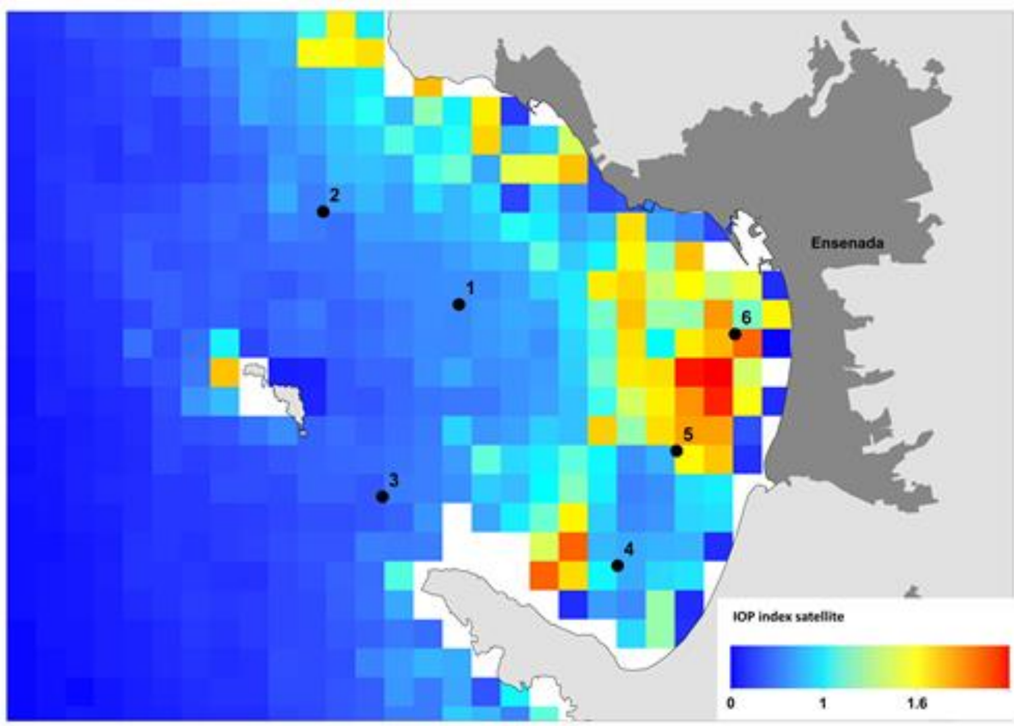

Figure 20. Satellite IOP index in Todos Santos Bay, composite image since 25 May to 10 June 2017. White pixels are due to cloud cover and absence of satellite information.

These results were the base for deciding to build the satellite IOP index baseline for sampling points 4 and 6. That is points near the coast with high IOP index values. Sampling point 4 was chosen also because it is located in Rincón de Ballenas, where blooms have been recurrent in recent years (COFEPRIS, 2018). The IOP index baseline was built for the years 2003 to 2016 (Equation 3), years with COFEPRIS reports available. Table 4 summarizes the data available for sampling point 4, there were 101 available data for May and 115 for June. Table 5 summarizes the data available for sampling point 6, there were 111 available data for May and 146 for June. Cloud cover in TSB is usually high and prevented us from having daily images.

Table 4. Monthly average per year of $a_{phy,GIOP}$ and $a_{dCDOM,GIOP}$ for sampling point 6 and average satellite IOP index. Observed days column refers to number of days with satellite information available. Cloud cover prevent from having daily information

May	$a_{dCDOM,GIOP}$	$a_{phy,GIOP}$	# Observed days	June	$a_{dCDOM,GIOP}$	$a_{phy,GIOP}$	# Observed days
2003	0.378	0.750	8	2003	0.181	0.233	5
2004	0.508	0.284	11	2004	0.442	0.503	8
2005	0.681	0.331	6	2005	0.396	0.677	10
2006	0.203	0.077	6	2006	0.147	0.274	7
2007	0.355	0.355	6	2007	0.371	0.329	14
2008	0.410	0.358	9	2008	0.242	0.282	9
2009	0.162	0.225	4	2009	0.291	0.452	5
2010	0.272	0.092	12	2010	0.134	0.084	5
2011	0.279	0.204	9	2011	0.112	0.466	9
2012	0.140	0.110	5	2012	0.246	0.157	10
2013	0.282	0.146	7	2013	0.304	0.070	7
2014	0.183	0.069	8	2014	0.179	0.082	9

2015	0.139	0.040	1	2015	0.346	0.088	7
2016	0.284	0.221	9	2016	0.207	0.139	10
Total			101				115
Average Satellite IOP index (Baseline)			**0.002**				**0.009**

Table. 5. Monthly average per year of $a_{phy,GIOP}$ and $a_{dCDOM,GIOP}$ for sampling point 4 and average satellite IOP index. Observed days column refers to number of days with satellite information available. Cloud cover prevent from having daily information.

May	$a_{dCDOM,GIOP}$	$a_{phy,GIOP}$	**# Observed days**	**June**	$a_{dCDOM,GIOP}$	$a_{phy,GIOP}$	**# Observed days**
2003	0.132	1.110	9	2003	0.300	0.337	6
2004	0.235	0.799	13	2004	0.249	0.462	11
2005	0.247	0.463	12	2005	0.187	0.537	9
2006	0.330	0.380	7	2006	0.152	0.312	10
2007	0.302	0.199	6	2007	0.368	0.260	15
2008	0.250	0.445	9	2008	0.186	0.164	11
2009	0.146	0.109	8	2009	0.309	0.685	5
2010	0.209	0.120	7	2010	0.147	0.174	11
2011	0.206	0.110	5	2011	1.115	0.087	15
2012	0.138	0.069	10	2012	0.146	0.049	15
2013	0.138	0.143	5	2013	0.185	0.058	8
2014	0.175	0.080	9	2014	0.182	0.091	13
2015	0.243	0.081	5	2015	0.177	0.065	6
2016	0.209	1.184	6	2016	0.070	0.091	11
Total			111				146
Average Satellite IOP index (Baseline)			**0.001**				**0.006**

Average satellite IOP index for sampling point 6 was 0.002 in May and 0.009 in June (Table 4), for sampling point 4 it was 0.001 in May and 0.006 in June (Table 5). These IOP index values can be considered as the baseline for May and June in the selected points. As time goes by the data base of $\boldsymbol{a_{phy,GIOP}}$ and

$\boldsymbol{a_{dCDOM,GIOP}}$ will be increasing with new data, and consequently the baseline can be modified. To be able to distinguish a bloom event, daily $\boldsymbol{a_{phy,GIOP}}$ and $\boldsymbol{a_{dCDOM,GIOP}}$ must be compared with this baseline. As an example, the bloom event of May to June 2017 was monitored in sampling points 4 and 6, and compared with the baseline. That is, the satellite IOP index was calculated with Equation 3, contrasting each daily value with the baseline information.

Figure 21 shows the behavior of $\boldsymbol{a_{phy,GIOP}}$ and $\boldsymbol{a_{dCDOM,GIOP}}$ of point 6, which was the point observed in situ that could be presumed to be in phytoplankton blooms, that is observed in the figure is the growth of $\boldsymbol{a_{phy,GIOP}}$ until June 8, and from this point a gradual decrease until the end of the month, with a rebound on June 14. The growth of $\boldsymbol{a_{phy,GIOP}}$ for this point 6 was fast and constant, this can be affirmed when observing $\boldsymbol{a_{dCDOM,GIOP}}$, which never reached $\boldsymbol{a_{phy,GIOP}}$, that is to say the production of phytoplankton biomass was never exceeded due to its degradation.

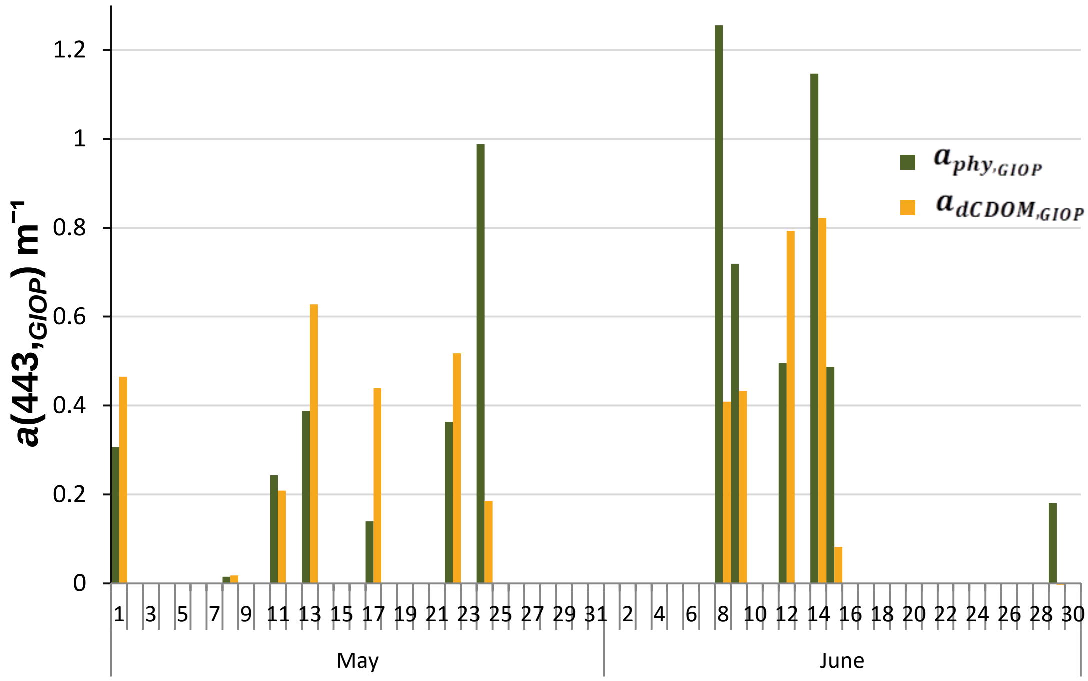

Figure 21. Daily values available from $\boldsymbol{a_{phy,GIOP}}$ (green) and $\boldsymbol{a_{dCDOM,GIOP}}$ (orange color) for sampling station 6 in the months of May (a) and June (b).

In the case of sampling station 4 it is different, since the values of $\boldsymbol{a_{phy,GIOP}}$ are lower compared with station 6 (Fig. 22). It can be seen that also on June 8, its highest $\boldsymbol{a_{phy,GIOP}}$, levels are reached, but the $\boldsymbol{a_{dCDOM,GIOP}}$ reaches it on June 12, which means that the production levels of phytoplankton biomass were slower than in season 6, which allowed that the degradation of this phytoplankton biomass will reach production. This is in accordance with that described by Gaxiola-Castro et al. (2008), which describes a strong seasonal and interannual variability in phytoplankton biomass, which is also forced by diverse local mesoscale processes such as coastal upwellings, eddies, fronts and meanders (Espinosa-Carreón et al., 2004, Barocio-León et al. 2007).

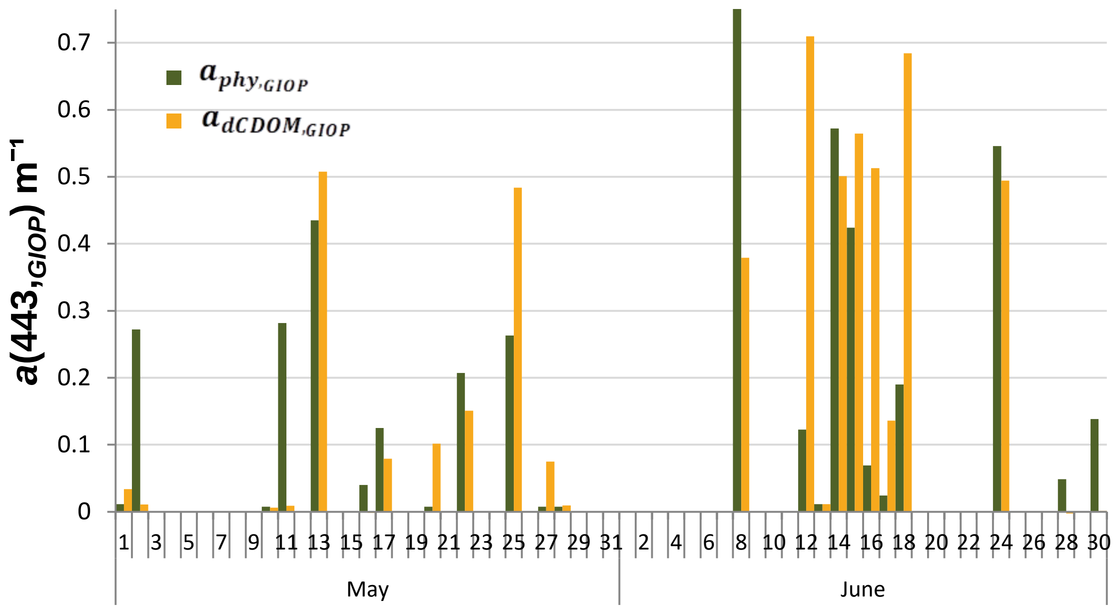

Figure 22. Daily values of $a_{phy,GIOP}$ (green color) and $a_{dCDOM,GIOP}$ (orange color) for sampling station 4 in the months of May (a) and June (b).

The percentages shown in figure 23 make it possible to observe that sampling station 6 had on average a greater growth of $a_{phy,GIOP}$ between May and June 2017 compared to station 4. Also if we compare the percentages of figure 23 with the data From figure 23, we can see that the balance between $a_{phy,GIOP}$ and $a_{dCDOM,GIOP}$ for season 6 in the month of May (Figure 23a) is related to the normal behavior of the index in the month of May (Figure 24) ; but when the balance of $a_{phy,GIOP}$ and $a_{dCDOM,GIOP}$ breaks in station 6 in June (Figure 23b) the satellite IOP index reacts to anomalous data (Figure 24), in this case towards an active bloom, and it is the $\boldsymbol{a_{phy,GIOP}}$ that grew in the month of June.

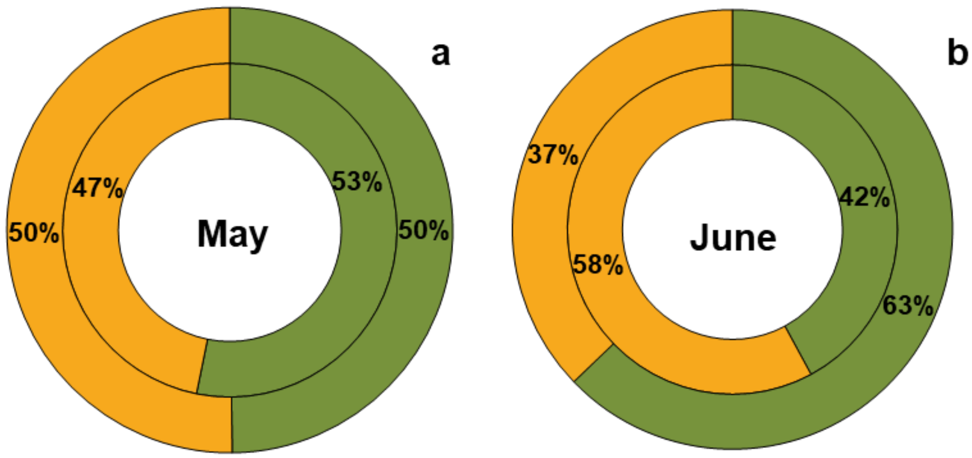

Figure 23. Percentages of $\boldsymbol{a_{phy,GIOP}}$ (green color) and $\boldsymbol{a_{dCDOM,GIOP}}$ (orange color) for sampling stations 6 (outer circumference) and 4 (inner circumference) in the months of May (a) and June (b).

Figures 24 and 25 shows the temporal evolution of satellite IOP index 1 May to 30 June 2017 in sampling points 6 and 4 respectively. IOP index bars have been colored to facilitate interpretation as follows: (1) green color for values in the interval (−1, 1) show the normal values of the specific site or non-bloom conditions; (2) yellow color for values in the interval (1, 1.6) are above the average and represent a transition from anomalous values to normal values or decaying bloom conditions, and can be considered as a pre-alert situation, and (3) red color for values higher than 1.6 are anomalous and indicate an active phytoplankton bloom, and can be considered as an alert situation.

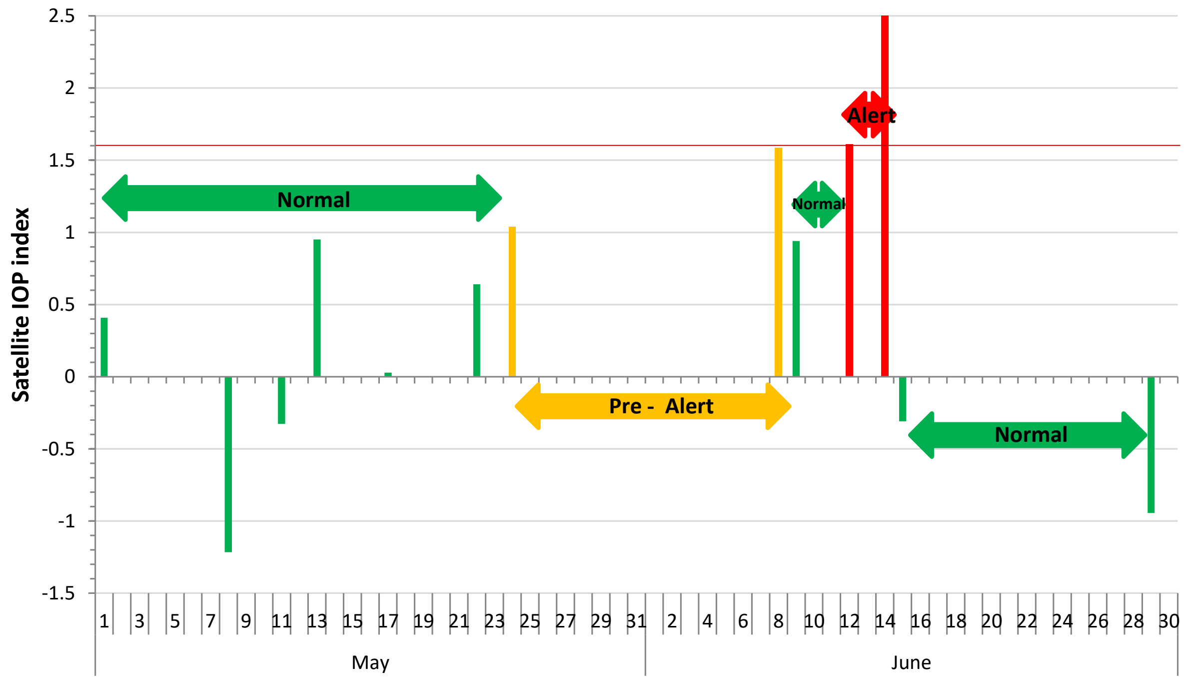

Figure 24. Temporal evolution of satellite IOP index 1 May to 30 June 2017 in sampling point 6. The red line defines the limit of anomalous conditions (> 1.6 standard deviations of IOP index) and active bloom conditions. Green color bars show non-bloom conditions; yellow color bars show decaying bloom conditions, and red color bars show active phytoplankton bloom. Absence of bars is due to cloud cover.

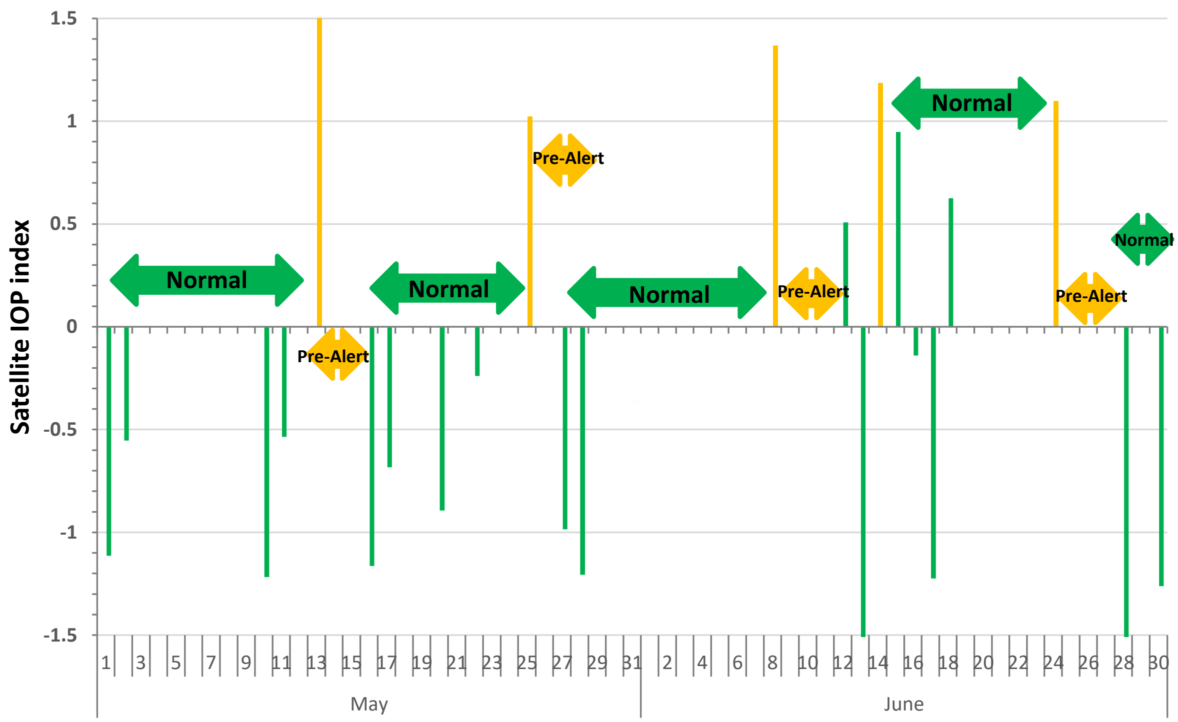

Figure 25. Temporal evolution of satellite IOP index 1 May to 30 June 2017 in sampling point 4. The red line defines the limit of anomalous conditions (> 1.6 standard deviations of IOP index) and active bloom conditions. Green color bars show non-bloom conditions; yellow color bars show decaying bloom conditions, and red color bars show active phytoplankton bloom. Absence of bars is due to cloud cover.

In Figures 24 and 25 we can observe that daily data available for sampling point 6 is more reduced than for sampling point 4 (13 days as compared to 23 days). No information was available for the in situ sampling day (2 June 2017) in either sampling points. Working with a conservative approach in the absence of satellite images it should be considered that the worst scenery remains until new information could be processed. In sampling point 6 (Figure 24) a pre-alert situation (yellow color) started on 24 May and was kept until 8 June 2017, as there was no satellite information during 14 days the pre-alert was kept. Because there is available information of in situ sampling, it is known that on 2 June there was active bloom conditions. For this reason, it is important to clearly define which management measures should be adopted during pre-alert. On 10 June there was a decrease in IOP index reaching normal values or non-bloom conditions, but it lasted only until 14 June when active blooms condition was detected. In sampling point 4, pre-alert situation was reached several times but it expanded as maximum 4 days because satellite data availability was higher and new data confirmed the decrease of the IOP index value to normal or non-bloom conditions.

TSB is a highly cloudy area which prevents the availability of daily satellite images. In the example of May-June Bloom event the maximum period without satellite information was 14 days.

The Mexican Bivalve Mollusks Health Program (in Spanish "Programa Mexicano de Sanidad de Moluscos Bivalvos" (PMSMB)) aims at creating a historical database in order to background information of phytoplankton species by regions and microregions of the Mexican littoral. It also pretends to establish a timely warning system for harmful algal blooms in the coastal states of the country (COFEPRIS, 2016). For this purpose, a Permanent and Systematic Sampling Program is defined for sampling and analysis of bivalve mollusks, gastropods and seawater, under normal conditions in previously determined sampling stations. The State Health Authority establishes a monthly sampling frequency for the determination of marine biotoxins in product and weekly for phytoplankton cell count in normal conditions in wild and cultivation areas. When the maximum permissible levels of phytoplankton established are exceeded during routine monitoring, a sample of the product will be taken in order to carry out a rapid detection test for marine biotoxins. If the result is negative, routine phytoplankton monitoring will continue. If positive, the sanitary closure will be implemented, consisting of the temporary prohibition of capture, commercialization and consumption of mollusks and other marine species for human consumption from an area affected by an event of harmful algal blooms, in order to protect the health of the population. However, not all the Mexican states have the facilities either for phytoplankton quantitative analysis or biotoxin tests (COFEPRIS, 2016). The incidence of marine biotoxins is important however the lack of a monitoring program in the Baja California region as well as specialized laboratories have not allowed a real record of its incidence (Bustillos-Guzmán, 2018). The satellite IOP index methodology proposed in this study aims to be a supplementary tool for permanent in situ monitoring programs. This methodology offers several advantages. While in situ sampling has to be limited to previously fixed sampling stations, mapping the IOP index allow to have a complete spatial coverage of BTS (or any other coastal area). This can be very helpful to determine the extent of blooms events and affected areas, and also may avoid missing bloom events in non-monitored areas.

Regarding sampling frequency, the Permanent Sampling Program is quite ambitious in his principles, it purposes weekly frequency for phytoplankton quantitative analysis, but this is not easy to accomplish. MODIS GIOP products, which are the base for calculating the satellite IOP index, are available at a daily frequency (NASA, 2018). However, this frequency could be reduced due to cloud cover. In this study, BTS was selected to test the methodology and despite being an especially cloudy area the satellite IOP index proved to be useful. So, it is expected that in less cloudy areas temporal resolution will be improved. Finally, one of the objectives of permanent monitoring programs is to obtain background information of phytoplankton. The quantitative analysis of collected water samples can offer information at species level it has some limitations. The first one is that is not possible to have quantitative information always due to limited laboratory facilities and personal, so the Mexican Bivalve Mollusks Health Program stablishes that in that case qualitative analysis will be enough, with the consequent loss of information (COFEPRIS, 2016). The second one is the complexity of having high quality data of quantitative phytoplankton analysis (Almazán-Becerril et al. 2016; Sebastiá et al., 2012). In this sense, the use of the satellite IOP index provides reliable information that can be more objective than phytoplankton traditional analysis. It is true that this method cannot offer taxonomic information at present state, but it provides important information about the background levels of phytoplankton, CDM and CDOM that can be very useful for detecting anomalies. So it can serve as a first-level permanent monitoring tool to support decisions about when and where it is necessary to take in situ samples.

5.5 Conclusions

TSB is a highly cloudy area which prevents the availability of daily satellite images. Despite this disadvantage the GIOP satellite products from MODIS have proved to be useful for monitoring temporal evolution of IOP index, and phytoplankton bloom conditions.

Acknowledgments: This research was funded by CONACYT with a doctorate scholarship to Jesús A. Aguilar-Maldonado, with the announcement number 291025 in 2015. María-Teresa Sebastiá-Frasquet was a beneficiary of the CAS18/00107 post-doctoral research grant, supported by the Spanish Ministry of Education Culture and Sports during her stay at the Universidad Autónoma de Baja California (Mexico).

5.6 References

Aguilar-Maldonado, J.A.; Santamaría-del-Ángel, E.; González-Silvera, A.; Cervantes-Rosas, O.; López, L.M.; Gutiérrez-Magness, A.; Cerdeira-Estrada, S.; Sebastiá-Frasquet, M.T. **2018a**. Identification of Phytoplankton Blooms under the Index of Inherent Optical Properties (IOP Index) in Optically Complex Waters. *Water* 10, 129. doi:10.3390/w10020129

Aguilar-Maldonado JA.; Santamaría-Del-Ángel E.; González-Silvera A.; Cervantes-Rosas OD.; Sebastiá-Frasquet M-T. **2018b**. Mapping Satellite Inherent Optical Properties Index in Coastal Waters of the Yucatán Peninsula (Mexico). *Sustainability*. 10(6),1894. doi:10.3390/su10061894

Almazán-Becerril, A.; Aké-Castillo, J.A.; García-Mendoza, E.; Sánchez-Bravo, Y. A.; Escobar-Morales, S.; Valadez-Cruz, F. **2016**. Catálogo de microalgas de Bahía de Todos Santos, Baja California. México: *CICESE*. ISBN: 978-607-95688-7-0

Andersen, P. **1996**. Design and Implementation of some Harmful Algal Monitoring Systems
IOC Technical Series No. 44, *UNESCO*

Barocio-León, OA.; Millán-Nuñez, R.; Santamaria-del-Angel, E.; González-Silvera A. **2007**. Phytoplankton primary productivity in the euphotic zone of the California Current System estimated by CZCS imagery. *Cienc. Mar*. 33: 59–72.

Barocio-Leon, O. A.; Millan-Nunez, R.; Santamaría-del-Ángel, E.; Gonzalez-Silvera, A. **2008**. Trees, C. C., & Orellana-Cepeda, E. Bio-optical characteristics of a phytoplankton bloom event off Baja California Peninsula (30–31 N). *Cont Shelf Res.*. 28(4-5), 672-681.

Blondeau-Patissier, D.; Gower, J. F.; Dekker, A. G.; Phinn, S. R.; Brando, V. E. **2014**. A review of ocean color remote sensing methods and statistical techniques for the detection, mapping and analysis of phytoplankton blooms in coastal and open oceans. *Prog. Oceanogr*., 123, 123-144. doi.org/10.1016/j.pocean.2013.12.008

Bustillos-Guzmán, JJ. **2018**. Available online: https://www.cibnor.gob.mx/investigacion/planeacion-ambiental-y-conservacion/lineas-y-proyectos-de-investigacion/sistemas-costeros/415-biotoxinas-marinas-monitoreo-y-efectos-en-organismos (accessed on 27 July 2018).

Carstensen, J.; Klais, R.; Cloern, J.E. **2015**. Phytoplankton blooms in estuarine and coastal waters: Seasonal patterns and key species. *Estuar. Coast. Shelf Sci*. 162, 98-109. doi.org/10.1016/j.ecss.2015.05.005

Cepeda-Morales, J.; Durazo, R.; Millán-Nuñez, E.; De la Cruz-Orozco, M.; Sosa-Ávalos, R.; Espinosa-Carreón, T.L.; Soto-Mardones, L.; Gaxiola-Castro, G. **2017**.

Response of primary producers to the hydrographic variability in the southern region of the California Current System. *Cienc. Mar*. 43, 123–135.

COFEPRIS (Comisión Federal para la Protección contra Riesgos Sanitarios/Federal Commission for Protection against Health Risks). Available online: http://www.cofepris.gob.mx/AZ/Paginas/Marea%20Roja/EmergenciasSanitariasEstatales.aspx (accessed on 27 July 2018).

COFEPRIS (Comisión Federal para la Protección contra Riesgos Sanitarios/Federal Commission for Protection against Health Risks). **2016**. Lineamiento de trabajo para el muestreo de fitoplancton y detección de biotoxinas marinas. Available online: http://www.cofepris.gob.mx/AZ/Documents/Lineamiento%20de%20Trabajo%20Muestreo%20y%20Deteccion.pdf (accessed on 27 July 2018).

Espinosa-Carreón TL.; Strub PT.; Beier E.; Ocampo-Torres F.; Gaxiola-Castro G. **2004**. Seasonal and interannual variability of satellite-derived chlorophyll pigment, Surface height, and temperature off Baja California. *J Geophys Res Oceans*. 109, (C3). doi.org/10.1029/2003JC002105

García-Mendoza, E; Rivas, D; Olivos-Ortiz, A; Almazán-Becerril, A; Castañeda-Vega, C; Peña-Manjarrez, JL. **2009**. A toxic Pseudo-nitzschia bloom in Todos Santos Bay, northwestern Baja California, Mexico. *Harmful Algae*. 8 (3), 493-503, https://doi.org/10.1016/j.hal.2008.10.002

Garver, S. A.; and Siegel, D. A. **1997**. Inherent optical property inversion of ocean color spectra and its biogeochemical interpretation: 1. Time series from the Sargasso Sea. *J Geophys Res Oceans*.102(C8), 18607-18625. doi.org/10.1029/96JC03243

Gaxiola-Castro G.; Durazo R.; Lavaniegos B.; De la Cruz-Orozco M.E.; Millán-Núñez E.; Soto Mardones L.; Cepeda-Morales J. **2008**. Pelagic ecosystem response to interanual variability off Baja California. *Cienc. Mar*.34: 263–270

Goela, P. C.; Icely, J.; Cristina, S.; Newton, A.; Moore, G.; Cordeiro, C. **2013**. Specific absorption coefficient of phytoplankton off the Southwest coast of the Iberian Peninsula: A contribution to algorithm development for ocean colour remote sensing. *Cont. Shelf Res*. 52, 119-132. doi.org/10.1016/j.csr.2012.11.009

Gregg, W. W. and Casey, N. W. **2004**. Global and regional evaluation of the SeaWiFS chlorophyll data set. *Rem Sens Environ*. 93: 463-479. doi.org/10.1016/j.rse.2003.12.012

INEGI (Instituto Nacional de Estadística y Geografía/ National Institute of Statistic and Geography) Available online http://www.beta.inegi.org.mx/contenidos/proyectos/ccpv/2010/tabulados/Basico/01_01B_MUNICIPAL_02.pdf (accessed on 2 August 2018).

IOCCG, **2012**. Mission requirements for future ocean-colour sensors. In: McClain, C., Meister, G. (Eds.), Reports of the International Ocean Colour Coordinating Group. NASA Goddard Space Flight Center, Greenbelt (MD, USA), p. 106.

Kirk, J.T.O. **2011**. Light and Photosynthesis in Aquatic Ecosystems, 3rd ed.; Cambridge Univ. Press., ISBN: 9780521151757.

Mélin, F., and Vantrepotte, V. **2015**. How optically diverse is the coastal ocean?. *Remote Sens Environ*. 160, 235-251. doi.org/10.1016/j.rse.2015.01.023

Millán-Núñez, E.; Macias-Carballo, M. **2014**. Phytogeography associated at spectral absorption shapes in the southern region of the California current. Calif. Ocean. Fish. Investig. Rep. 55, 183–196

Mitchell, B.G.; Kahru, M.; Wieland, J.; Stramska, M. **2002**. Determination of spectral absorption coefficients of particles, dissolved material and phytoplankton for discrete water samples. In Ocean Optics Protocols for Satellite Ocean Color Sensor Validation; NASA, Mueller, J.L., Fargion, G.S., Eds.; Flight Space Center: Greenbelt, MD, USA. Volume 3, pp. 231–257.

Morel, A., **2001**. Bio-optical models. In: Steele, J.H. et al. (Eds.), Encyclopedia of Ocean Sciences. Academic Press, New York, pp. 317–326.

Morel, A. **2006**. Meeting the Challenge of Monitoring Chlorophyll in the Ocean from Outer Space. In Chlorophylls and Bacteriochlorophylls: Biochemistry, Biophysics, Functions and Applications; Grimm B., Porra R., Rüdiger W., Scheer H., Eds.; Springer, Dordrecht. Vol. 25, pp 521-534. ISBN: 978-1-4020-4516-5.

Orellana-Cepeda, E.; Granados-Machuca, C., & Serrano-Esquer, J. **2004**. Ceratium furca: One possible cause of mass mortality of cultured blue fin tuna at Baja California, Mexico. In K. A. Steidinger, J. H. Landsberg, C. R. Tomas & G. A. Vargo (Eds.), Harmful Algae 2002 (514-516). St. Petersburg, FL, USA: Florida Fish and Wildlife Conservation Comission, Florida Institute of Oceanography and Intergovernmental Oceanographic Comission of UNESCO.

Peña-Manjarrez, J.L.; Gaxiola-Castro, G.; Helenes-Escamilla, J. **2009.** Environmental factors influencing the variability of Lingulodinium polyedrum and Scrippsiella trochoidea (Dinophyceae) cyst production *Cienc. Mar*. 35(1): 1–14. doi.org/10.7773/cm.v35i1.1406

Santamaría-del-Ángel, E.; Millán Núñez, R.; González-Silvera, A.; Cajal-Medrano, R. **2010**. Comparison of In Situ and Remotely-Sensed Chl-a concentrations: a Statistical Examination of the Match-up Approach. Chap. 15 in the Handbook of Satellite Remote Sensing Image Interpretation: Applications for Marine Living Resources Conservation and Management, J. Morales, V. Stuart, T. Platt and S. Sathyendranath, eds. EU PRESPO and IOCCG. pp. 221-238.

Santamaría-del-Angel, E.; Soto, I.; Millán-Nuñez, R.; González-Silvera, A.; Wolny, J.; Cerdeira-Estrada, S.; Cajal-Medrano, R.; Muller-Karger, F.; Cannizzaro, J.; Padilla-Rosas, Y.; et al. **2015**. Experiences and Recommendations for Environmental Monitoring Programs. In Environmental Science, Engineering and Technology;

Sebastia-Frasquet, M.-T., Ed.; Nova Science Publishers: Hauppauge, NY, USA, p. 32, ISBN 978-1-63482-189-6.

Sebastiá Frasquet, M.T.; Estornell Cremades, J.; Rodilla Alamá, M.; Marti Gavila, J.; Falco Giaccaglia, S.L. **2012a**. Estimation of chlorophyll «A» on the Mediterranean coast using a QuickBird image. Revista de Teledetección. . 37, 23–33.

Sebastiá, M.T.; Rodilla, M.; Sanchis, J.A.; Altur, V.; Gadea, I.; Falco, S. **2012b**. Influence of nutrient inputs from a wetland dominated by agriculture on the phytoplankton community in a shallow harbour at the Spanish Mediterranean coast. *Agric Ecosyst Environ*. 152, 10-20. doi.org/10.1016/j.agee.2012.02.006

Smayda, T. J.; Borkman, D. G.; Beaugrand, G.; Belgrano, A. **2004**. Responses of marine phytoplankton populations to fluctuations in marine climate. MarineEcosystems and Climate Variation: The North Atlantic: A Comparative Perspective. Oxford University Press, Oxford, 49-58.

Werdell, P. J.; McKinna, L. I.; Boss, E.; Ackleson, S. G.; Craig, S. E.; Gregg, W. W.; Stramski, D. **2018**. An overview of approaches and challenges for retrieving marine inherent optical properties from ocean color remote sensing. *Prog Oceanogr*. 160, 186-212. doi.org/10.1016/j.pocean.2018.01.001

Conclusiones generales

Una vez analizados y discutidos conjuntamente los resultados obtenidos durante la realización de esta tesis, se han obtenido las siguientes conclusiones generales:

- La variedad de áreas de estudio seleccionadas permitieron aplicar el índice IOP dentro de la amplia variabilidad de las aguas costeras ópticamente complejas. Dentro de esta variabilidad se encontraron áreas con dominancia de detrito o CDOM, a pesar de que los muestreos se desarrollaron en áreas con florecimientos fitoplanctónicos observados. Esto permitió discernir entre los puntos de muestreo en condiciones de florecimiento activo con los puntos en condiciones de florecimiento en degradación, esto en función de la presencia de CDOM y detrito.

- Los coeficientes de absorción medidos en muestras tomadas *in situ*, datos de campo, y los datos de satélite del modelo GIOP tienen una relación significativa positiva, si bien no son idénticas, si tiene una misma tendencia. Así pues el modelo GIOP puede ser utilizado como referencia de coeficientes de absorción de fitoplancton y CDOM+detrito para el cálculo del índide IOP satelital.

- Las diferencias entre los lugares muestreados permitieron definir los límites espaciales del índice IOP, ya que una gran extensión bajo estudio homogeniza la línea base o el comportamiento medio, no permitiendo resaltar los datos anómalos, o por el controraio, una muy reuducida área de estudio no refleja la variabiidad de las estaciones de muestreo, haciendo que los datos anómalos se manifiesten con mayor frecuencia.

- El índice IOP satelital demostró ser útil para diferenciar florecimientos fitoplanctónicos de la variabilidad natural de un área. El uso del modelo GIOP obtenido del satélite MODIS para un conjunto de años permitió definir la línea de base para la interpretación del índice de IOP satelital. Lo cual permite identificar las localizaciones o los píxeles que tienen valores anómalos.

- El uso de sensores remotos ayudó a definir el índice IOP, mejorando las posibilidades de un monitoreo *in situ* más puntual y mejor orientado, ya que ofrece una mayor resolución espacial y temporal a un costo menor.

- El índice IOP ofrece una metodología más precisa que los métodos de conteo de células , porque tiene en cuenta todos los componentes del agua (es decir, fitoplancton, CDOM y detrito) para identificar un florecimiento activo o en degradación.

- La metodología del índice IOP satelital propuesta en este estudio puede ser una herramienta complementaria para los programas permanentes de monitoreo *in situ*. Esta metodología ofrece varias ventajas: una cobertura espacial completa del área costera específica en estudio, una resolución temporal apropiada y una herramienta para construir una línea base objetiva para detectar la desviación de las condiciones normales durante los eventos de florecimientos fitoplanctónicos.

Futuras líneas de Investigación

Durante el desarrollo de la investigación, tanto en la Universidad Autónoma de Baja California como en las tres estancias académicas en la Universidad Politécnica de Valencia se identificó y analizó el creciente uso de los datos de satélite en el desarrollo de observación y análisis terrestre, especialmente en el estudio de los océanos, donde su aplicación puede hacer más eficiente el uso de los recursos humanos y económicos en los planes de monitoreo y muestreo. Específicamente en el monitoreo de florecimientos fitoplanctónicos pudimos constatar los beneficios que tiene el uso de datos provenientes de sensores remotos, especialmente en el uso de los productos satelitales del modelo GIOP que deben ser comparados con datos *in situ* de diferentes lugares que contengan diferentes proporciones de los tres componentes de absorción de luz en el agua, esto con el fin de cubrir todos los espectros de posibilidad en las aguas y contar con un comportamiento conocido del índice IOP en todos los escenarios posibles.

Uno de los aspectos que deben ser cubiertos en un futuro inmediato, debe ser la puesta en internet, sobre una plataforma institucional, del índice IOP satelital. El índice IOP satelital debe ser calculado para todo un conjunto de pixeles que constituyan un área de estudio o monitoreo constante. Los resultados del índice deben ser convertidos a formato ráster y ya como una imagen ser colocadas en el sistema como un semáforo diario que ofrezca visualizar la calidad de las aguas en base al índice IOP satelital.

La principal línea de investigación en la que se va a trabajar a partir de la conclusión de la tesis es en la simplificación y optimización de la metodología. El objetivo es calcular el índice IOP satelital a partir de los valores más básicos que se obtienen del satélite, es decir, a partir de las reflectancias satelitales. La finalidad trabajar con datos más fieles a la respuesta original de la luz i*n situ*, ya que se estaría evitando procesar los datos bajo algoritmos que los manipulan y modifican, tal como ocurre en el modelo GIOP.

Referencias generales

Brody, S.R.; Lozier, M.S.; Dunne, J.P. **2013**. A comparison of methods to determine phytoplankton Bloom initiation. *J. Geophys. Res. Oceans*. 118, 2345–2357.

Castillo-Pavón, O.; Méndez-Ramírez, J.J. **2017**. The tourist developments and their environmental effects in the Mayan Riviera, 1980–2015. *Quivera*. 19, 101–118.

Carstensen, J.; Henriksen, P.; Heiskanen, A.-S. **2007**. Summer algal blooms in shallow estuaries: Definition,mechanisms, and link to eutrophication. *Limnol. Oceanogr*. 52, 370–384.

Carstensen, J.; Klais, R.; Cloern, J.E.. **2015**. Phytoplankton blooms in estuarine and coastal waters: Seasonal patterns and key species. *Estuar. Coast. Shelf Sci*. 162, 98–109.

Cui, T.; Cao,W.; Zhang, J.; Hao, Y.; Yu, Y.; Zu, T.;Wang, D. **2013**. Diurnal variability of ocean optical properties during a coastal algal bloom: Implications for ocean colour remote sensing. *Int. J. Remote Sens*. 34, 8301–8318.

Huppert, A.; Blasius, B.; Stone, L. **2002**. A Model of Phytoplankton Blooms. *Am. Nat*. 159, 156–171

Ji, R.; Edwards, M.; Mackas, D.; Runge, J.; Thomas, A. **2010**. Marine plankton phenology and life history in a changing climate: Current research and future directions. *J. Plankton Res.* 32, 1355–1368.

Kirk, J.T.O. **2011**. Light and Photosynthesis in Aquatic Ecosystems, 3rd ed.; Cambridge Univ. *Press: Cambridge*, UK, ISBN 9780521151757

Kudela, R.M.; Bickel, A.; Carter, M.L.; Howard, M.D.; Rosenfeld, L. **2015**. The monitoring of harmful algal blooms through ocean observing: The development of the California Harmful Algal Bloom Monitoring and Alert Program. *Coast. Ocean Obs. Syst*. 58–75.

Loisel, H.; Vantrepotte, V.; Norkvist, K.; Mériaux, X.; Kheireddine, M.; Ras, J.; Pujo-Pay, M.; Combet, Y.; Leblanc, K.; Dall'Olmo, G.; Mauriac R.; Dessailly D.; Moutin T. **2011**. Characterization of the Bio-Optical Anomaly and Diurnal Variability of Particulate Matter, as Seen from Scattering and Backscattering Coefficients, in Ultra-Oligotrophic Eddies of the Mediterranean Sea. *Biogeosciences.* 8(11), 3295–3317.

Mercado, J.M.; Ramírez, T.; Cortés, D.; Sebastián, M.; Reul, A.; Bautista, B. **2006**. Diurnal Changes in the Bio Optical Properties of the Phytoplankton in the Alborán Sea (Mediterranean Sea). *Estuar. Coast. Shelf Sci*. 69, 459–470.

Morel, A. **2006**. Meeting the Challenge of Monitoring Chlorophyll in the Ocean from Outer Space. In Chlorophylls and Bacteriochlorophylls: Biochemistry, Biophysics, Functions and Applications; Grimm, B., Porra, R., Rüdiger, W., Scheer, H., Eds.; Springer: Dordrecht, The Netherlands; Volume 25, pp. 521–534, ISBN 978-1-4020-4516-5.

NASA Goddard Space Flight Center, Ocean Biology Processing Group. **2014**. Sea-viewing Wide Field-of-view Sensor (SeaWiFS) Ocean Color Data, NASA OB.DAAC, Greenbelt, MD, USA. http://doi.org/10.5067/ORBVIEW-2/SEAWIFS_OC.2014.0. Accessed 2018/08/20. Maintained by NASA Ocean Biology Distibuted Active Archive Center (OB.DAAC), Goddard Space Flight Center, Greenbelt MD.

Padilla, N.S. **2015**. The environmental effects of Tourism in Cancun, Mexico. Int. *J. Environ. Sci*. 6, 282 294.

Platt, T.; Sathyendranath, S.; White, G.; Fuentes-Yaco, C.; Zhai, L.; Devred, E.; Tang, C. **2009**. Diagnostic properties of phytoplankton time series from remote sensing. *Estuar. Coasts*. 33, 428–439.

Preisendorfer, R.W. **1961**. Application of Radiative Transfer Theory to Light Measurements in the Sea; IUGG: Potsdam, Germany. Volume 10, pp. 11–30.

RedFAN (Red Temática sobre Florecimientos Algales Nocivos/ Thematic Network on Harmful Algal Blooms). Available online: https://redfan.cicese.mx/Secciones/inicio (accessed on 13 August 2018).

Santamaría-del-Angel, E.; González-Silvera, A.; Millán-Nuñez, R.; Callejas-Jiménez, M.E.; Cajal-Medrano, R. **2011**. Determining Dynamic Biogeographic Regions using Remote Sensing Data. In Handbook of Satellite Remote Sensing Image Interpretation: Applications for Marine Living Resources Conservation and Management; Morales, J., Stuart, V., Platt, T., Sathyendranath, S., Eds.; EU PRESPO and IOCCG: Dartmouth, NS, Canada, Chapter 19, pp. 273–293.

Santamaría-del-Angel, E.; Soto, I.; Millán-Nuñez, R.; González-Silvera, A.;Wolny, J.; Cerdeira-Estrada, S.; Cajal-Medrano, R.; Muller-Karger, F.; Cannizzaro, J.; Padilla-Rosas, Y.; et al. **2015**. Experiences and Recommendations for Environmental Monitoring Programs. In Environmental Science, Engineering and Technology; Sebastia-Frasquet, M.-T., Ed.; Nova Science Publishers: Hauppauge, NY, USA, p. 32, ISBN 978-1-63482-189-6.

Schneider, B.; Kaitala, S.; Maunula, P. **2006**. Identification and quantification of plankton bloom events in the Baltic Sea by continuous pCO2 and chlorophyll a measurements on a cargo ship. *J. Mar. Syst*. 59, 238–248.